Characterizing Rare Disease-Causing Mutations in Genes Affecting Cation-Coupled Chloride Cotransport

By

Salma Omer

Dissertation

Submitted to the Faculty of the

Graduate School of Vanderbilt University

in partial fulfillment of the requirements

for the degree of

DOCTOR OF PHILOSOPHY

in

Neuroscience

May 8th, 2020

Nashville, Tennessee

Approved:

Eric J. Delpire, Ph.D.
Laura L. Dugan, M.D.
Carrie A. Grueter, Ph.D.
Fiona E. Harrison, Ph.D. (Chair)

بِسْمِ اللَّهِ الرَّحْمَٰنِ الرَّحِيمِ

I dedicate this work to my mother, and guardian angel, Rawhia El-Mahdy (1953-2013), and father, Abuobieda Omer for all their sacrifices

and

To my beloved siblings and branches of my life, Sumaiyah, Abdel-Rahman, Asma, Aisha, Zuhair, El-Tayeb, and Sarah

and most importantly

to my nephews and nieces, for keeping me lighthearted through the most difficult times

ACKNOWLEDGEMENTS

I would like to thank key individuals for their guidance, mentorship, and training throughout my PhD. None of the work in this dissertation would have been made possible without their unending support. First and foremost, I would like to thank my advisor Dr. Eric Delpire for his unwavering patience, and for fostering my independence as a scientist. With his open-door policy, and limitless sponsorship, there was never a time where he opposed my ideas or withheld from funding or sponsoring my experiments. His work ethic, enthusiasm for science, and perseverance, were extremely inspiring and motivating throughout my training. I am fortunate to have trained in the lab of a pioneer in the field of the Cation Chloride Cotransporters.

Second, I would like to individually thank members of my thesis committee, Dr. Fiona Harrison, Dr. Carrie Grueter, and Dr. Laura Dugan for their endless encouragement, advice, and for continuing to push and challenge me. As my thesis committee chair, Dr. Harrison always went above and beyond to ensure I was receiving the best possible training from performing proper statistical analysis methods to rodent neurobehavior and handling, and spent hours and days on end training and mentoring me. I owe all my expertise in mouse behavior and animal handling to her. Further, Dr. Carrie Grueter, always made herself available to me and at many times was the reason I held my head up high. I am extremely thankful for her serving as the expert in metabolism for Chapter III of my dissertation. I would also like to thank Dr. Laura Dugan, for always believing in me and convincing me that I am capable of all my career and scientific aspirations.

I am extremely grateful for the professional relationships I built with all the current members of my laboratory, which resulted in life-long friendships, and made time spent in lab extremely enjoyable. I would like to recognize Kerri Rios for all her contributions of molecular cloning of constructs, allowing many of my experiments to be possible. Thank you Ghalli Abdelmessih for handling the husbandry and breeding of my mouse lines, which is not an easy feat. I also really appreciated having Bianca Flores in the lab as another PhD student, where we endured all the happy and tough times together. Lastly, I would especially like to thank Dr. Rainelli Koumangoye for his endless efforts in training and mentoring me as a Research Instructor in the lab. I owe many of my *in vitro* technical expertise to him, as he was extremely patient and thorough with every aspect of his training. I am thankful for the many opportunities he offered to collaborate on projects, resulting in several co-authorships of his publications.

I want to thank the leadership of the Initiative for Maximizing Student Diversity (IMSD) Program at Vanderbilt, Dr. Roger Chalkley, Dr. Linda Sealy, and Dr. Christina Keeton, for equipping me with all the resources, and knowledge to succeed in graduate school, especially as an under-represented minority in STEM. These wonderful individuals and scientists recognized and fostered my scientific intellect, before I had the confidence to, and for that I am forever indebted to them. I'm grateful for the Vanderbilt Brain Institute (VBI) and the T-32 Training in Fundamentals of Neuroscience training grant for serving as the foundation in my knowledge of neuroscience basic science research.

Finally, I would like to thank my most wonderful and endlessly supportive parents, and siblings for their love, emotional and financial support, and guidance. By immigrating to America, my parents sacrificed so much and left everything they knew and loved behind to provide a better

life for me and my siblings. Thank you for serving as my role models of success, for inspiring me to always be kind to others, and for cultivating my growth as the best person I can possibly be. I love you.

TABLE OF CONTENTS

LIST OF TABLES

LIST OF FIGURES

CHAPTER I

CATION CHLORIDE COTRANSPORTERS

Rare Disease-Causing Mutations in Genes Affecting Chloride Cotransport

According to the World Health Organization, and the NIH Genetic and Rare Diseases information center, a rare disease is classified as a condition that affects less than 1 in 2000 individuals (Henrard & Arickx, 2016; NIH genetic and rare disease information center, 2017). Approximately 7000 rare diseases have been reported, including well known rare diseases such as cystic fibrosis, Angelmann syndrome, and muscular dystrophy. However, unlike cystic fibrosis, which occurs in about 1 in 3400 people, there are diseases that are only found in single individuals (Humphreys, 2012), which this dissertation body of work is based on. Rare diseases affect approximately 25-30 million Americans, and even more individuals are thought to have a rare disease that is unreported. Rare diseases are caused by several factors, but mainly are caused by genetic changes such as inherited and non-inherited genetic mutations, in the form of heterozygous *de novo* mutations (which is the genetic mutation discussed in this dissertation). Genetic mutations in individuals with rare diseases are identified via whole-exome sequencing. While these unique patients are being treated for their symptoms, the identification of mutations in specific genes does not necessarily provide a clear path to disease understanding and treatment. In our studies, we will aim at establishing causality between unique genetic mutations and the clinical features that these patients present. This will be helped by the generation of mouse models that reproduce one single mutation in a gene of interest.

This dissertation is based on two single cases or two individuals with rare diseases. They each carry deleterious heterozygous *de novo* mutations in genes of interest to this laboratory. One individual carries a heterozygous *de novo* mutation in the gene encoding for protein kinase D1 (PKD1), suffering from central and peripheral nervous system deficits (discussed in chapter 2). This patient is being treated by a current collaborator at Yale University. The second individual carries a heterozygous *de novo* mutation in the gene encoding for the Na^+-K^+-$2Cl^-$ cotransporter 1 (NKCC1), with multi-organ failure and metabolic deficits (Discussed in Chapter 3). This patient was admitted into the NIH Undiagnosed Diseases Program (UDP). The purpose of the UDP is to bring together clinical and research experts from across the United States to identify the mysterious symptoms of patients, and establish causality between genetic mutations and diseases. The original NIH-based UDP became UDN, a network that now branches into 12 research sites, where Vanderbilt University serves as one hub of the network. Typically, whole exome sequencing is conducted on individuals admitted into the UDN to identify pathogenic DNA variants. Researchers will then generate model organisms carrying the mutation of interest, to understand how specific genetic changes contribute to disease. A common factor between our two single cases with rare diseases, is that the genetic mutations they carry affect chloride cotransport.

The tight regulation of intracellular Cl^- concentrations ($[Cl^-]_i$) is critical for many cellular physiological processes including: cell volume regulation, the modulation of inhibitory synaptic neurotransmission, muscle contraction, and epithelial transport in the direction of absorption or

secretion (Gamba, 2005; Gagnon & Delpire, 2016). The solute carrier 12 (*SLC12*) gene family, which encodes several electroneutral cation-coupled chloride transporters (CCCs), is primarily responsible for the regulation of intracellular Cl^-, in addition to regulating intracellular Na^+ and K^+. The *SLC12* gene family comprises nine members and is divided into two main functional branches based on their ability to transport Na^+ (Figure1-1). The members are differentially sensitive to pharmacological inhibitors, and they show various stoichiometry, amino acid topology, and phylogeny. The first branch of the *SLC12* gene family consists of four Na^+ independent and K^+ coupled Cl^- cotransporters (KCCs) (Gillen et al., 1996; Race et al., 1999; Hiki et al., 1999; Mount et al., 1999; Payne et al., 1996), encoded by the *SLC12A4-A7* genes (Table1-1). The second branch consists of the Na^+ coupled and dependent Cl^- cotransporters (one NCC and two NKCCs) (Gamba et al., 1993; Gamba et al., 1994; Payne et al., 1995; Payne & Forbush 1994; Xu et al., 1994; Delpire et al., 1994). They are encoded by the *SLC12A1-A3* genes. Two additional orphan members of the SLC12 family encodes for *SLC12A8 (*or CCC8) and *SLC12A9* (or CIP, CCC9), but they have unknown function.

From their cloning from 1993-1996, and hydropathy plot of their primary amino acid sequence, it was clear that the CCCs consist of a core of 12 transmembrane domains (TMDs), flanked by intracellular amino- and carboxyl-terminal domains (Gagnon & Delpire, 2013). The NKCCs contain a larger extracellular loop between TMD7 and TMD8, whereas the KCCs contain a large extracellular loop between TMD5 and TMD6. Several studies have identified domains that participate in the dimerization of the CCCs at the plasma membrane, and the correct dimerization of CCCs is necessary for proper function and activity where studies have identified an increase in

ion flux in the dimeric state of the cotransporters (Casula et al., 2001; Starremans et al., 2003). Once activated by extracellular osmolar conditions, followed by phosphorylation or dephosphorylation by kinases or phosphatases, the cotransporters function in membrane or transepithelial transport of Cl^- ions along with Na^+ and/or K^+ ions, resulting in cell volume regulation by extrusion or influx of the ions. The crystal structures of KCC1, KCC4, and NKCC1 have been identified in 2019, revealing the confirmation state of the transporters, the importance of the extracellular, transmembrane and cytosolic domains for dimerization, and key residues in the transmembrane domain that function in ion transport, which will be discussed in more detail in the representative cotransporter description (Chew et al., 2019; Liu et al., 2019; Reid et al., 2019).

The large transmembrane Na^+ and K^+ gradients established by the Na^+-K^+-ATPase energetically drive the chloride cotransporters, resulting in secondary active transport of the cotransporters since they do not utilize ATP (Geck et al., 1980; Dunham et al., 1980; Lauf & Theg, 1980). The CCCs function to transport an equivalent number of positive and negative ions across the membrane, resulting in electroneutral transport. The large electrochemically-favorable inward gradient for Na^+ works in the favor of Na^+ coupled chloride cotransporters and allows them to transport Cl^- into the cell, raising $[Cl^-]_i$ above the Cl^- electrochemical equilibrium or reversal potential (E_{Cl}). Similarly, the K^+ coupled chloride cotransporters take advantage of

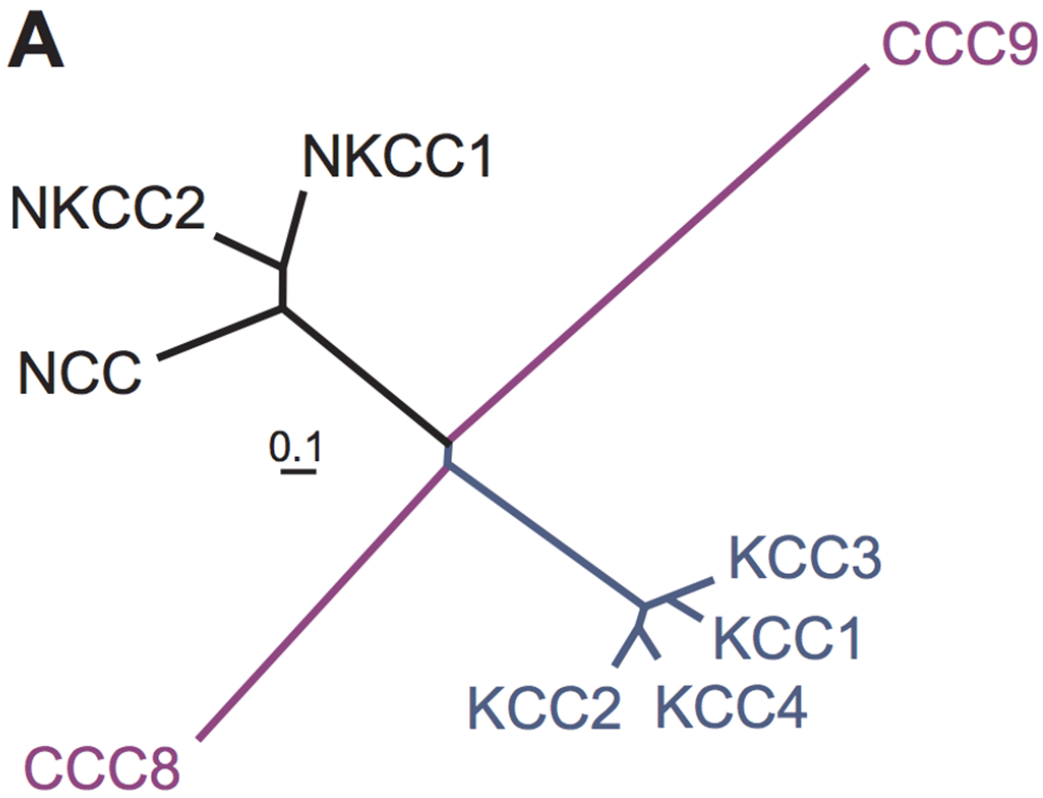

Figure 1-1. SLC12A cation chloride cotransporter homology tree. Homology tree adapted from Gagnon et al., illustrating a cluster dendrogram of the *SLC12A* gene family delineating the branching of the Na-dependent (NCC, NKCC1-2) and Na-independent (KCC1-4) CCCs. The functionally uncharacterized CCC8 and CCC9 are separated early during evolution from the Na-independent and Na-dependent cotransporters, respectively (Gagnon & Delpire, 2013).

the outward gradient for K^+ by transporting Cl^- out of the cell, reducing $[Cl^-]_i$ below E_{Cl} (Zhu et al., 2016; Leefmans et al., 2010). The degree to which each transporter is active in mediating Cl^- efflux or influx determines the $[Cl^-]_i$ in various cell types, resulting in the regulation of neuronal excitability, cell volume, and transport of Na^+, K^+ and water across epithelia.

The cation-chloride cotransporters are expressed in a wide range of cell types. NKCC1, NKCC2, KCC1, KCC3, and KCC4 are expressed in several tissue types, whereas KCC2 expression is confined to the central nervous system (Table 1-1). An imbalance in intracellular Cl^- and mutations in genes involving the transport of Cl^- have been linked to inherited as well as non-inherited forms of human disease. For example, disease variants of KCC2 result in human epilepsy (Kahle et al., 2014; Puskarjov et al., 2014; Stödberg et al., 2015; Saitsu et al., 2016); inactivating mutations in KCC3 result in agenesis of the corpus callosum with peripheral neuropathy (ACCPN) (Howard et al., 2002; Boettger et al., 2003); various mutations in NCC and NKCC2 are associated with the salt wasting disorders such as Gitelman and Bartter syndromes, respectively (Simon et al., 1996); and abnormal developmental regulation of NKCC1 in premature neurons result in hyperexcitability and neonatal seizures (Dzhala et al., 2005). Recently we identified a nonsense mutation in NKCC1 resulting in multi-organ failure (Delpire et al., 2016), where I determined that this mutation results in metabolic deficits, which will be discussed in this dissertation. This dissertation will also outline studies I performed to characterize a mutation in the gene encoding for protein kinase D1 (PKD1) resulting in abnormal KCC3 activity, peripheral neuropathy, and central nervous system deficits.

Table 1-1. Summary of SLC12 Family of Electroneutral Cation-Coupled Cotransporters

Gene name	Protein	Gene locus	Phosphorylation sites	Tissue distribution	Human disease association	Mouse KO phenotype
SLC12A1	NKCC2/ BSC1	15q21.1	T100, T105, S130	Kidney	Type 1 Bartter syndrome	Hypotension, Hypokalemia, hypocalciuria, metabolic alkalosis
SLC12A2	NKCC1/ BSC2	5q23.3	T184, T189, S202	Ubiquitous	Multiorgan failure	Sensorineural deafness, decreased enolymph secretion, decreased salivation, infertility in males, reduced intestinal secretion, abnormal sensory perception
SLC12A3	NCC	16q13	T53, T58, S71	Kidney and bone	Gitelman syndrome	Hypotension, hypocalciuria, hypomagnesemia, hypokalemia
SLC12A4	KCC1	16q22	T926, T983	Ubiquitous	Sickle cell anemia	No phenotype
SLC12A5	KCC2	20q13	T906, T1007	Central nervous system (Brain and Spinal cord)	Human epilepsy	Premature death due to respiratory failure, epilepsy
SLC12A6	KCC3	15q14	T991, T1048	Brain and spinal cord, peripheral nerves, red blood cells, kidney, pancreas, lung	ACCPN (Andermann Syndrome)	Peripheral motor neuropathy

SLC12A7	KCC4	5p15	T926, T980	Brain, kidney, heart	Renal abnormalities	Sensorineural deafness, renal tubular acidosis
SLC12A8	CCC9	3q21	Unknown	Widespread	Unknown	Unknown
SLC12A9	CCC8/ CIP	7q22	Unkown	Widespread	Unkown	Unkown

Table 1-1. Chromosomal location, phosphorylation sites, and tissue distribution of the cation-coupled cotransporters. Several cotransporters have been associated with human disease and respective KO mouse models of have been generated.

Protein Structure of CCCs

The SLC12 family of transporters have a typical membrane topology with a rather short hydrophilic (and therefore outside the membrane) N-terminus, a 12 transmembrane hydrophobic core domain, and a large hydrophilic C-terminus (Figure 1-2). The cytoplasmic N-terminal and carboxyl terminal carry the sites of phospho-regulation and protein binding (Flemmer et al., 2002; Rinehart et al., 2009; De Los Heros et al., 2014). The 12 TMD hydrophobic core of the protein is where the transporters share the largest degree of homology. In fact, TMD2 is where differences in ion affinities seem to be encoded (Isenring et al., 1998) and site specific mutagenesis in NKCC1 and NKCC2 resulted in reduced Na^+ or Rb^+ affinity. Similarly, Isenring and collaborators have identified through point mutation and chimera studies, that TMD2, 4, and 7 are important for ion transport affinities in the NKCCs (Isenring et al., 1998a; Isenringet al., 1998; Isenring & Forbush, 1997). As discussed above, the solved structures of the zebrafish Na-K-2Cl cotransporter and human KCC1 identifies other transmembrane domains as providing residues key to ion coordination. Each member of the SLC12 family contains a large extracellular loop, with N-linked glycosylation sites necessary for plasma membrane transport from the ER (Singh et al., 2015). The location of the N-glycosylation sites differs between the NCC/NKCCs and the KCCs/CIP, due to the large extracellular loop being placed between TMD7 and TMD8 in the NKCCs, and TMD5 and TMD6 in the KCCs and CIP (Delpire et al., 1994; Mount et al., 1999). The amino- and carboxyl- termini are necessary for the cotransporters to exist as homo-oligomeric or heterodimeric structural units at the plasma membrane (Casula et al., 2001; Moore-Hoon & Turner, 2000). Using chemical cross linking studies via the reversible chemical cross-linker DTSSP [3,3‘-dithiobis (sulfosuccinimidyl propionate)], NKCC1 was determined to form homo-oligomeric

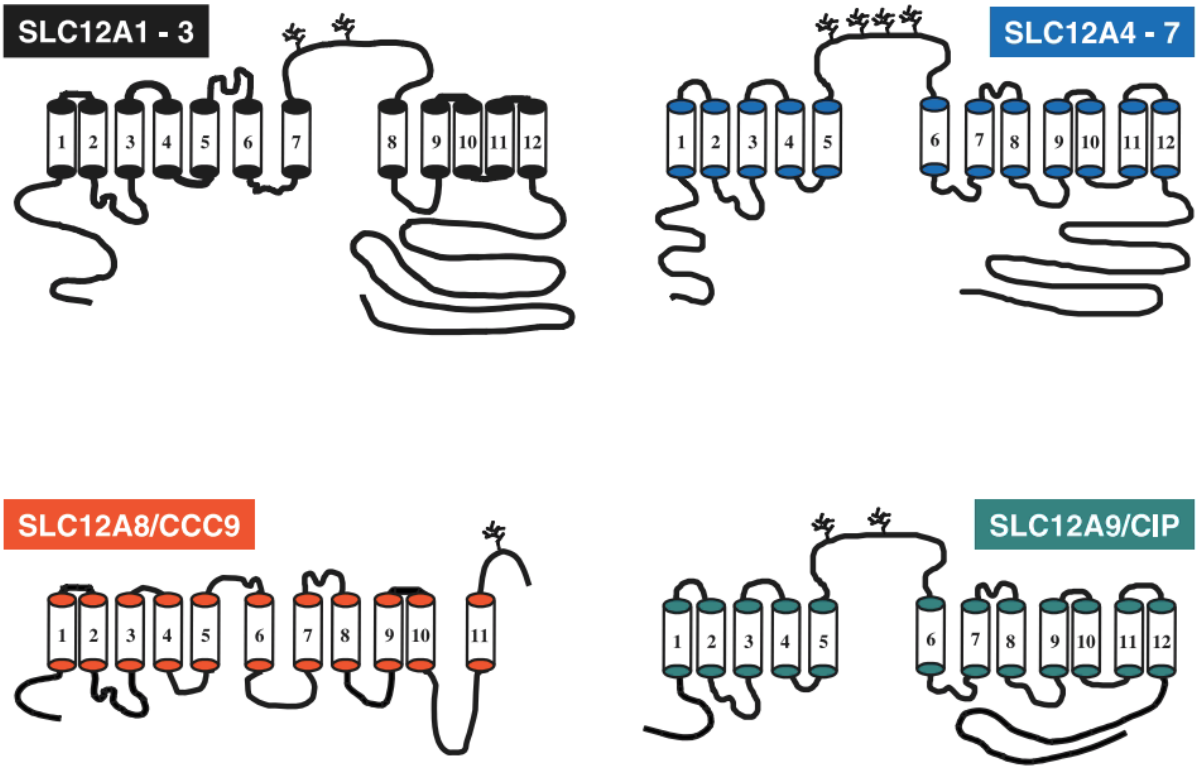

Figure 1-2. Kyte-Doolittle topology of SLC12A cation chloride cotransporters. The cation chloride cotransporters share several structural and topological characteristics according to the Kyte-Doolittle hydropathy plot analyses adapted from (Gamba, 2005). There are 12 hydrophobic transmembrane domains, flanked by a large hydrophilic intracellular carboxyl terminal, and a shorter hydrophilic amino terminal. All CCCs contain a large extracellular glycosylated loop between: transmembrane domains 7 and 8 in SLC12A1-3 (NKCCs), and transmembrane domains 5 and 6 in SLC12A4-7 (KCCs) and CIP (CCC8).

structural units at the plasma membrane with a molecular size twice the size of the monomeric state (Moore-Hoon & Turner, 2000). Yeast two-hybrid studies also revealed that two domains located at the C-terminal tail of NKCC1 are responsible for the homo-oligomeric and self-interaction of NKCC1 (Simard et al., 2004). Similarly, NKCC2 can also self-interact via the C-terminal, in addition to forming a homo-oligomeric state at the cell membrane (Brunet et al., 2005). This suggests that independent of phosphorylation, the C-terminal can act a self-regulatory mechanism. Additionally, in heterologous expression systems NKCC2 co-immunoprecipitates with itself, and NCC also co-immunoprecipitates with itself (Starremans et al., 2003; De Jong et al., 2003).

Other studies have shown that the KCCs exist in dimeric states, where initially a study identified that KCC1 exists in a homo-oligomeric state at the plasma membrane, and truncating the amino and carboxyl termini abolished function (Casula et al., 2001). Another immunoblot study (Blaesse et al., 2006) discovered that KCC2 exists in multimeric states. However, it was unclear whether the oligomer is a homo-oligomeric or hetero-oligomeric structure. Shortly after, GST pull-down and yeast two-hybrid assays revealed that the KCCs can exist as homodimers, as well as functional heterodimers in some complexes (Simard et al., 2007). For example, KCC2 can form complexes with KCC2 and KCC4, and KCC4 can form complexes with KCC4, KCC2, and even NKCC1. Furthermore, immunoprecipitation assays by our group demonstrated that KCC3 and KCC2 can also exist as heterodimer complexes, although this complex is not properly trafficked to the plasma membrane, reducing cotransporter function (Ding et al., 2013). Ultimately,

dimerization of the cotransporters is absolutely necessary for transporter function, although it is still unclear whether the CCCs can form functional relevant heterooligomers.

Function, Regulation, and Pharmacology of CCCs

Function

The first line evidence of electroneutral coupled transport of Na^+, K^+, and Cl^- was provided by Geck et al., (1980) in mouse Ehrlich cells. The work showed that net fluxes of Na^+, K^+, and Cl^- were furosemide sensitive (diuretic used in clinic to inhibit renal absorption of NaCl) (Greger & Schlatter, 1981), unaffected by the membrane potential, and that the transport of Na^+, K^+, and Cl^- was with a ratio of 1 Na^+:1K^+:2Cl^-. The transporters responsible for the electroneutral transport of Na^+, K^+, and Cl^- were molecularly identified to be NKCC1 and NKCC2 in 1994 by our group and others (Delpire et al., 1994; Gamba et al., 1994; Xu et al., 1994; Igarashi et al., 1995). NCC on the other hand was identified a year earlier (1993) by Gerardo Gamba and Steven Hebert. It was from the flounder bladder and was the first member of the SLC12A family to be molecularly cloned (Gamba et al., 1993). NCC is a thiazide-sensitive sodium chloride cotransporter, in contrast to the other cotransporters, it does not carry K^+ and is insensitive to loop diuretics, e.g. furosemide and bumetanide. It functions as an electroneutral transport of Na^+ and Cl^-, in a ratio of 1Na^+:1Cl^-. The Na^+ independent K-Cl cotransporters (KCCs) have an ion stoichiometry of 1K^+:1Cl^-. They have been first described in mammalian red blood cells (Dunham & Ellory, 1980; Lauf & Theg, 1980). KCC1 was the first K-Cl cotransporter to be molecularly characterized (Gillen et al., 1996), followed by KCC2, KCC3, and KCC4 (Payne et al., 1996; Mount et al., 1999). The

transport properties (if any) of the last two members of the SLC12 family, CCC8 and CCC9, have yet to be discovered.

Regulation

The cation-chloride cotransporters fulfill major physiological roles in the body, including ion homeostasis, epithelial transport, and maintenance and regulation of cell volume. Consequently, the regulation of the electroneutral ion transport by these cotransporters is critical for proper physiological processes and survival. Most cation-chloride cotransporters respond to perturbations in extracellular osmolality and participate in regulatory volume increase (RVI) following a hypertonic shock and regulatory volume decrease (RVD) following a hypotonic shock (Hoffmann & Dunham, 1995; Hoffmann et al., 2009; Adragna & Lauf, 2007; Kregenow, 1971a, b; Kregenow, 1981) (Figure 1-3). Phosphorylation and dephosphorylation are the key mechanisms by which acute modulation of the CCC activity occurs, whereas long-term modulation of their activity is mediated by gene transcription, protein trafficking and degradation (Table 1-1).

In many cells, a decrease in intracellular $[Cl^-]_i$, or a decrease in cell volume (shrinkage) triggers the activation of a series of kinases leading to cotransporter phosphorylation. The kinases are with no K (lysine) (WNK), STE20 (sterile 20)/SPS1-related proline/ alanine-rich kinase (SPAK), and oxidative stress-responsive kinase-1 (OSR1) (Piechotta et al., 2002; Piechotta et al., 2003; Gagnon et al., 2006; Piala et al., 2014). The activation of the WNK-SPAK/OSR signaling cascade stimulates the Na-K-2Cl cotransporters and inhibits the K-Cl cotransporters (Figure 1-3). In Cl^-sec-

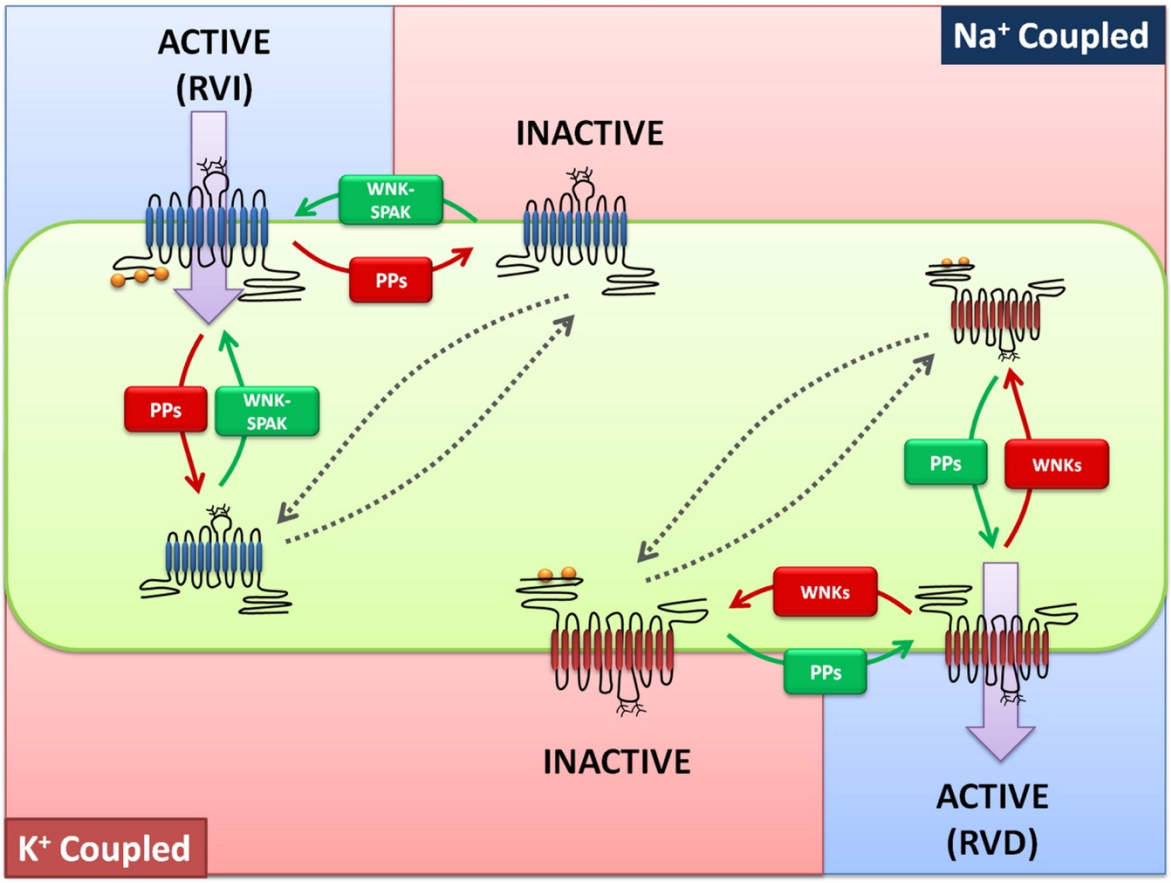

Figure 1-3. Schematic of functional regulation of the chloride coupled transporters leading to Na^+ coupled regulatory volume increase (RVI) and K^+ coupled regulatory volume decrease (RVD). Figure adapted from Arroyo et al., 2013, illustrating extracellular hypotonicity, cell swelling, and dephosphorylation by phosphatases (PPs), activating the K^+ coupled and Na^+ independent KCCs, leads to RVD. Conversely, extracellular hypertonicity, cell shrinkage, and phosphorylation by WNK-SPAK/OSR kinases, activates Na^+ coupled NKCCs, leads to RVI.

reting epithelial cells, like intestinal enterocytes for instance, the activation of Cl^- exit by Cl^- channels (e.g. the cystic fibrosis transmembrane conductance regulator, CFTR) at the apical membrane leads to a decrease in intracellular Cl^- which stimulates the basolateral Na-K-2Cl cotransporter and the replenishment of the anion (Matthews et al., 1998). Thus, sustained trans-epithelial Cl^- secretion requires the combined activities of apical channels and basolateral cotransporters. Similarly, in the distal convoluted tubule, a decrease in intracellular Cl^- stimulates the kinase cascades and the Na-Cl cotransporter, leading to increased Na^+ reabsorption (Gamba, 2009). Upon cell shrinkage, also depending upon the level of intracellular Cl^-, NKCC1 activity is increased, leading to the uptake of ions and obligatory water and RVI, helping the cells recover their volume (Figure 1-3).

Conversely, when cells swell, protein phosphatase-1 (PP1) is activated leading to K-Cl cotransporter dephosphorylation and activation, leading to increased KCC activity, loss of Cl^-, and regulatory volume decrease (Figure 1-3) (Jennings & Schulz, 1991; Kaji & Tsukitani, 1991; Krarup & Dunham, 1996; Krarup et al., 1998). Transporter phosphorylation occurs at very specific threonine or serine residues (Table1-1). Depending on the type of tissue and cell type, different cation-chloride cotransporters are involved in the maintenance and regulation of cell volume. Hence, the SLC12 family are important plasmalemmal facilitators of RVI and RVD. Interestingly, PP1 was the first protein identified as a regulator of CCC function (Jennings & Schulz, 1991; Kaji & Tsukitani, 1991; Krarup et al., 1998; Krarup & Dunham, 1996). The identification of the kinases (WNK-SPAK/OSR1) was not done until the early 2000s by our group (Piechotta et al., 2002; Piechotta et al., 2003). The identification of SPAK and OSR1 as interactors of the cation-chloride

cotransporters was made by yeast two-hybrid screens. First, SPAK was identified as an interactor of the N-terminus of KCC3, then NKCC1 and other transporters (Piechotta et al., 2002). Second, WNK kinases were identified as SPAK interactors through a screen that utilized the regulatory domain of SPAK as the bait (Piechotta et al., 2003). A year later (2004), the lab functionally demonstrated that WNK4 kinase activated SPAK, which in turn activated the cotransporter. It took 2 years for this study to be accepted for publication (Gagnon et al, 2006), as the model of successive activation that we proposed was against the prevalent idea at the time that WNK kinases were inhibitory to cotransporter function (Wilson et al., 2003). The original functional work was then confirmed by two biochemical studies (Morigushi et al., 2005; Vitari et al., 2005) and later functional studies (Kahle et al., 2005).

SPAK had been previously cloned and characterized from rat brain by Ushiro (Ushiro et al., 1998) and mouse by Johnston (Johnston et al., 2000). Immunohistochemical analyses found SPAK to be expressed abundantly in brain and epithelial tissue, coincidentally where most transporters are functionally expressed (Ushiro et al., 1998). In addition to identifying that WNK is a binding substrate of SPAK and OSR1, Piechotta et al., discovered the binding of SPAK with KCC3, NKCC1, and NKCC2, the transporters that are functionally expressed in abundance in brain and transport epithelial tissue (Kaplan et al., 1996; Dharmsathaphorn et al., 1985; Pearson et al., 2001). To confirm interaction of SPAK with the transporters, Piechotta et al., demonstrated with immunohistochemistry the expression (co-localization) of SPAK with NKCC1 along the apical membrane of the choroid plexus (Piechotta et al., 2003). In contrast, in the absence of the cotransporter (NKCC1 knockout mouse), SPAK expression was confined to the cytoplasm of the

same choroid plexus epithelial cells. In addition, when NKCC1 was found on the basolateral membrane (i.e. in salivary gland), the kinase was also found located on the basolateral membrane.

The molecular identity of the WNK kinases was identified in the early 2000s (Xu et al., 2000; Veríssimo & Jordan, 2001). Simultaneously, it was shown that mutations in human WNK1 leads to a blood pressure disorder, called Gordon syndrome, by affecting the activity of the thiazide-sensitive Na-Cl cotransporter (Wilson et al., 2001). Mutations in WNK4 are also responsible for Gordon syndrome cases (Wilson et al., 2003).

Pharmacology

One classification method of distinguishing the transporters from one another is based on their sensitivity to pharmacological inhibitors and loop diuretics: thiazide, furosemide, and bumetanide. Loop diuretics (furosemide and bumetanide) are named based on their mechanism of action at the loop of Henle in the kidney, where they function to reduce excess bodily fluid (edema) by increasing urine output. Thiazides can also be used to treat hypertension and congestive heart failure (Andreasen & Mikkelsen, 1977; Materson, 1983). Thiazides inhibit the distal convoluted tubule Na-Cl cotransporter, whereas furosemide and bumetanide inhibit the thick ascending loop of Henle Na-K-2Cl cotransporter 2 or NKCC2 (Forbush & Palfrey, 1983; Gamba et al., 1993; Payne et al., 1996). Kunau and coworkers were the first to demonstrate inhibition of renal Cl^- reabsorption by thiazides (Kunau et al., 1975). NCC is inhibited by the

thiazide diuretics with IC_{50} of about $4x10^{-7}$ M in mouse, $3x10^{-7}$ in rat, and $7x10^{-6}$ in winter flounder (Vázquez et al., 2002; Sabath et al., 2004; Monroy et al., 2000).

Loop diuretics also inhibit K-Cl cotransporters, but with a much lower affinity than the Na-K-2Cl cotransporters (Lauf, 1984). There are also slight differences in bumetanide pharmacokinetics and ion affinities between NKCC1 and NKCC2 (Isenring et al., 1998). For instance, NKCC2 has several fold greater sensitivity to bumetanide, than NKCC1 where the NKCC1 K_m for bumetanide is 0.28 µM, and NKCC2 bumetanide K_m is 0.08 µM. The ion affinity of Cl^- is similar between NKCC1 and NKCC2, however NKCC2 has a higher affinity to Na^+, and NKCC1 has a larger affinity towards Rb^+/K^+. In addition, NKCC2 is more sensitive to changes in intracellular Cl^- levels and responds therein more acutely. Differences in pharmacokinetics can be attributed to differences in expression patterns of NKCC1 and NKCC2 and to the fact that the diuretics are mostly bound to albumin in the circulation and difficult to reach peripheral tissues, while the diuretic can be concentrated in the urine and free to act as the protein content of the urine should be low.

In contrast to NKCCs, K-Cl cotransporters have much lower affinity for loop diuretics, and some differences between isoforms also exist. KCC4, for instance is much less sensitive to furosemide inhibition than KCC1, as the half-maximum inhibition values $K_{(0.5)}$ for KCC4 and KCC1 were measured to be 900 µM and 180 µM, respectively. The IC_{50} of furosemide and bumetanide for rat KCC2 were determined to 6×10^4M (Delpire et al., 1999). On the other hand, KCC3 $K_{(0.5)}$ were measured at ~200 µM and ~35 µM for KCC3a and KCC3b, respectively (Tanis et al., 2009;

Mercado et al., 2005). In an effort to generate better inhibitors of KCC2, our group undertook a screen of 300,000 compounds and identified novel inhibitory compounds that were several order of magnitudes more potent than the loop diuretics. The original screen identified ML077 with an affinity of 560 nM for KCC2 (Delpire et al., 1999). Additional chemistry around the ML077 scaffold identified an inhibitor with an EC50 of 60 nM (Delpire et al., 2012).

Epithelial ion transport

The Na-Cl, K-Cl, and Na-K-2Cl cotransporters play important roles in transepithelial transport. Expression of NCC and NKCC2 at the apical membrane of epithelial cells is important for salt reabsorption in the kidney. In contrast, expression of NKCC1 at the basolateral membrane of epithelial cells is important for salt secretion. Expression of KCC3 and KCC4 in the inner ear is important for transepithelial movement of K^+ and auditory perception, as the loss of either KCC3 or KCC4 results in deafness (Boettger et al., 2003; Boettger et al., 2002). KCC1 is also thought to be involved in transepithelial ion movement, salt reabsorption, and glucose reabsorption in the kidney, where it is expressed along with a splice variant of KCC3, and KCC4 (Liapis et al., 1998; Melo et al., 2013). KCC2 is the only cotransporter that is not affiliated with epithelial transport, as its expression is restricted to central neurons.

Regulation of Cl^- in the central nervous system

In the mammalian nervous system, the primary permeant anion is Cl^-. Tight regulation of its movement in and out of cells is critical for a variety of neurophysiological processes (Kahle & Staley 2012). Intracellular Cl^- levels in neurons must be fine-tuned to ensure proper electrical

output responses to the amino acid neurotransmitters: γ-aminobutyric acid (GABA) and glycine. GABA is the primary inhibitory neurotransmitter in the adult brain, gating electrical activity and serving as a balance against glutamatergic excitatory inputs. In neurons, GABA binds ligand-gated $GABA_A$ receptors ($GABA_AR$), triggering conformational changes that facilitate the passive influx or efflux of Cl^- depending on the reversal equilibrium potential for Cl^- (E_{Cl}). The $[Cl^-]_i$ serves as an indicator of how a cell will respond to GABA: when $[Cl^-]_i$ is low, such that E_{Cl} is negative relative to the neuron membrane potential (Vm), activation of $GABA_AR$ causes an influx of Cl^- and hyperpolarization of the neuron, but when $[Cl^-]_i$ is high, and E_{Cl} is positive compared to Vm, activation of $GABA_AR$ results in an efflux of Cl^- and depolarization of the neuron.

Stage of development is a key determinant of the $[Cl^-]_i$ of a neuron in the central nervous system. During the postnatal period, as the brain matures in rodents, there is a developmental switch that causes GABA to shift from being excitatory to inhibitory, (Rivera et al., 1999; Ganguly et al., 2001). Mature neurons in the central nervous system (CNS) maintain a low $[Cl^-]_i$. This results in E_{Cl} being close to the neuron's resting Vm and for GABA to elicit a hyperpolarizing effect on the membrane potential of the neuron. The low levels of intracellular Cl^- in the mature CNS is primarily the result of higher expression levels of KCC2, which is only expressed in neurons in the CNS (Lu et al., 1997; Stein et al., 2004), and low levels of NKCC1 (Plotkin et al., 1997; Wang & Kriegstein, 2011). During embryonic development and the perinatal period, KCC2 expression is low in the brain; while NKCC1 levels are high, facilitating GABA depolarizing and excitatory responses. As a result of this expression pattern, immature CNS neurons have a high $[Cl^-]_i$ (20-40 mM higher than mature neurons), with the electrochemical driving force of Cl^- out of the cell

leading to a depolarizing Cl^- equilibrium potential (Sung et al., 2000; Ben-Ari et al., 1989). The evolutionary advantage of the switch in NKCC1 expression remains an unanswered question in the field. Still, even minute changes in the $[Cl^-]_i$ of a neuron can drastically alter synaptic strength as well as the polarity of GABAergic neurotransmission.

Intracellular levels of Cl^- is also an important factor for cell volume, as is setting the direction of $GABA_AR$-mediated currents, since water flows in the same direction as the flux of ions (Kahle & Staley 2012). Neurons, glia, and other cells in the brain utilize $[Cl^-]_i$ as a tool to defend against cell volume perturbations such as fluctuations in extracellular osmolality or intracellular solute or ion content that can compromise their structural integrity. Chloride homeostasis in neurons is thus a balance between cell volume regulation and GABAergic signaling; imbalance of this homeostasis has been linked to human diseases where the robust activity of NKCC1 is thought to contribute to neonatal seizures (Gamba, 2005). NKCC1 is also highly expressed in the mammalian choroid plexus, a specialized epithelium that plays an important role in the production and regulation of CSF. The choroid plexus is composed of a single layer of epithelial cells that forms a tight barrier resulting from the tight junction of complexes between the cells, effectively separating the cerebrospinal fluid (CSF) from the blood (Kim & Jung, 2012). The choroid plexus thus restricts the passage of molecules and ions into the CSF. Additionally, the choroid plexus lines the ventricles of the brain, and by doing so supplies neurons and glia with essential nutrients from the periphery, removes toxins from the CNS, and facilitates communication between the neuroendocrine system and the brain (Wu et al., 2012). In contrast to NKCC1 expression on the basolateral membrane of secretory epithelia, NKCC1 is expressed on

the apical membrane of the choroid plexus where it somehow participates in the production of the cerebrospinal fluid (Plotkin et al., 1997; Karimy et al., 2016). There is still controversy as to which direction the ions flow through the cotransporter: from inside the epithelial cell to the CSF or from CSF to epithelial cell (Koumangoye et al., 2019; Wu et al., 2012; Steffensen, 2018; Gregoriades et al., 2019).

Regulation of Cl^- in the peripheral nervous system

In addition to regulating Cl^- in developing CNS neurons and choroid plexus, cation-chloride cotransporters play key roles in maintaining Cl^- homeostasis in the peripheral nervous system (PNS). For example, NKCC1 is implicated in mammalian cochlear and vestibular function: SLC12A2 knockout mice are deaf and display head bobbing and circling behavior known as "shaker/waltzer" behavior (Abbas & Whitfield, 2009; Delpire et al., 1999). These phenotypes are associated with pathologies in the chambers of the inner ear. The inner ear contains a specialized extracellular fluid known as the endolymph, which bathes the sensory organs of the inner ear. The endolymph contains high K^+ and low Na^+ levels, an atypical ion composition for an extracellular space that instead more closely resembles that of the intracellular milieu. The endolymph is generated by marginal cells of the stria vascularis in the cochlea, as well as by dark cells in the vestibular system (Zdebik et al., 2009).

Endolymph volume is largely regulated by secretion of K^+ ions. Mutations in the genes encoding for proteins that regulate K^+ endolymphatic homeostasis results in a loss of endocochlear potential, a reduction in endolymphatic volume, and sensorineural deafness due

to hair cell degeneration (Abbas & Whitfield, 2009). NKCC1 is a key contributor to K^+ secretion in the endolymph. NKCC1 is expressed on the basolateral membrane of marginal cells (Zdebik et al., 2009) and transports K^+ ions into the marginal cells from the intrastriatal fluid, which is then channeled out from the cell into the endolymph by K^+ channels. Mice with complete loss of NKCC1 function demonstrate reduced endolymph volume and degeneration of hair cells (Delpire et al., 1999; Abbas & Whitfield, 2009). Interestingly, over-administration of loop diuretics in pediatric subjects can lead to reversible hearing loss (Bourke, 1976; Vargish et al., 1970). This ototoxicity is the result of decreased K^+ secretion and loss of the endolymphatic potential (Marcus et al., 1987).

NKCC1 and its regulation of intracellular Cl^- are also important for sensory afferent signaling in the PNS. Unlike the CNS where NKCC1 undergoes a developmental downregulation from immature neurons to mature neurons, high NKCC1 expression persists in sensory afferent neurons throughout development and adulthood (Alvarez-Leefmans et al., 1988; Sung et al., 2000). This is the case for cranial ganglia such as the vestibular and spiral ganglia, as well as for dorsal root ganglia (DRG) (Mao et al., 2012). DRGs contain the cell soma of primary afferent sensory neurons, which modulate, gate, and transduce sensory information from the periphery to the spinal cord (Kishi et al., 2002). Several classifications of DRG neurons exist, and they are characterized by the size of their cell bodies and function. Type A DRG neurons are large and are coupled to touch, vibration, and proprioception (Krames, 2014), whereas type B neurons are smaller than their type A counterparts. Although smaller, type B neurons exceed the number of

type A neurons with a ratio of 71:29 and are associated with the sensation of pain or nociception (Sharpee, 2014).

Not only do DRG cell bodies function as metabolic stores for peripheral processes, but studies have shown that they are also heavily involved in signaling. DRG cells identify specific sensory stimuli and respond by producing neurotransmitters in order to modulate the signaling processes (Devor, 1999). Humans have 31 pairs of spinal nerves carrying autonomic and sensorimotor information located between the spinal cord and the periphery (Gelderd & Chopin 1977). The spinal nerves are composed of dorsal afferent sensory axons that become dorsal roots, as well as ventral efferent motor axons that become ventral roots. The spinal nerves emerge from the intervertebral neural foramina located between adjacent vertebrae and between the superior and inferior pedicles. The dorsal sensory root fibers travel laterally to connect their processes at a T-junction with their cell bodies, making up the DRG. Anatomically, the primary sensory nerve arises from the distal axons of the dorsal sensory root. The neuron's peripheral receptive field is the start of the primary sensory neuron (Aldskogius et al., 1986). The receptive field is the region in which a stimulus, such as touch, injury, or inflammation, initiates neuronal firing, and ends at the CNS. The primary afferent neurons (PANs) are the largest neurons in the human body, reaching up to 1.5 m in length (Hogan, 2010).

As stated previously, NKCC1 expression is high in PANs in DRG to maintain a high $[Cl^-]_i$ (Sung et al., 2000; Mao et al., 2012; Rocha-González et al., 2008). This makes it possible for PANs to be consistently depolarized by GABA throughout adulthood (Desarmenien et al., 1984). GABAergic depolarization in PANs is mediated by Cl^- efflux facilitated by $GABA_AR$ channels: the

electrochemical driving force of Cl^- is outward because E_{Cl} is positive compared to Vm (Gallagher et al., 1978). The outward Cl^- gradient is maintained throughout the entire cell surface of the PAN, including the cell soma in the DRGs, the central processes, as well as the peripheral processes (Alvarez-Leefmans et al., 1988). The exact mechanism of the excitatory depolarizing effect of GABAARs remains unknown, as is why excitatory depolarization does not lead to shunting inhibition as seen in mature neurons of the CNS. However, the extent of our current knowledge on the depolarization effect of GABA is that an increase in NKCC1 activity results in an increase in $[Cl^-]_i$, thereby increasing $GABA_A$-mediated depolarization above action potential threshold (Figure 1-4).

It is also thought that voltage-gated Ca^{2+} channel activation can lead to GABAergic depolarization by depolarizing the membrane enough to reach action potential threshold, resulting in a depolarization amplification effect (Aptel et al., 2007). Although Cl^--mediated GABA depolarization is the main depolarization mechanism in sensory afferents, a subset of DRG neurons involved in nociception depolarize via the Ca^{2+}-dependent depolarization mechanism. Data demonstrate that NKCC1 mRNAs and protein are expressed in virtually all types of DRG neurons (Mao et al., 2012). In addition to confirming that NKCC1 is the key player in maintaining $[Cl^-]_i$ above equilibrium, studies have revealed that there is a downward "drift" in $[Cl^-]_i$, at various postnatal ages in single DRG neurons, although $[Cl^-]_i$, remains higher than E_{Cl} (Alvarez-Leefmans et al., 1988). However, a rapid transition in $[Cl^-]_i$ does not occur as observed in neurons of CNS. In fact, KCC2 transcripts and protein are absent in DRG neurons, suggesting that Cl^- homeostasis cannot be attributed to KCC2. These findings suggest that Cl^- influx is unopposed by KCC2- media-

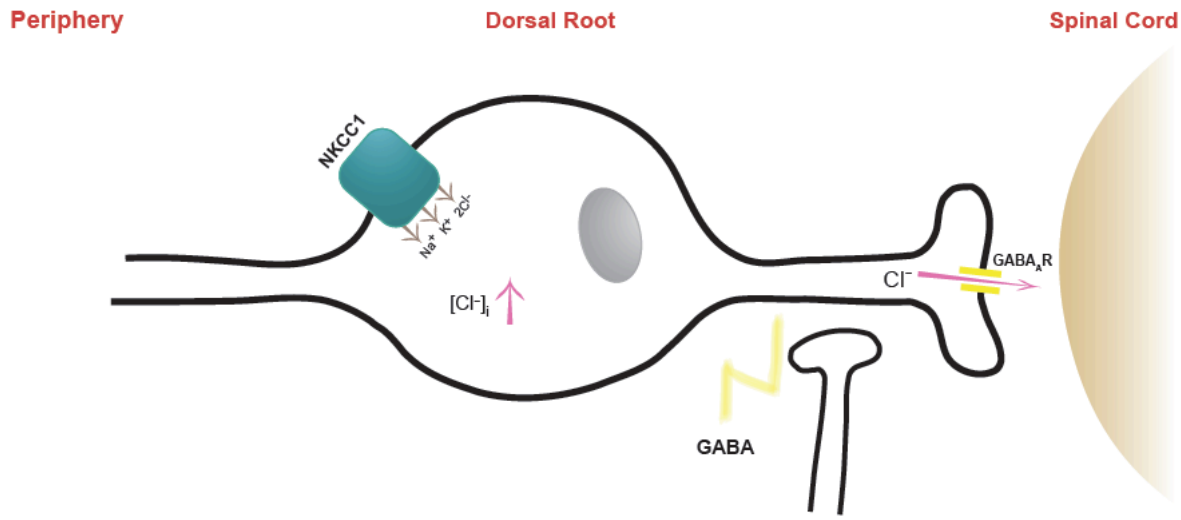

Figure 1-4. Depolarization effect of GABA in sensory afferents. High expression of NKCC1 in dorsal root ganglia maintains a high $[Cl^-]_i$. The electrochemical driving force for Cl^- causes $GABA_AR$ mediated Cl^- efflux, leading to membrane depolarization.

ted outward Cl^- transport and support the Cl^--mediated GABAergic depolarization model underlying PAD in the spinal cord. Nevertheless, the Cl^- gradient in PANs plays a significant role at the peripheral endings by contributing to the rapid excitation of nociceptors by chemical mediators of pain that are released at the time of tissue damage (Alvarez-Leefmans & Delpire, 2009). Similarly, at the central terminals, the Cl^- gradient eventually gives rise to GABA-mediated PAD by spinal interneurons. PAD underlies presynaptic inhibition, a pervasive mechanism that is crucial in the gating and modulation of somatosensory information (Rudomin & Schmidt, 1999). Particularly, PAD decreases the relative intensity of incoming action potentials resulting in reduced PAN neurotransmitter release. $GABA_AR$ antagonists reduce the effect of PAD suggesting that PAD is mediated by spinal interneuron GABA release (Witschi et al., 2011). Supporting this hypothesis are data from behavioral tests conducted on NKCC1 knockout mice measuring pain. NKCC1 knockout mice exhibited a reduced response to noxious heat and touch-evoked pain (Sung et al., 2000; Laird et al., 2004). To further confirm the association of NKCC1 and the pain pathway, mice were treated with the NKCC1 specific inhibitor bumetanide via intrathecal delivery (Granados-Soto et al., 2005). Bumetanide was found to inhibit nocifensive behavior in formalin tests. Furthermore, intracolonic capsaicin injections in mice stimulated a rapid and transient increase in spinal phosphorylated NKCC1, which is the activated state of the transporter, and persistent trafficking of NKCC1 to the cell surface (Galan & Cervero 2005). In enhanced pain states, the enhancements of PAD might be necessary for inducing direct activation of spinal nociceptors instead of inhibiting incoming action potentials, a phenomenon known as dorsal root reflexes (Willis, 1999). Taken together, these findings indicate that NKCC1 might be a fundamental regulator of inflammatory and tissue damage in the sensory afferent pain pathway.

KCC3

Chapter 2 is based on characterizing a human mutation in Protein Kinase D1 (PKD1) associated with human epilepsy and peripheral nerve hypermyelination, which causes KCC3 cotransporter activation. To appreciate the potential effect of this mutation on KCC3, it is important to understand the functional relevance of KCC3 at a cell and molecular level, as well as the association of KCC3 with disease. KCC3 was identified and cloned by 3 independent groups in 1999 (Mount et al., 1999; Hiki et al., 1999; Race et al., 1999) and shares 75% homology with KCC1, 67% homology with KCC2, and 65 % homology with KCC4. Similar to the CCCs, KCC3 consists of 12 transmembrane domains, flanked by large intracellular -NH2 and -COOH domains, and a large extracellular loop between domains 5 and 6 (unique to the KCCs). Although KCC3 is well characterized, the quaternary protein structure of KCC3 has not yet been solved. KCC3 is encoded by the *SLC12A6* gene, and has been identified to have several N-terminally spliced variants (Pearson et al., 2001; Shekarabi et al., 2011a; Mercado et al., 2005) with two main isoforms: KCC3a, primarily expressed in the nervous system, and KCC3b, mainly expressed in the kidney. KCC3 is widely expressed in various tissue, such as brain, heart, muscle, kidney, placenta and red blood cells (Hiki et al., 1999; Mount et al., 1999; Race et al., 1999). Like all of the CCC family of transporters, KCC3 is subject to regulation by extracellular conditions and phosphorylation. Extracellular hypotonicity triggering cell swelling, high $[Cl^-]_i$, and protein phosphatases (PPs) involved in cotransporter dephosphorylation at sites Thr991 and Thr1048 activates KCC3 (Table 1-1), thereby decreasing $[Cl^-]_i$, and resulting in regulatory volume decrease (RVD) of the cell. KCC3 is subsequently inactivated by phosphorylation via WNK/SPAK and OSR at

active sites Thr991 and Thr1048. KCC3 was recently identified as an interacting partner of PKD1 in a functional kinomic screen (Zhang et al., 2016). In this screen, a decrease in PKD1 resulted in increased P-KCC3 levels at its important phosphoregulatory sites Thr991 and Thr1048, consistent with the inhibitor effect of kinases on K-Cl cotransport.

KCC3 is expressed in the peripheral and central nervous system. During development, expression of KCC3 is low at birth and in immature central neurons, subsequently increasing during postnatal development resulting in high expression in mature neurons (Pearson et al., 2001). In the peripheral nervous system, KCC3 is expressed at relatively low amounts, particularly in dorsal root ganglia (DRG) neurons, sciatic nerves, and parvalbumin positive (PV+) sensory interneurons (Pearson et al., 2001; Ding & Delpire 2014). KCC3 is detected at high levels in the central nervous system, specifically in the brain and spinal cord. Tissue and cellular localization of KCC3 is predominantly found in the choroid plexus, amygdala, and interneurons of the hypothalamus (Pearson et al., 2001; Byun & Delpire 2007b; Shekarabi et al., 2011b). More importantly KCC3 is known to be confined to the myelinated tracts of neurons, where disrupting KCC3 in mice results in abrogation of nerve signal propagation, denoting KCC3's important role in saltatory conduction (Sun et al., 2010). Saltatory conduction of an action potential is the speed at which an action potential is propagated through a nerve axon (Nave & Werner 2014). This mechanism is regulated by the movement of ions by ion channels at the nodes of Ranvier, so it is not surprising that affecting the transport of ions via KCC3 interferes with saltatory conduction.

KCC3 has been mapped to human chromosome 15q14 (Howard et al., 2002; Casaubon et al., 1996) and disruption of KCC3 in humans, results in a disorder, called ACCPN. ACCPN or

HSMN/ACC is an inherited genetic disorder due to a mutation in *SLC12A6* resulting in loss of KCC3 function. The disorder is prevalent in Quebec, Canada but also found sporadically in families throughout the world. Individuals with this disorder have different degrees of agenesis of the corpus callosum, but all suffer from severe sensorimotor neuropathy. The inherited Quebec mutation is 2436delG (Thr813fsX813) and individuals need to be homozygous to be diseased. As heterozygous individuals are asymptomatic, they are carriers and in some regions of Quebec, the frequency of diseased individuals is 1 in 2000; whereas the frequency of carriers is as high as 1 in 20 people. The pathogenesis of the disease includes progressive motor and sensory neuropathies (Auer et al., 2016) with delays in motor and sensory function, mental disabilities, generalized hypotonia, and areflexia, resulting in the loss of the ability to walk and being confined to a wheelchair in most individuals.

Severity of the agenesis of the corpus callosum can range between individuals: from complete loss of corpus callosum to partial or no loss at all. Damage to myelin or axons can result in several forms of neuropathies, so it is not unusual that a post-mortem study (Auer et al., 2016) revealed that individuals with ACCPN have a larger brain mass compared to matched control individuals, and exhibit axonopathies and tumor-like axon overgrowth. Since KCC3 participates in cell volume regulation and RVD in the nervous system, one can conclude that aberrant KCC3 function affects the homeostatic osmotic set point of peripheral and central nerves resulting in cell swelling in ACCPN individuals.

Interestingly, a *de novo* KCC3 gain of function (GOF) mutation was identified and characterized by our group, in an individual with a rare form of peripheral neuropathy (Kahle et al., 2016), with neither parent displaying peripheral neuropathy nor carrying mutations in KCC3. The missense mutation resulted in Thr991 to Ala substitution, Thr991 being one of the two main phospho-regulatory sites of the protein. The mutation leads to a constitutively active cotransporter. The other phospho-regulatory site Thr1048, was intact in the patient, and did not appear to compensate for the missense mutation at position 991. Unlike individuals with ACCPN, this patient did not exhibit any cognitive abnormalities, and only displayed a severe motor neuropathy. The motor component was more severe than the sensory component in the neuropathy.

To understand the role of this mutation in KCC3 *in vivo*, and physiology, our group generated the first GOF KCC3 mouse model via CRISP/Cas9, expressing the same T991A mutation in the patient (Kahle et al., 2016). In this study, Bianca Flores in the laboratory assessed locomotor behavior in heterozygous and homozygous T991A mice via the accelerated rotarod and balance beam assays. Homozygous T991A performed significantly worse than WT and heterozygous mice in both the accelerated rotarod and balance beam assays, indicating poor coordination and balance, respectively. To assess the physiological implications of a GOF mutation in KCC3 on peripheral nerves on T991A mice, she also carried out nerve conduction experiments to characterize motor amplitude in latencies. This method of analyzing the efficiency of nerve conduction, teases apart whether the damage to nerves is axonal (by affecting the amplitude of signal) or due to myelin (by affecting its latency). This analysis helps with diagnosing the type of

neuropathy patients have. It was also established that the latency was increased, and the peak amplitude was decreased in both heterozygous and homozygous mice, indicating that the peripheral nerves are undergoing both demyelination and axonopathy. This is also illustrated in EM images that were taken on sciatic nerves of T991A mice through damage to myelin as well as changes in axonal diameters. These studies were in line with the patient's phenotype, highlighting the detriment a point mutation at a regulatory site in KCC3 can make in peripheral neve pathology, nerve conduction, and motor coordination.

In addition to the degeneration in nerves that occurs due to an abnormally functioning KCC3, it is important to note the osmotic imbalance that resulted from an over-active KCC3. In 2002, the lab demonstrated that loss of KCC3 function resulted in axonal swelling (Byun & Delpire 2007a). In the case of the KCC3 GOF mice, axonal shrinkage was demonstrated (Flores et al., 2018), clearly establishing that KCC3 is involved in the maintenance and regulation of nerve fiber volume. The importance of KCC3 on nerve integrity and excitability, gave rise to the central hypothesis of Chapter 2: *PKD1 is involved in maintaining nerve integrity and excitability through KCC3.* Aside from peripheral neuropathy, KCC3 LOF mutations also result in deficits in the central nervous system. Many HSMN/ACC patients present some degree of agenesis of the corpus callosum. Abnormal swelling and vacuolization is also observed in the brain. KCC3 knockout mice also have lower seizure thresholds as shown by field potential recordings in freely moving WT and $KCC3^{-/-}$ (Boettger et al., 2003).

NKCC1

The body of work outlined in Chapter 3 is based on a single human case: a *de novo* mutation in the gene encoding NKCC1. This study addresses the cellular consequences of expressing the mutant NKCC1, shedding light into the metabolic complications experienced by the patient. Participation of NKCC1 in cell metabolism has never been reported, and Chapter 3 explores how a mutation in NKCC1 can result in metabolic deficits. The Na-K-2Cl cotransporter 1, NKCC1 (formerly known as BSC2) is encoded by the *SLC12A2* gene and is located in human chromosome 5q23.3, and similar to NKCC2 transports Na^+, K^+, and Cl^- in a 1:1:2 stoichiometry (Delpire et al., 1994a). NKCC1 has a molecular weight of 130 kDa, and is ubiquitously expressed and sensitive to the loop-diuretic, bumetanide. Like all CCCs, NKCC1 is regulated by the WNK-SPAK/OSR kinases, at residues Thr184, Thr189, and Ser202 (Delpire & Austin 2010) (Table 1-1). The structure of the zebrafish NKCC1 has recently been solved by cryo-EM. In this study, ion binding domains for Na^+, K^+, and Cl^- have been identified, where there are two binding residues for Cl^-. The Na^+, K^+ and Cl^- binding sites in TM1 and TM6 are strategically in close proximity suggesting cooperative binding. The ion binding sites form between the scaffold domain and the core. This study also revealed that the C-terminal domain of one transporter interacts with a transmembrane domain of another transporter, forming the dimer interface (Chew et al., 2019). There are two alternatively spliced isoforms of NKCC1: NKCC1a and NKCC1b (Randall et al., 1997; Cutler & Cramb 2002). NKCC1b lacks exon 21, where it was previously thought exon 21 plays a role in trafficking to the basolateral membrane in polarized cells (Carmosino et al., 2008). NKCC1 is expressed on the basolateral membrane of secretory epithelia (lung, salivary gland, sweat gland, lacrimal gland, intestine), the apical membrane of the choroid plexus of the blood brain

barrier, and in sensory afferents of the peripheral nervous system. Several motifs are thought to play important roles in trafficking NKCC1 to the basolateral membrane. Work by Carmosino et al., showed a dileucine motif in exon 21 of NKCC1, that is not present in NKCC2, is responsible for being targeted to the basolateral membrane (Carmosino et al., 2008). Our group further demonstrated the existence and importance of another dileucine motif close to the carboxyl terminal end that seemingly regulates NKCC1 trafficking to the basolateral membrane in 3-D cultures of MDCK cells (Koumangoye et al., 2018). Therefore, several sites might contribute to the differential targeting of NKCC1 in polarized cells.

Mouse models of NKCC1

NKCC1's ubiquitous expression leads to the regulation of several physiological processes such as vascular smooth muscle cell contraction (VSMC), renal function, and indirect neuronal depolarization (Chipperfield & Harper, 2000; Soo et al., 2008; Dzhala et al., 2005). Delpire and coworkers were first to demonstrate the importance of NKCC1 function *in vivo*, by generating a NKCC1 knockout mouse model (Delpire et al, 1999). NKCC1 knockout mice exhibited severe phenotypes, including deafness due to deficits in K^+ and endolymph secretion in the inner ear; pain perception, which is not surprising given NKCC1's role in maintaining intracellular Cl^- in sensory afferents; impaired intestinal secretion; decrease in salivation due to impaired parotid gland; infertility as seen by absence of spermatocyte production; and low blood pressure possibly explained by the role of NKCC1 in smooth muscle cells in the vasculature (Delpire et al., 1999; Flagella et al., 1999; Sung et al., 2000; Laird et al., 2004; Pace et al., 2000). In epithelial cells lining the intestine, NKCC1 is expressed in the basolateral membrane, and plays a role in intestinal fluid

secretion. It is one of the major basolateral Cl^- entry pathway and Cl^- secretion through apical Cl^- channels is the main drive for intestinal water secretion. As previously stated, NKCC1 is highly expressed in the peripheral nervous system where it is important for maintaining intraneuronal Cl^- levels, necessary for the depolarizing act of the GABA (Sung et al., 2000). Other studies have demonstrated the effect of NKCC1 on sensory afferents in mice, where mice display prolonged response times to nociception and allodynia (Sung et al., 2000; Valencia-de Ita et al., 2006).

The importance of NKCC1 function, and the generation of a novel NKCC1 mouse model, is highlighted by the first human clinical case with a mutation in the NKCC1 gene. Until recently, NKCC1 has not been linked to any inherited or non-inherited forms of human disease, which could have been interpreted as either evidence for multiple redundancy pathways to a loss of NKCC1 function or to early embryonic lethality in humans. However, this changed when an 8 year old patient with multi-organ failure was admitted to the Undiagnosed Diseases Program (UDP) at the NIH (Delpire et al., 2016). The patient suffers from orthostatic intolerance, complete bladder and gastrointestinal shut down, and endocrine insufficiencies (Delpire et al., 2016). Labs conducted on the patient, identified an abnormal increase in glycogen content as well as mitochondrial DNA copy number in the patient muscle and liver cells. In addition to identifying what seemed to be a metabolic deficit, whole exome sequencing conducted on the patient genome revealed that she had several mutations in protein encoding genes, including a *de novo* mutation in *SLC12A2*, the gene encoding NKCC1. Due to the widespread expression of NKCC1 and its importance in many cellular functions, the NKCC1 mutation was given the highest investigative priority.

This case was presented to our laboratory to further investigate the impact of the specific NKCC1 mutation. We confirmed that the patient carries an 11 base pair deletion in the *SLC12A2* gene, leading to a frameshift and to the introduction of a stop codon resulting in premature termination of the COOH-terminal end of the protein. The mutant was termed DFX for the last "intact" residue, aspartic residue (D), followed by the introduced residue, phenylalanine (F), and finally the stop codon (X). Rubidium tracer flux assays in *Xenopus laevis* oocytes expressing the NKCC1-DFX mutation showed that the transporter was non-functional. Concomitantly, immunocytochemistry performed in HeLa cells transfected with mutant NKCC1-DFX and WT NKCC1 revealed that the cells transfected with mutated NKCC1 had a diffuse expression of GFP tagged NKCC1-DFX in the cytoplasm compared to the stronger expression at the plasma membranes in cells expressing WT tdTomato tagged NKCC1. Similarly, immunocytochemistry on MDCK cells expressing NKCC1-DFX revealed that NKCC1 was targeted to both the apical and basolateral membrane, a profound effect since NKCC1 is endogenously expressed at the basolateral membrane of epithelial cells for proper function (Koumangoye et al., 2018; Koumangoye et al., 2019). Western blot analysis uncovered an increase in dimerization between the wild-type and mutant transporter, indicating that the mutant protein might exert a dominant negative effect on the wild-type transporter. To understand the effect of NKCC1-DFX *in vivo*, the lab generated a mouse model of the NKCC1-DFX human mutation via CRISPR/Cas9. NKCC1 expression in secretory epithelia was assessed in salivary glands and intestine, and resulted in abnormal NKCC1 expression at the apical membrane. NKCC1-DFX mice also showed impaired water and goblet cell mucus secretion (Koumangoye et al., 2020). This phenotype supports the impairment of intestinal secretion observed in the NKCC1 KO mouse (Flagella et al., 1999). I have

utilized the NKCC1-DFX mouse to address the deficits in energy homeostasis in the patient. The relationship between NKCC1-DFX and cell metabolism will be addressed in chapter 3. Interestingly, the publication of this first clinical case resulted in several physicians and investigators reaching out to our group with several additional cases of patients carrying mutations in NKCC1. Current studies are ongoing to identifying the regions of the protein most likely to result in human disorders when mutated.

Dissertation Goals

It is quite apparent that the CCCs are vital for main physiological functions, especially in the kidney and nervous system. Although the expression of KCC3 in several tissue and its involvement in human disease has been established, its true function in the peripheral nervous system still remains a mystery. Similarly, the role of KCC3 in chloride regulation in the developed nervous system is well understudied, especially since NKCC1 is primarily responsible for the maintenance of intracellular Cl^-. In particular, mechanistic pathways of interacting partners of the CCCs are not well understood, and for the first time, project 1 of this dissertation uncovers a possibly novel interacting partner of KCC3, PKD1, which we have several reasons to believe leads to peripheral neuropathy and neuronal hyperexcitability. We now know that affecting regulation of the transporters, leads to several diseased states in humans, and here we report for the first time the disruption of KCC3 function by a heterozygous *de novo* mutation (E79X) in protein kinase D1 (PKD1) resulting in its inactivation. The nonsense mutation in PKD1 (PKD1-E79X) was first identified in an individual presented with peripheral neuropathy, abnormal gait, and seizures. A previous study identified a novel interaction between PKD1 and KCC3, where inactive PKD1

results in decreased P-KCC3 at positions Thr991 and Thr1048, suggesting the increase in KCC3 activity. This study, along with the association of KCC3 with peripheral neuropathy led to the central hypothesis that *PKD1 is involved in maintaining the integrity of peripheral and central nerves through KCC3.* We generated a mouse expressing the mutation PKD1-E77X to test the central hypothesis using the following aims, which is discussed in detail in Chapter II:

Project 1: Peripheral nerve deficits and seizures associated with defective protein kinase D1

- Specific Aim 1: Characterize PKD1 effect on activity and membrane expression of KCC3. *Hypothesis: Inactive PKD1 results in increased KCC3 activity in Xenopus oocytes injected with cRNA of WT and inactive PKD1 and WT KCC3*

- Specific Aim 2: Establish PKD1 effect on peripheral nerve integrity in PKD1-E77X mice. *Hypothesis: Inactive PKD1 results in nerve tomacula pathology and abnormal myelin thickness in peripheral nerves imaged with Electron Microscopy.*

- Specific Aim 3: Determine sensory/locomotor and CNS nerve behavior of PKD1-E77X mice. *Hypothesis: Inactive PKD1 leads to sensory/locomotor deficits, and seizures in mice in battery of neurobehavioral tasks and pharmacological seizure induction.*

The second project of my dissertation is a personal feat, as it was the first to identify a novel role for NKCC1 in energy homeostasis, described in further detail in Chapter III. This work began when an individual with multi-organ failure, and fatigue, was admitted to the undiagnosed diseases program (UDP) at the NIH (Delpire et al., 2016). Lab reports revealed abnormally high

mitochondrial DNA content and glycogen levels in the liver and muscle cells of the patient. Elevated levels of mitochondrial DNA in muscle cells is a hallmark and biomarker of metabolic disease, explaining the nature of the patient's fatigue. Whole-exome sequencing on the individual's genome identified multiple mutations, including a heterozygous *de novo* mutation in the gene encoding for NKCC1 (NKCC1-DFX). Due to the widespread expression of NKCC1 in tissue, and its physiological importance, it was given the highest priority of investigation. We generated a novel mouse model expressing the NKCC1-DFX mutation using CRISPR/Cas-9 where we characterized the effect of the mutation in epithelial tissue, and its consequential impairment of intestinal secretion (Koumangoye et al., 2019; Koumangoye et al., 2018). In addition, I led the investigation of determining the impact of NKCC1-DFX on metabolism, where the central hypothesis is *NKCC1 inactivation affects metabolic and energy homeostasis*, tested by the following aims:

Project 2: A mutation in the Na-K-2Cl cotransporter-1 leads to changes in cellular metabolism

- Specific Aim 1: Establish mitochondrial DNA content and characterize mitochondrial and glycolytic respiration in NKCC1-DFX human fibroblasts, epithelial cells, and NKCC1 $^{+/DFX}$ and NKCC1 $^{DFX/DFX}$ mice. *Hypothesis: NKCC1-DFX leads to elevated mitochondrial respiration and lower glycolysis in human fibroblasts expressing NKCC1-DFX, epithelial cells, and mouse fibroblasts expressing NKCC1-DFX*

- Specific Aim 2: Establish ER and oxidative stress in NKCC1-DFX mice. *Hypothesis: Fibroblasts isolated from NKCC1 $^{+/DFX}$ NKCC1 $^{DFX/DFX}$ elicit mitochondrial oxidative stress, in addition to ER stress.*

CHAPTER II

PERIPHERAL NERVE DEFICITS AND SEIZURES ASSOCIATED WITH DEFECTIVE PROTEIN KINASE D 1

Introduction

Peripheral neuropathy

As previously mentioned in Chapter I, genes affecting the CCCs result in damage to nerves in the PNS and CNS (Howard et al., 2002; Delpire 2007b; Kahle et al., 2016). Damage to nerves can be in the form of damage to myelin or axon of nerves leading to neuropathies (Pisciotta & Shy 2018; Barrell & Smith 2019). Damage affecting peripheral nerves leads to a disease termed peripheral neuropathy. There are different pathological forms of peripheral neuropathy, such as demyelinative neuropathy, hypertrophic “onion bulb” neuropathy, and axonal neuropathy (Katona & Weis 2018). Any type of peripheral neuropathy consequently affects signal conduction, which affects the function of many organs and lead to several disease states in humans (Uncini & Kuwabara 2015; Oh et al., 2015). Damage of myelin for instance highlights the importance of intact nerves on nerve function and physiology. Once a signal is received by the cell body of a neuron, myelin plays a critical role in its propagation throughout the axon via the nodes of Ranvier, through a process known as saltatory conduction (Akaishi, 2018; Waxman &Ritchie 1993; Rosenbluth, 2009; Ulzheimer et al., 2004). At the nodes of Ranvier, the part of the axon that is unmyelinated, ions are exchanged across the axon membrane, regenerating the axon potential between the regions of the axon that are myelinated. Therefore, the signal is propagated along the axon at high speeds, without compromising or degrading the signal.

Because the exchange of ions plays a vital role in saltatory conduction, it is expected that a LOF in KCC3, which is expressed in neurons, results in abnormal myelin pathologies, thus peripheral neuropathies and ACCPN in humans (Kahle et al., 2016). Since peripheral neuropathy can affect peripheral nerve function, nerve conduction studies on KCC3 KO and KCC3-T991A (LOF) mice displayed slower nerve conduction velocities, with poor performance on locomotor tasks (Byun & Delpire 2007b; Kahle et al., 2016).

Epilepsy

Abnormal neuronal function as a result of myelin damage, axonal atrophy, metabolic alterations, infections, pharmacology, traumatic brain injury, stroke, or brain tumor can result in permanent or transient alterations of the brain electrical activity (Chen et al., 2016; Imad et al., 2015; Zoons et al., 2008; Ferguson et al., 2010; You et al., 2011). For instance, a seizure is defined as a transient increase in electrical activity in the brain. The occurrence of multiple spontaneous seizures in individuals, is considered epilepsy (Stafstrom & Carmant, 2015). Epilepsy is thought to arise as a result of an imbalance between neuronal excitability and inhibition, leading to a hyperexcitable state, where seizures occur. Characterized by recurrent and unprovoked seizures, and depending on the type of seizure, epilepsy causes abnormal motor behavior, and/or loss of consciousness. According to the World Health Organization, epilepsy is the most common serious brain disorder worldwide, affecting ~50 million people worldwide (World Health Organization 2019). In the year 2015, epilepsy affected about 1.2 percent of the population – 3.4 million individuals in the United States (Zack & Kobau, 2017). Epilepsy is currently treated by antiepileptic drugs (AEDs), aiming to restore the imbalance of neuronal excitation and inhibition,

by altering neuronal inhibition or repressing excitation (Kaeberle, 2018). Although extensive medical research has contributed to developing novel AEDs for decades, about a third to 50 percent of patients continue to have seizures following the use of medication, also known as medication refractory epilepsy (Golyala & Kwan, 2017; Shorvon & Luciano, 2007; Kwan & Brodie, 2000). The absence of a truly affective AED highlights the gap in knowledge, of understanding mechanisms by which epileptogenesis occurs. Several studies have identified the CCCs as contributors to the hyperexcitability or inhibition of neurons via GABA (Dzhala et al., 2005; Deeb et al., 2011). NKCC1 is responsible for maintaining high E_{Cl} in immature neurons and sensory afferents, leading to the depolarizing affect in GABA. Whereas KCC2 is important for maintaining low E_{Cl} in mature neurons in the brain and spinal cord, contributing to the hyperpolarizing GABAergic currents. Further, genetic variants resulting in LOF mutations in KCC2 have been identified in epileptic individuals (Kahle et al., 2014; Puskarjov et al., 2014; Huberfeld et al., 2007). Preclinical studies in rodents that were genetically engineered to have KCC2 or KCC3 LOF mutation, also displayed reduced Cl^- efflux, decreased neuronal excitability, and epileptic seizures (Hübner et al., 2001a; Boettger et al., 2003; Tanis et al., 2009). Interestingly, in both cases of epilepsy associated with KCC2 and KCC3, K-Cl cotransport is diminished/reduced.

There are many neurological disorders that have some overlap between peripheral nerve disease and brain hyperexcitability. For instance, Charcot-Marie-Tooth disease (CMT) and Multiple Sclerosis (MS) are prime examples of chronic neurological diseases that are primarily caused by damage to the myelin sheath of a neuron and/or nerve axon, abnormal myelination in the central nervous system (CNS) and peripheral nervous system (PNS). CMT is classified as a rare

hereditary peripheral neuropathy, affecting ~1 in 2500 people in the United States. Peripheral neuropathies are categorized into acquired neuropathies, hereditary neuropathies, and idiopathic neuropathies. Damage to myelin, demyelinative neuropathy, hypertrophic "onion-bulb" neuropathy, axonal neuropathy, and hypermyelination are all forms of peripheral neuropathy. Peripheral neuropathy can be heterogenous depending on the gene mutation. For example, there are many forms of CMT depending on the type of gene that is affected. CMT1 is caused by abnormalities in the myelin sheath, and has several types. CMT1A for instance, is a result of a duplication event within chromosome 17 that contains the peripheral myelin protein-22 (PMP22) gene (Thomas et al., 1997). PMP22 is an essential component of peripheral nerve myelin. The outcome of the duplication is an overexpression of the PMP22 gene resulting in hypermyelination and abnormal peripheral nerve function. Patients with this disease variant experience muscle weakness and sensory loss. Whereas patients with hereditary neuropathy with predisposition to pressure palsy (HNPP) (van Paassen et al., 2014), have a deleted copy of the PMP22 gene resulting in markedly lower levels of PMP22. Abnormal lower levels of PMP22 leads to demyelinating neuropathy in HNPP patients, where they experience muscle atrophy, foot drop, and carpel tunnel syndrome.

Similarly, MS is a heterogenous demyelinating disease in CNS neurons, and is the most common form of demyelinating disease (Love, 2006). Caused by both genetic and environmental factors, MS occurs due to the attack of the immune system (macrophages and T-cells) on CNS myelin (van der Valk and De Groot, 2000). MS affects 309.2 per 100,000 adults in the United States (Wallin et al., 2019), and clinical manifestations of the disease can vary from experiencing

no symptoms, to muscle weakness, ataxia, autonomic motor dysfunction, and sensory loss. Since damage to the myelin sheath results in abnormal neuronal activity, it is not surprising that a recent study identified MS patients are three – six times more likely to develop epileptic seizures compared to non-MS individuals (Lapato et al., 2017). It was demonstrated that MS mouse models have higher EEG activity, hippocampal demyelination, and loss of parvalbumin (PV+) interneurons, which are responsible for preventing neuronal hyperexcitability. Although both MS and CMT are treatable diseases, they are uncurable to date.

Here, I describe a patient with myoclonic gait dyspraxia, jerky tremors, EEG generalized discharges, and peripheral neuropathy that affects primarily sensory neurons with normal brain structure. We show that the patient carries a *de novo* mutation in protein kinase D1 (PKD1). PKD1 is a member of a family of serine/threonine kinases consisting of: PKD1, PKD2, and PKD3 (Rozengurt et al., 2005). Phosphorylation of PKD1-3 plays an important role in intracellular transduction pathways leading to several cell functions but also leads to the mediation of neurogenic inflammation and pain transmission through protease-activated receptor 2 (PAR_2) (Amadesi et al., 2009). Studies have shown that PKD1 is involved in inflammation and oxidative stress (Chiu et al., 2007; Storz et al., 2004), tumor pathogenesis (Guha et al., 2010; LaValle et al., 2010), and cardiomyopathies (Fielitz et al., 2008; Harrison et al., 2006). Although, PKD1 has been shown to regulate protein trafficking and mediate dendritic branch stabilization in neurons (Bencsik et al., 2015; Bisbal et al., 2008), its role in the nervous system has been primarily studied *in vitro* and its role in in vivo models of neurodegenerative disease is understudied.

In a functional kinomics screen, we previously identified PKD1 as an interacting partner of the potassium chloride cotransporter, KCC3 (Zhang et al., 2016). KCC3 is an electroneutral cotransporter of K^+ and Cl^-, expressed in both the central and peripheral nervous system (Pearson et al., 2001; Shekarabi et al., 2011). The cotransporter is activated by dephosphorylation, and inactivated by phosphorylation at two specific residues: Thr991, and Thr1048 (Rinehart et al., 2009). Inactivating mutations in human KCC3 are the cause of peripheral neuropathy associated with agenesis of the corpus callosum (ACCPN or Anderman syndrome) (Boettger et al., 2003; Howard et al., 2002). We and others have also previously shown that KCC3 loss-of-function and gain-of-function mutations yield peripheral and central nervous system neurodegeneration, locomotor deficits, and decreased seizure threshold *in vivo* (Boettger et al., 2003; Ding and Delpire, 2014; Howard et al., 2002; Kahle et al., 2016; Shekarabi et al., 2012). In this study, we generated a mouse model expressing the human mutation in PKD1 and confirmed that PKD1 affects KCC3 activity *in vitro*. In addition, we demonstrate that mice expressing the mutant kinase exhibit similar nerve pathology to the patient, and are more susceptible to seizures.

Material and Methods

Kinship analysis

Relationship between proband, siblings, and parents in the Family NG1917 was estimated using the pairwise identity-by-descent (IBD) calculation in PLINK (Purcell et al., 2007). The IBD sharing between the proband, siblings and parents is between 45% and 55%.

Principal component analysis

To determine the ethnicity of each sample, the EIGENSTRAT (Price et al., 2006) software was used to analyze tag SNPs in cases, controls, and HapMap subjects as described before (Jin et al., 2017).

Mapping and variant calling

Whole exome sequencing was performed at the Yale Center for Genome Analysis. Genomic DNA was captured using the Nimblegen SeqxCap EZ MedExome Target Enrichment Kit (Roche) followed by Illumina DNA sequencing as previously described (Jin et al., 2017). At each site sequence reads were independently mapped to the reference genome (GRCh37) with BWA-MEM and further processed using GATK Best Practice workflows, which include duplication marking, indel realignment, and base quality recalibration, as previously described(Li and Durbin, 2010; McKenna et al., 2010; Van der Auwera et al., 2013). Single nucleotide variants and small indels were called with GATK HaplotypeCaller and annotated using ANNOVAR (Wang et al., 2010) and Genome Aggregation Database (gnomAD) (Lek et al., 2016). The MetaSVM algorithm was used to predict deleteriousness of missense variants ("D-Mis", defined as MetaSVM-deleterious or CADD ≥ 20)(Dong et al., 2015; Kircher et al., 2014). Inferred LoF variants consist of stop-gain, stop-loss, frameshift insertions/deletions, canonical splice site, and start-loss. LoF + D-Mis mutations were considered "damaging". Variant calls were reconciled between Yale and PCH prior to downstream statistical analyses. Variants were considered by mode of inheritance, including DNMs, RGs, and X-linked variants.

CRISPR/Cas9 generation of PKD1-E77X mice

A mouse carrying the patient p.Glu79X mutation was generated using CRISPR/cas9 technology. A 20-bp sequence (CGATGGAACAAGCCATCTCC), located in exon 1 of the mouse PRKD1 gene, and followed by CGG as protospacer adjacent motif was selected for guide RNA targeting sequence. This sequence flanked by *BbsI* sites was inserted in pX330, a vector expressing the guide RNA under U6 promoter, and cas9 under a hybrid chicken β-actin promoter. The vector was injected alongside a 196-bp repair oligonucleotide into 429 0.5 day B6D2 mouse embryos. The repair oligo contained 90-bp homology arms, a codon introducing a stop codon, a unique *Nhe* I restriction site, and a few additional third base mutations that prevent re-targeting of cas9 to the repaired DNA. Of 429 embryos injected, 301 survived and were transferred to 14 pseudo-pregnant females, thereby generating 27 pups. At weaning, genotyping was done by amplifying a 384-bp fragment followed by sequencing. Two animals out of 24 (as 3 died, 8.7%) were identified as having a mutant allele. One male mouse (#19) was shown to have the stop codon at amino acid 77, but lacked the designed NheI restriction site (Figure 2-3). The other mouse had a frame shift that introduced a stop codon, 6 residues downstream of the cut site. We carried line 19 and crossed it to C57BL/6J female mice to demonstrate germline transmission. The lines were then further bred to the C57BL/6J mouse strain to dilute any possible off-target effects.

Transmission electron microscopy

Sural nerves were dissected from adult mice, then fixed with 2.5% glutaraldehyde in 0.1 M sodium cacodylate for 1 hour at room temperature (RT) and then at 4°C overnight. The

Vanderbilt Electron Microscopy core further processed the sural nerve samples by washing and fixing them in 1% osmium tetroxide solution for 1 hour at RT and then with 0.5% OsO4 for 24 hours. Then, the tissue samples underwent a series of ethanol dehydration steps (50% for 5 min, 75% for 15 min, 95% twice for 15 min each, and 100% thrice, 20 min each) before they were embedded in Spurr resin at 60°C for 24 to 48 hours. Semi-thin sections (500 nm) were stained with toluidine blue and examined for positioning. Ultrathin sections (80 nm) were then cut and stained with uranyl acetate and lead citrate and placed on copper grids. Images were observed using a Philips/FEI T-12 transmission electron microscope.

PRKD1$^{+/E77X}$ brain water content

Fresh brains isolated from WT and PRKD1$^{+/E77X}$ mice were immediately weighed following extraction. Brains were placed in desiccating vacuum oven (VWR 1400E) at 110 °C for 48 hours. Desiccated brains weights were obtained to measure water content (wet brain – dry brain)/ (dry brain).

Accelerated rotarod assay

A neuromotor coordination task was performed using an accelerating rotating cylinder (model 47600; Ugo Basile, S.R. Biological Research Apparatus). Both controls (wild-types) PRKD1$^{+/+}$ and heterozygous PRKD1$^{+/E77X}$ mice were tested. The cylinder was 3 cm in diameter and was covered with scored plastic. Mice were confined to a 4-cm-long section of the cylinder by gray Plexiglass dividers. Two to five mice were placed on the cylinder at once. The rotation rate of the cylinder increased over a 4-min period from 4 to 40 rpm. The latency of each mouse to fall

off the rotating cylinder was automatically recorded by the device. Mice that remained on the rotarod after the 300-s trial period were removed and given a score of 300 s. The test was performed as three trials daily for three consecutive days with an inter-trial interval of at least 30 min.

Balance beam assay

To assess fine motor coordination and balance, we used a 1m-long steel balance beams of either 12 mm or 6 mm thickness. The beams were placed about 50 cm from the ground and positioned between two pillars. At the start of the test, mice began on an open, square platform and ended in an enclosed black box with bedding as motivation for the mice to cross. Mice were trained for 2 days (three trials per day for each beam) beginning with the thicker beam (12 mm) and progressing to the thinner beam (6 mm). The mice were tested consecutively on each beam with 10-min relief periods between each trial. The third day was used as the test day with three trials for each beam. The mice had about 60 s to traverse the beam and were scored on the neurological scoring system for beam walking adapted from Feeney and colleagues (Feeney et al., 1982). This scoring system is based on the ability of the mouse to cross the beam and accounts for the number of paw slips. The mice received a score ranging from 1 to 7, based on their ability to complete the task, to place affected limbs on beam, and on the number of paw slips. This neurological scoring system considers a high score of 7 to be indicative of a wild-type mouse phenotype with no coordination deficits, and a low score of 1 indicative of severe motor defects.

Foot-print (Gait) assay

Gait was measured by coating the hind paws of each mouse with non-toxic black ink (Carters Brand Neat-Flo Inker for Felt/Foam Stamp Pads; Hill et al., 2004). Each mouse received a single trial in which it was placed at the beginning of a 40 × 10 cm runway paper and permitted to run freely to the end. The middle toe print was used for gait measurement, recorded as the mean distance (in cm) of three consecutive right hind paw prints.

Open-field

Exploratory locomotor activity was measured in specially designed chambers measuring 27 x 27 cm (Med Associates), housed in sound-attenuating cases over a 30 minute period. Infrared beams and detectors automatically record movement in the open field. Locomotor activity was measured over a period of 30 min.

Porsolt forced swim test

For this test, mice were placed in a large beaker, filled with 25-27°C water, such that they cannot escape from the beaker and cannot touch the bottom. On each of two consecutive days each mouse is individually placed in the beaker for 5-15 min. Latency to float, and amount of time spent struggling are measured. The mouse is monitored during the task, either by direct observation, or with a live video feed. If a mouse is struggling to keep its mouth above water or seem in danger of drowning, it is removed from the beaker immediately and excluded from the study. At the completion of the test, the animal is removed from the beaker, towel dried, and recovered for 10-20 min in a warm cage (~35-37°C) sitting on a heating pad.

Hot plate assay

Hotplate assay was performed by placing the mice individually on a platform maintained at 52-55°C (Hotplate Analgesia Meter, Columbus Instruments, Columbus, OH). A plastic cylinder 15-cm in diameter and 20-cm high confined the mouse to the surface of the hotplate. The time necessary for the mouse to respond to the thermal stimulus (hindpaw fluttering, licking, or withdrawal) was measured with a stopwatch. After the initial response or the maximum cut-off time of 15 sec, the mice were removed from the hotplate and returned to the home cage. A minimum recovery period of 1 h was implemented between hotplate assay sessions.

Von-Frey filaments

Somatosensory responsiveness was assessed using Von Frey filaments. Filaments of various diameters were pressed against the plantar surface of the mouse's foot. The filaments bend, producing a constant force of application from 0.01 to 10 mN. The filaments were used in ascending order until a foot withdrawal response was observed. The force exerted by the filament that elicits a withdrawal response was taken as the threshold.

Kainic acid administration and behavioral scoring of seizures

Behavioral observations began immediately following intraperitoneal administration of 20 mg/Kg kainic acid per mouse and continued for up to 1 hour, after which, mice were returned to their home cage or sacrificed. Cages were not returned to the vivarium until at least 3 hours after drug administration when it was confirmed that no further seizures were observed. Mice

were scored live at the time of the treatment and videotaped for additional coding of activity levels by a second experimenter, who was fully blinded to experimental conditions. Mice were rated for immobility time (Table 2-1) across three continuous 10-min time bins. Kainic acid was scored according to a modified Racine scale in which stage 3 head bobs represents myoclonic jerks.

Xenopus laevis oocytes

Oocyte-positive *Xenopus laevis* female frogs were maintained in static aquaria as previously described (Delpire and Gagnon 2011). For surgery, frogs were anesthetized with buffered tricaine (1.7 g/L + 3.4 g/L Na-bicarbonate), placed on a wet stack of paper placed on ice, and a small 4- to 6-mm incision was made on the lower abdomen by using a disposable sterile scalpel (Feather #11; Fisher Scientific). Ovarian lobes were externalized with sterile curved forceps, removed with sharp scissors, and placed in a 10-cm plastic culture dish containing Ca^{2+}-free ND96 (96 mM NaCl, 4 mM KCl, 0.8 mM MgSO4, HEPES 5 mM, pH 7.4—185 mOsM). The incision was sutured with three to four stitches by using 4–0 monofilament nylon surgical suture (DemeTech; 18-mm needle, three-eighth circle, reverse cutting). After the frogs recovered from anesthesia in shallow water, they were returned to their housing and recovered for a minimum of 8 wk. Oocytes (stages V–VI) were defolliculated by 4 × 90-min treatments (vigorous shaking at 4°C) with 5 mL divalent-free ND96 containing 9.5 mg/mL collagenase D with washes between treatments. After the final wash, oocytes were placed in modified L15 (250 mL Leibovitz L15 Ringer [Invitrogen], 200 mL deionized water, 952 mg HEPES [acid form], and 400 µL of 50 mg/mL

Table 2-1. Modified Racine Scale

Stage 1	Immobility/flattening
Stage 2	Extension of forelimb and/or tail extension, rigid posture
Stage 3	Tics, repetitive movements, head bobs
Stage 4	Rearing and falling
Stage 5	Continuous rearing and falling, barrel rolling
Stage 6	Severe tonic-clonic seizures

Table 2-1. Modified Racine scale to score stages 1-6 of seizures in mice after kainic induction.

gentamycin [Invitrogen]; pH 7.0; 195–200 mOsM), filtered on 0.22 µm cellulose acetate membrane and allowed to recover overnight in a 16°C incubator.

cRNA Transcription and Injection

cDNA clones inserted in pBF were linearized with the restriction enzyme MluI and linearized DNA (2.5 µg) was transcribed into cRNA using the mMessage mMachine SP6 transcription kit (Ambion). cRNA quality was verified by gel electrophoresis (1% agarose, 0.693% formaldehyde) and quantitated by measurement of absorbance at 260, 280, and 320 nm. The day after isolation, oocytes were injected with 50 nL water or cRNA mixture (15 ng cRNA or as indicated) by using a 10-µL digital microdispenser (Drummond Scientific) fitted with sterile pulled glass capillary tubes.

K^+ Influx Measurements in oocytes

For 10 min in an isosmotic solution containing 140 mM NaCl, 5 mM KCl, 2 mM $CaCl_2$, 1 mM MgSO4, 5 mM Hepes (pH 7.4), and 1 mM glucose. At the end of the preincubation period, the medium was aspirated and replaced with identical solution containing 100 µM ouabain, and ^{86}Rb (5 mCi/ml). After a 1-hr ^{86}Rb uptake, the oocytes were washed three times with ice-cold buffer, individually placed in liquid scintillation vials with 200 µl of 0.25 N NaOH for 1 hour, and neutralized with 250 µl of acetic acid glacial. Liquid scintillation fluid (5 ml, Biosafe II) was added to each vial, and radioactivity was counted using a Packard Tri-Carb β-scintillation counter. K^+ flux was calculated from ^{86}Rb counts and expressed in nanomoles K^+ per oocyte per hour. Calculation was based on measuring and averaging the counts (cpm) of 5 ml of aliquots of radioactive

extracellular solution and relating these counts to the amount of K^+ contained in these aliquots (e.g. 1 cpm = 2.5 pmol K^+).

Cell culture and surface biotinylation

HEK293FT cells transfected with GFP-tagged KCC3 and His-6-strep II-tagged PKD1 were grown in 10-cm Corning culture dishes at 37°C, air/5% CO2. For biotinylation, cells were washed in ice cold $CaCl_2$ and $MgCl_2$ containing HBSS ($HBSS^{2+}$), then incubated with freshly prepared Sulfo-NHS-biotin (Thermo Scientific, Waltham, MA, 0.5 mg/mL in cold $HBSS^{2+}$ for 30 minutes at 4°C. After 2 washes with ice cold $HBSS^{2+}$, 1 mL of lysis buffer (150 mM NaCl, 50 mM Tris-HCl pH 7.5, 1% Triton X-100 with proteases inhibitors) was added to the plate and cells lysate was collected. Biotinylated (cell surface) proteins were isolated by immunoprecipitation with streptavidin agarose beads (Thermo Scientific). Streptavidin immuno-precipitated proteins and whole cell lysate were used to detect cell surface and total cellular KCC3 by immunoblotting.

Immunoblotting

Equal volumes (40 µL) of cell lysates in sample buffer was subjected to gradient (4-20%) SDS-polyacrylamide gel electrophoresis (PAGE) and proteins were transferred to polyvinylidene fluoride (PVDF) membranes (Thermo Fisher Scientific). Membranes were probed with primary antibodies overnight at 4°C (KCC3, His-6 [Millipore], and Ezrin [Millipore]), followed by horseradish peroxidase (HRP)-conjugated secondary anti-mouse (Jackson ImmunoResearch) or anti-rabbit antibodies (Sigma-Aldrich), and revealed using enhanced chemiluminescence (PerkinElmer).

Immunofluorescence

HEK293FT cells transfected with GFP-tagged KCC3 and His-6-strep II-tagged were cultured on glass coverslips until they reached 100% confluency. Cells were fixed with cold (−20°C) methanol, washed with 3 X 5 min with HBSS2+, and followed by incubation in blocking buffer (5% BSA, 0.1% Triton X-100, and 0.1% Tween 20 in HBSS2+) for 2 h and incubation with primary antibody overnight. Slides were washed 3 × 5 min with HBSS2+, and incubated with fluorophore-conjugated (Cy3 or FITC) secondary antibodies for 1 h. Chambers were removed from the microscope slide and mounted with ProLong Gold antifade reagent with DAPI (Invitrogen). Slides were imaged on a Zeiss LSM 880 laser scanning confocal microscope. Samples were scanned using a ×63 oil objective. The images were exported as TIFF files using Zeiss ZEN Lite 2012 software.

qRT-PCR

Sciatic nerves were isolated from WT or PRKD1+/E77X mice, lysed and processed using the RNeasy mini kit (Qiagen). RNA quality and quantity were assessed by measuring absorbance at 260, 280, and 320 nm. Reverse-Transcription was performed by incubating 1 µg RNA with random hexamers, dNTPs, and SuperScript II (Invitrogen), for 1 hour at 37^{o}C, followed by denaturation for 5 min at 95^{o}C. Quantitative PCR reactions contained 12.5 µl SYBR^{TM} Green PCR master mix (Applied Biosystems, Foster City, CA), 1 µl each primer (1 µM), 9.5 µl water, and 1 µl cDNA. Relative mRNA expression levels were calculated by the $\Delta\Delta$Ct method. Statistical analysis was performed using one-way analysis of variance (ANOVA).

Primers (mouse genes):

Target	Forward primer (5'-3')	Reverse primer (5'-3')
Mpz	CGGACAGGGAAATCTATGGTGC	TGGTAGCGCCAGGTAAAAGAG
Pmp22	CATCGCGGTGCTAGTGTTG	AAGGCGGATGTGGTACAGTTC
Mbp	ACACGAGAACTACCCATTATGGC	CCAGCTAAATCTGCTGAGGGA
Nrg1 type 3	TGCATTGCTGGCCTAAAGTG	GTTCTTCCGGGTGGGTACTG
Erbb11/2	ACCGACATGAAGTTGCGACTC	AGGTAAGCTCCAAATTGCCCT
Gapdh	AGGTCGGTGTGAACGGATTTG	GGGGTCGTTGATGGCAACA

Results

Clinical presentation of peripheral motor neuropathy and seizures

The PKD1 mutation was first discovered in a young female patient who developed an unusual and progressive seizure disorder. The patient presented at age 7 with a first-time seizure, during which she experienced an episode of whole body shaking and intermittent leg weakness. She continued to have similar episodes occurring multiple times during sleep, which typically occurred 2-3 hours after sleep onset, lasting 30 seconds to 2 minutes. At the time of first presentation, her past medical history was negative and family history significant only for a diagnosis of epilepsy in her sister (Figure 2-1A). Her exam was normal, and after initial workup, she was diagnosed with idiopathic generalized epilepsy syndrome after multifocal myoclonic seizures were captured on EEG. After further EEG studies and clinical evaluation, she was diagnosed with juvenile myoclonic epilepsy (JME) and her symptoms were partially responsive to valproic acid (VPA) and clonazepam. However, over the following couple of years her symptoms progressed despite treatment. She began having daytime seizures as well as progressive unsteadiness of her feet, gait and fine motor dyspraxia, worsening action/intention tremor of her

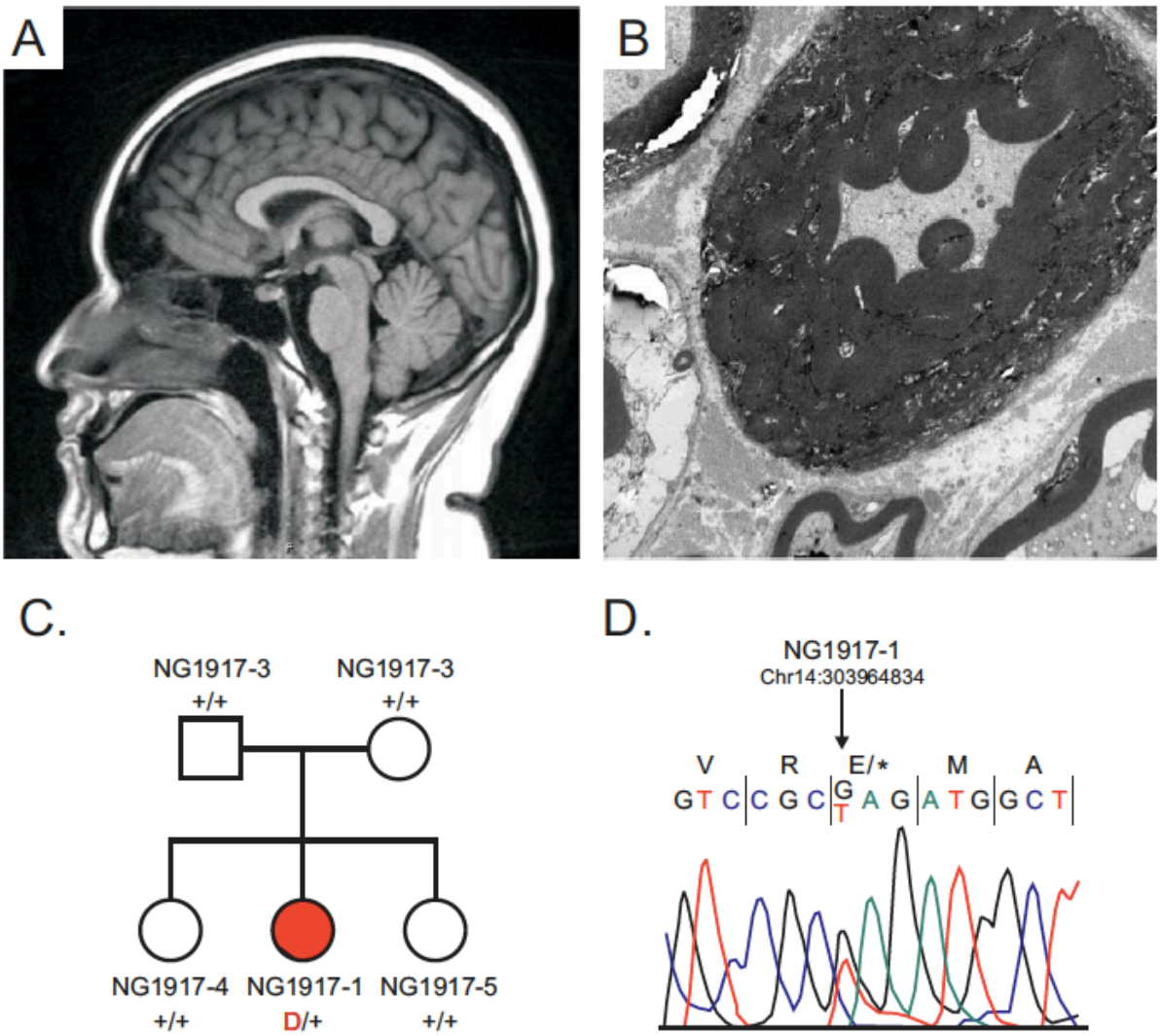

Figure 2-1. Patient with normal brain MRI and abnormal myelination of peripheral nerves. (A) Magnetic resonance imaging (MRI) of the brain no identifiable pathology. There is a normal sulcation pattern, hipoccampi are symmetric, and normal in signal and morphology. The brainstem is also normal in signal and morphology, with no evidence of atrophy. (B) Electron microscopy of sural nerve biopsy tissue showing highly abnormal degree and pattern of myelination, with hyper-myelinating fiber. (C) Pedigree of affected patient with *de novo* variant in *PRKD1* with epilepsy (red symbol) and healthy family members (open symbols). (D) Sanger sequencing chromatogram confirming E to Xaa PKD1 mutation in the proband.

hands and feet with development of a wide based and tremulous gate, and hyperreflexia. Given the progressive nature and unclear etiology of her condition, she underwent further diagnostics, including an MRI of the brain as well as sural nerve and muscle biopsies.

Identification of the mutation in the clinical case

Initial workup involved MRI of the brain, which revealed normal morphology, and a follow up MRI nine years later continued to show unremarkable findings (Figure 2-1C). The biopsies performed, however, suggested unusual abnormalities in myelination. The muscle biopsy tissue showed well preserved fascicles and normal staining. The sural nerve biopsy, however, demonstrated an abnormal degree and pattern of myelination. Electron microscopy of the nerve biopsy was then performed which demonstrated nonspecific nerve sheath degeneration and hyper-myelinating Schwann cells (Figure 2-1D). Metabolic and genetic testing performed initially did not uncover any known mutations, therefore, whole exome sequencing was performed, which uncovered the mutation in PKD1.

Effect of catalytically inactive PKD1 mutation on KCC3 function

PKD1 was identified as a hit in a kinome-wide RNAi screen carried out in HEK293 cells expressing KCC3. The screen was designed to recognize genes required for KCC3 phosphorylation at residue Thr^{991} (Zhang et al., 2016). In addition, this study demonstrated that PKD1 knockdown in HEK293 cells resulted in decreased KCC3 phosphorylation at residues Thr^{991} and Thr^{1048}. Given the importance of residue Thr^{991} phosphorylation in swelling-induced stimulation of KCC3 activity (de Los Heros et al., 2014; Rinehart et al., 2009), the swelling-regulated function of KCC3

was assessed in *Xenopus* laevis oocytes co-injected with wild-type or catalytically inactive PKD1 (Figure 2-2A). Oocytes expressing catalytically inactive PKD1 demonstrated a small but significant increase in K^+ influx, consistent with decreased phosphorylation of the cotransporter. To assess whether the increase was related to increased membrane expression, we co-transfected HEK293 cells with KCC3 and wild-type or mutant PKD1 kinase. Immunoblot assays (Figure 2-2C) revealed no change in the level of KCC3 expression at the plasma membrane, irrespective of PKD1 activity. Note that the kinase was shown to co-localize with the cotransporter (Figure 2-2B), indicating that the proteins are likely to be part of a multi-protein complex. These results indicate that an increasee in KCC3 mediated K^+ flux is due to the increase in KCC3 activity and not the expression at the plasma membrane.

Generation and characterization of PRKD1-E77X mice

Using CRISPR/Cas9 gene editing, we created a mouse that reproduces the PKD1-E79X mutation found in the human patient. In the mouse, residue E79 is located at position 77 and thus, we created a PKD1-E77X mouse line (Figure 2-3). After backcrossing a founder line to C57BL/6J mice for 4 generations, we crossed heterozygote mice to produce wild-type, heterozygous, and homozygous littermates. As seen In Figure 2-4, there was a significantly low number of homozygous animals generated. Out of 125 pups produced in 16 litters, only 3 homozygote animals were produced. Thus, in contrast to the sex of the mice which was distributed according to a Mendelian distribution ($X^2 = 3.53$, $P = 0.060$), the mutant PKD1 allele was not properly distributed ($X^2 = 34.186$, $P < 0.001$).

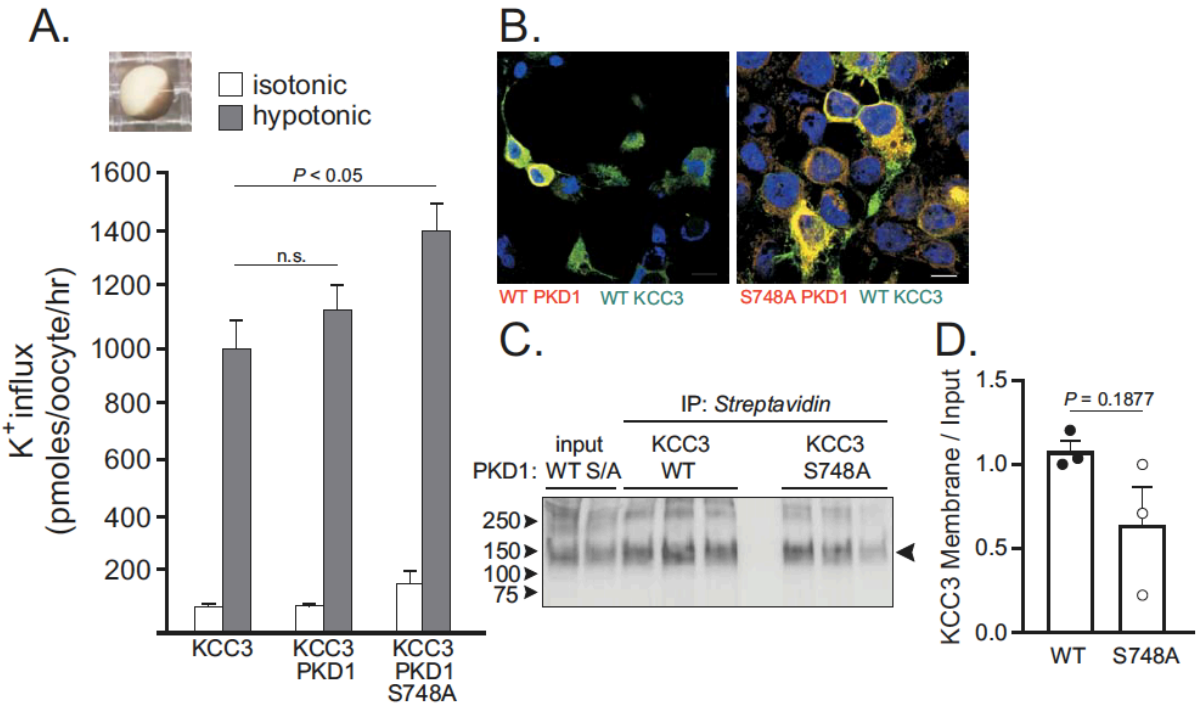

Figure 2-2. Catalytically inactive PKD1 results in increase in KCC3 mediated potassium flux and no change in expression at the membrane. (A) *Xenopus laevis* oocytes injected with KCC3, WT PKD1, or catalytically inactive PKD1 cRNA. Oocytes injected with mutant PKD1 result in increase in K^+ flux. One-Way ANOVA was used to measure significance ($P < 0.05$). (B) Immunofluorescence images of HEK293 cells transfected with WT KCC3 (right) and WT PKD1 or catalytically inactive PKD1 (left). (C) Western blot analysis of cell surface (biotinylated fraction) versus cell lysate KCC3 in HEK293 cells transfected with mutant or wild-type PKD1, and wild-type KCC3. SDS-PAGE contained 4-20% acrylamide. Membrane was probed with anti-KCC3 antibody. (D) Quantification of (C) unpaired t-test (not significant, p=0.1877).

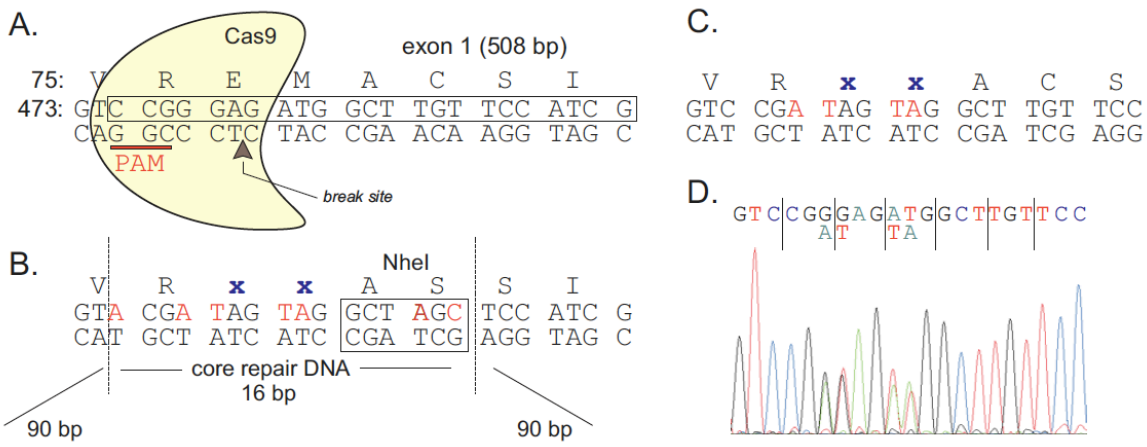

Figure 2-3. CRISPR design of PKD1 mutation. (A) Cas9 targeted to the DNA region of interest by guide RNA introduces a break site (arrowhead) in DNA where the mutation will be introduced. (B) Desired mutation introduced by single stranded repair DNA. (C) Actual mutation introduced by single stranded repair DNA. (D) Sanger sequencing chromatogram confirming the PKD1-E77X mutation in mice consisting of a nonsense mutation at position 77 of the protein resulting in a nonfunctional kinase.

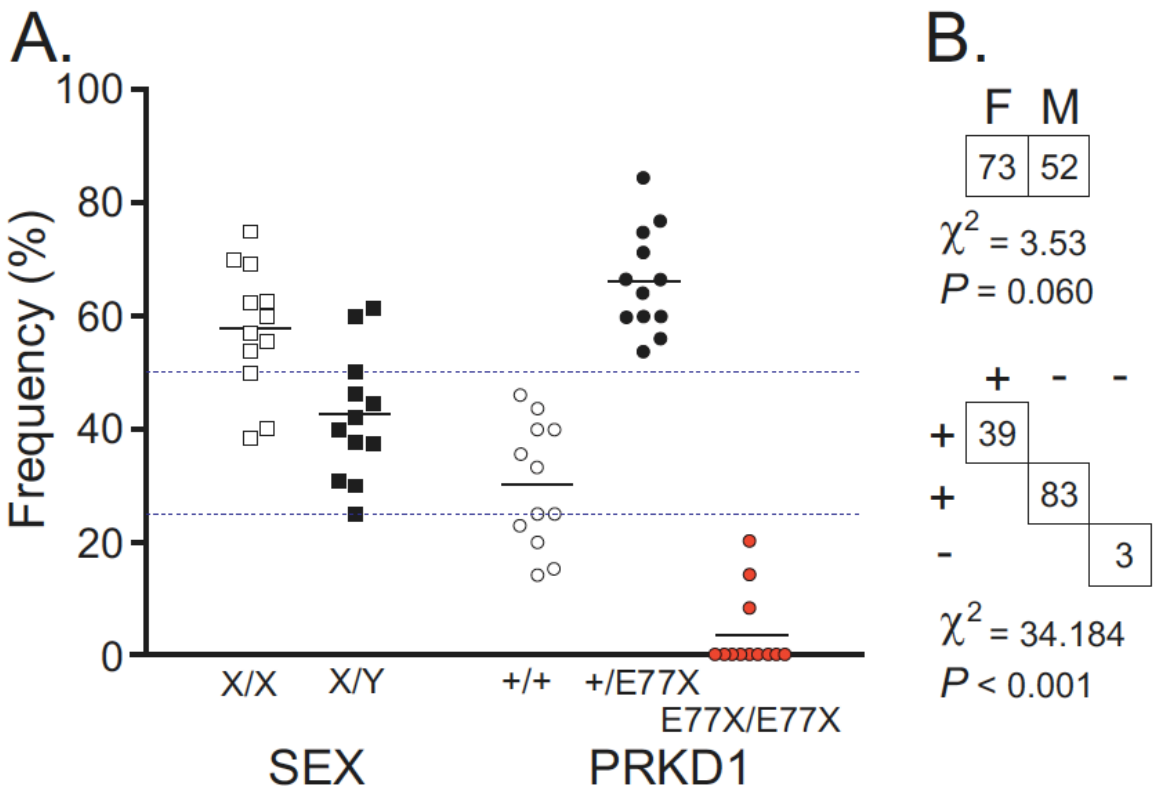

Figure 2-4. Deficit in homozygous offspring from PRKD1$^{+/E77X}$ breedings. Sex and genotypes of 125 pups generated from 18 litters. The number of females slightly exceeds 50% while the number of males comes slightly short of 50%. Chi square analysis revealed Mendelian distribution (P = 0.06, not statistically different from expected). Only 3 homozygote PRKD1 $^{E77X/E77X}$ mice were generated. Chi square analysis revealed non-Mendelian distribution ($p < 0.001$).

To assess nerve pathology in the PKD1 mutant mice, we isolated the sural nerves of WT, PRKD1$^{+/E77X}$, and PRKD1$^{E77X/E77X}$ mice and processed them for electron microscopy (Figure 2-5). While the morphology of the nerve fibers was overall normal (Figure 2-5, A-F), several nerve tomacula pathologies were identified in sural nerves of PRKD1$^{E77X/E77X}$ mice (Figure 5, H-I) similar to the pathology seen in the patient (Figure 1). We then assessed sural nerve fiber thickness, by measuring g-ratios on sural nerves isolated from WT, PRKD1$^{+/E77X}$, and PRKD1$^{E77X/E77X}$ mice. PRKD1$^{E77X/E77X}$ mice nerve fiber g-ratios were significantly lower than in wild-types and heterozygote mice ($P < 0.01$) (Figure 2-6A), possibly indicating larger fibers. To determine if the decrease in g-ratios was due to myelin thickness and/or axon diameter, we individually measured these two parameters on a large number of fibers, and could assign the increase in g-ratio solely to an increase in myelin thickness (Figure 2-6B). There was no measurable difference in axon diameter (Figure 2-6, C and D). Using qRT-PCR, we assessed sciatic nerve mRNA expression levels of protein that are involved in the regulation of myelin (Nrg1 type 3, ErbB1, PMP22, myelin P0, and MBP) but did not observe any differences between WT and PRKD1$^{E77X/E77X}$ (Figure 2-7).

To determine if the nerve pathology affected basal motor function and/or fine motor movement in the mice, we performed several neurobehavioral tests on wild-type and heterozygote mice, as unfortunately, the breeding did not produce homozygote mice for these experiments. Male and female mice of age P60-P70 were subjected to the accelerated rotarod (Figure 2-8A), balance beam (Figure 2-8, B and C), open-field (Figure 2-9, A-C), Porsolt forced swim (Figure 2-9D), and foot print (Figure 2-10, A-D) tests. There was no observed abnormal locomotor phenotype in the mutant PRKD1$^{+/E77X}$ mice, compared to their wild-type counterpart. As the sural nerve has a

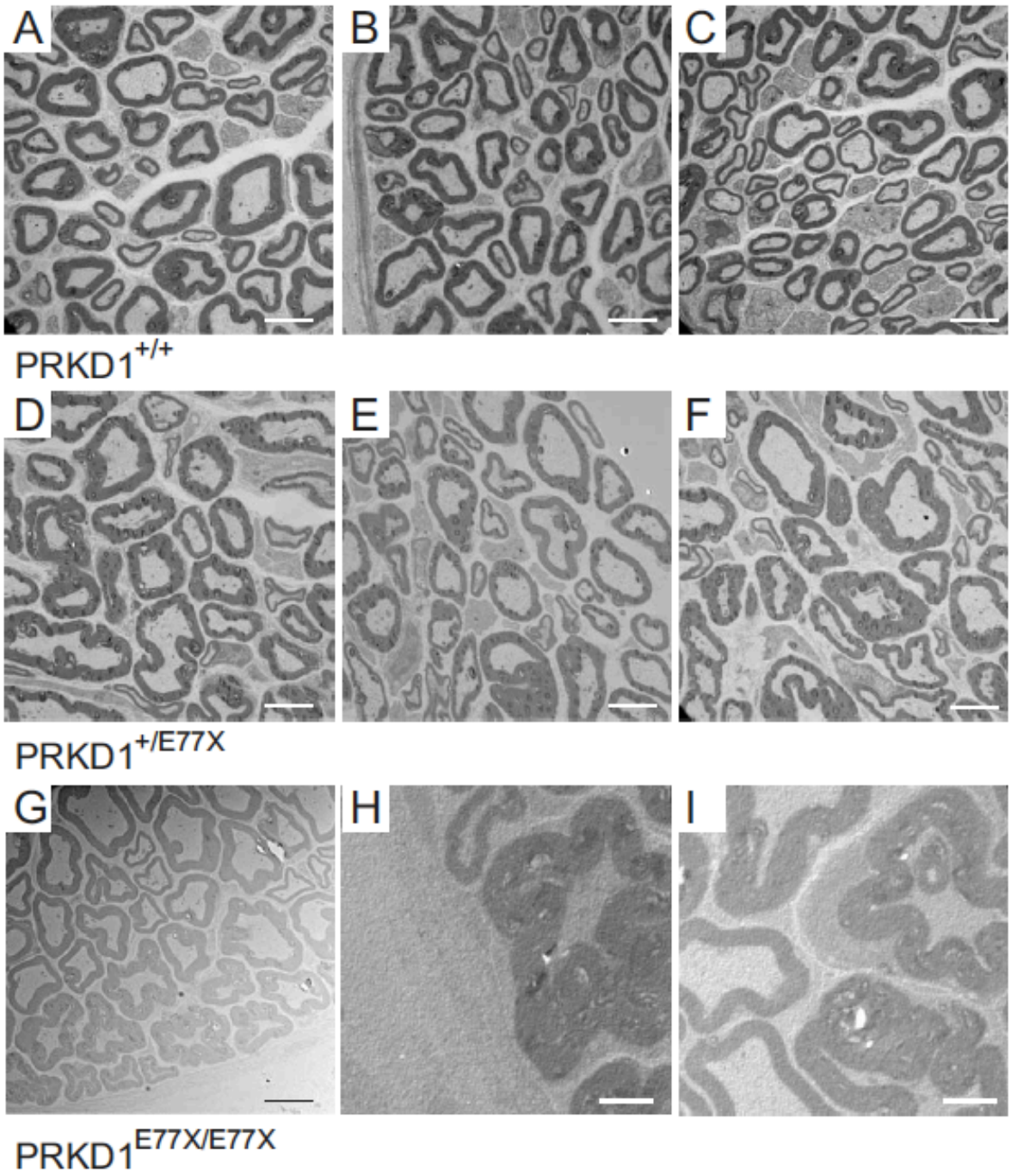

Figure 2-5. PRKD1$^{E77X/E77X}$ fibers exhibit the myelin tomacula pathology observed in sural nerve fibers of the patient. Electron micrographs of transverse sections of sural nerves extracted from wild-type (A-C), PRKD1 $^{+/E77X}$ (D-F), and PRKD1 $^{E77X/E77X}$ (G-I) mice. Scale bars = 5 μm (A-G) and 2 μm (H & I). Tomacula pathology observed in PRKD1 $^{E77X/E77X}$ homozygote mice (H-I).

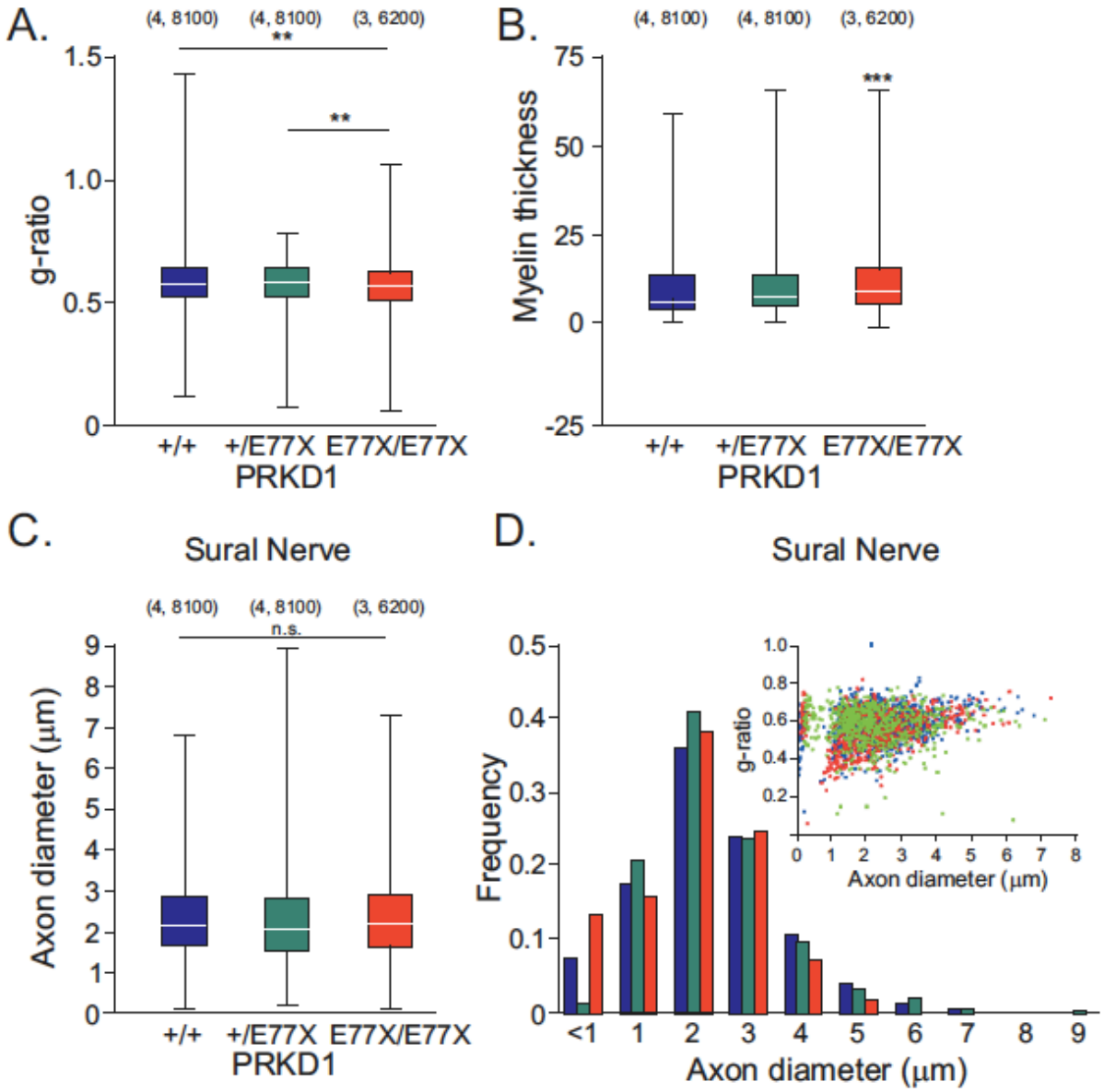

Figure 2-6. Normal axon diameter in PKD1 heterozygous and homozygous sural nerves, but lower g-ratio due to thicker myelin. (A) Box-and-whisker plot analysis of axon diameter of WT (n = 4 mice, 8100 fibers), PRKD1 $^{+/E77X}$ (n = 4, 8100), and PRKD1 $^{E77X/E77X}$ (n = 3, 6200) sural nerves. (B) Histogram analysis of axon diameter in WT, PRKD1 $^{+/E77X}$ and PRKD1 $^{E77X/E77X}$ sural nerves. (C) g-ratio analysis of sural nerves of WT, PRKD1 $^{+/E77X}$, and PRKD1 $^{E77X/E77X}$ axons, where PRKD1 $^{E77X/E77X}$ axons have lower g-ratio. The g-ratio is calculated as: axon diameter/fiber diameter. (D) Myelin thickness measured in WT, PRKD1 $^{+/E77X}$, and PRKD1 $^{E77X/E77X}$ sural nerves. PRKD1 $^{E77X/E77X}$ sural nerves have increased myelin thickness. One-way Analysis of Variance with **p < 0.0001, ***p <0.00001.

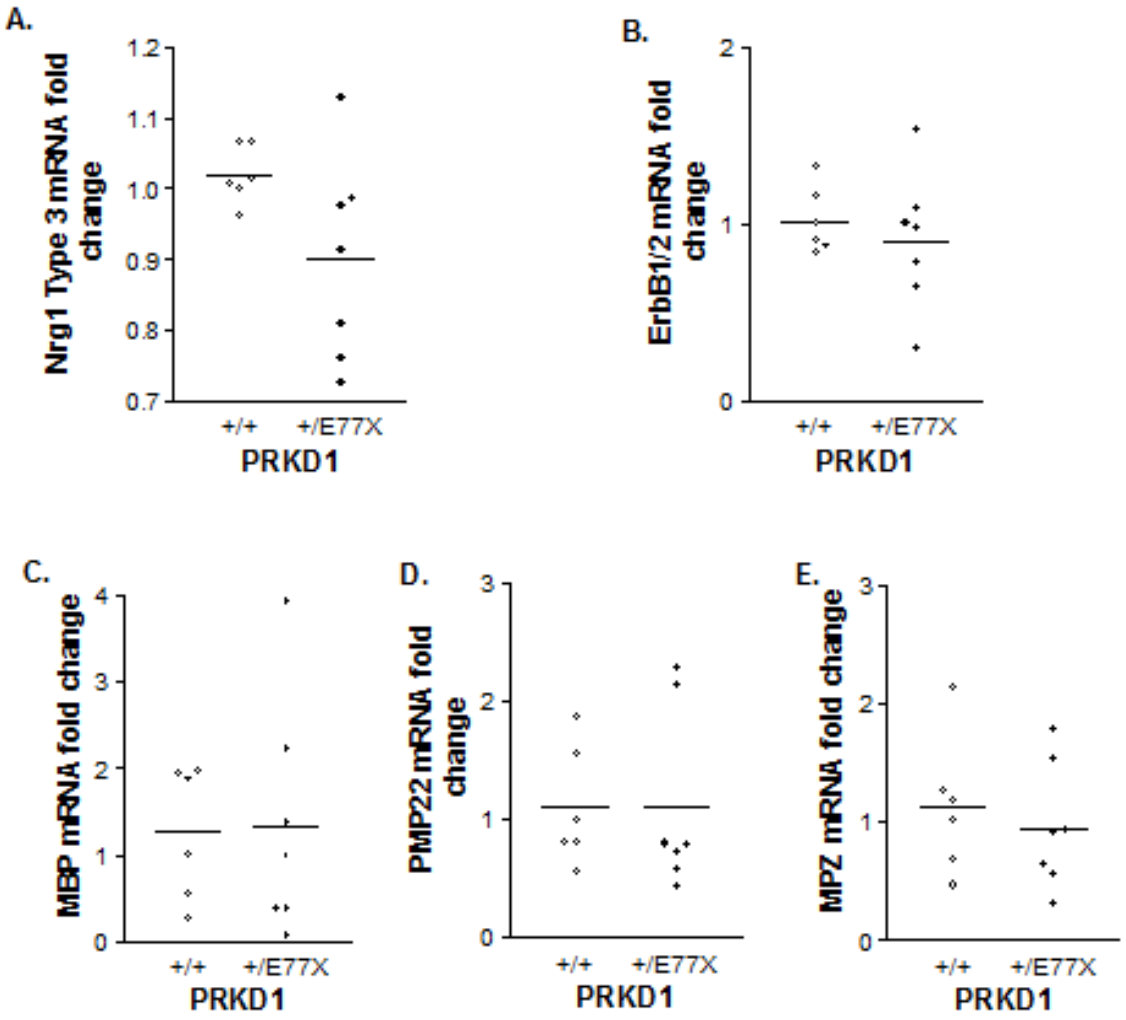

Figure 2-7. No change mRNA expression of various myelin protein in sciatic nerves of PRKD1$^{+/+}$ and PRKD1 $^{+/E77X}$. (A-E) Fold change of mRNA expression levels of Nrg1 type 3, ErbB1/2, MBP, PMP22, and MPZ in sciatic nerves of PRKD1$^{+/+}$ (white, n = 7), PRKD1$^{+/E77X}$ (black, n =7). Student's unpaired t-test, n.s. = non-significant. Fold change is normalized to WT and is calculated by the delta Ct method.

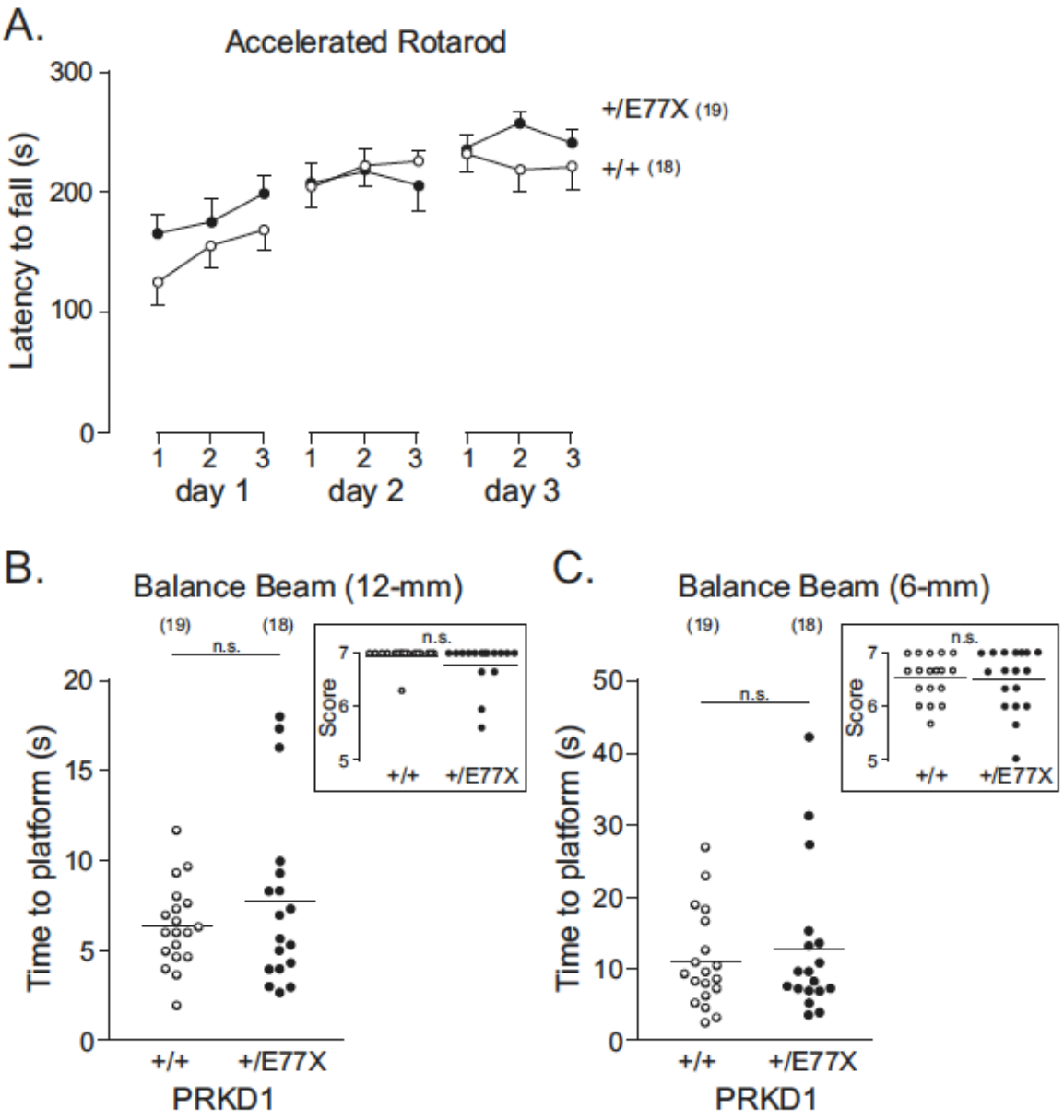

Figure 2-8. No change in motor coordination and balance as determined through accelerated rotarod and balance beam test. (A) Latency to fall on accelerated (4 rpm – 40 rpm) rotarod in WT (n = 19) and PRKD1 $^{+/E77X}$ (n = 18) mice. The mice underwent three trials a day for 3 days. Assessment of time (in sec) to platform and neurological score of mice placed on 12-mm (B) or 6-mm (C) beams. The number of mice analyzed was for WT (n = 19) and PRKD1 $^{+/E77X}$ (n = 18). Student's unpaired t-test, n.s.

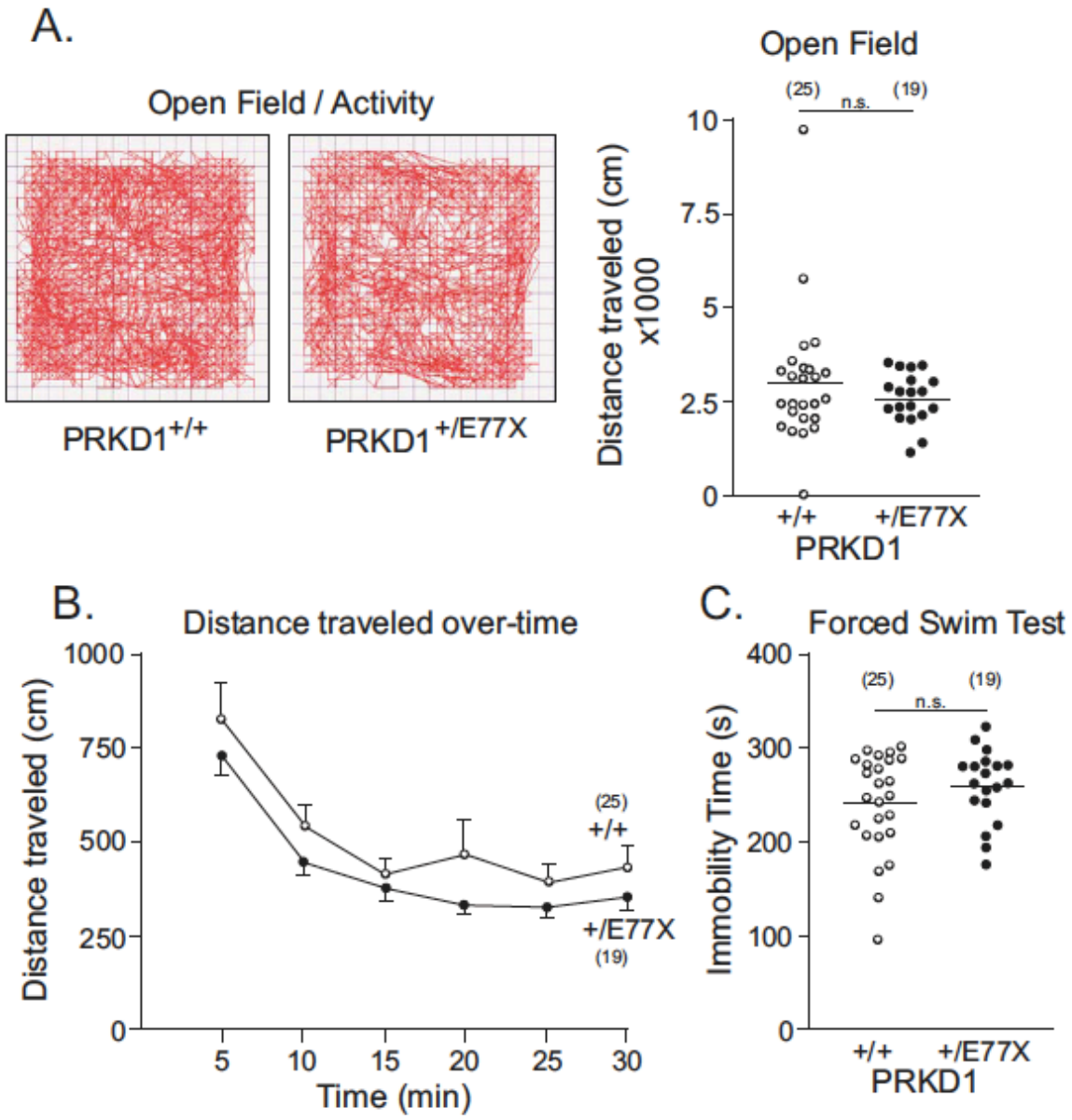

Figure 2-9. No difference in locomotor behavior between WT and PRKD1 $^{+/E77X}$ mice. (A) Open field assay assessing distance traveled by WT (n = 25) and PRKD1$^{+/E77X}$ mice (n = 19) over a 30 min trial. Laser tracking of WT and PRKD1 $^{+/E77X}$ mice subjected for 30 min to open field test. (B) Analysis of distance traveled as a function of time. Data were acquired by 5 min increments. (C) Time spent immobile during the Porsolt Forced Swim test in WT and PRKD1 $^{+/E77X}$ mice. Student's unpaired t-test, n.s.

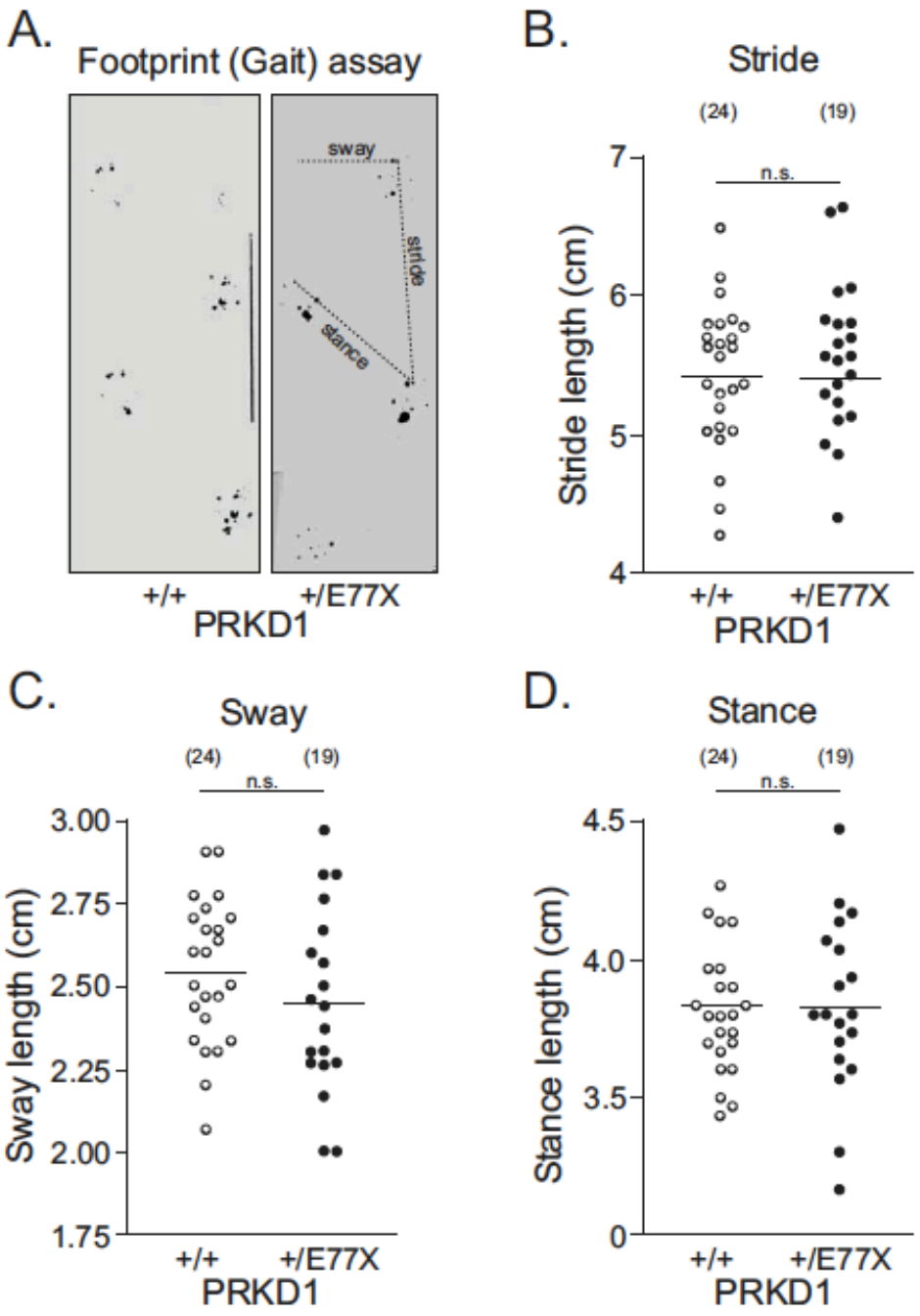

Figure 2-10. No abnormal gait identified via gait analysis in WT and PRKD1 $^{+/E77X}$ mice. (A) Representative measurement of the different gait parameters. (B) Stride length, (C) Sway length, and (D) Stance length measured in WT (n = 24) and PRKD1 $^{+/E77X}$ (n = 25) mice. All distances are represented in centimeters. Student's unpaired t-test, n.s.

purely sensory function, we also assessed response to noxious, mechanical and heat stimuli through von Frey (Figure 2-11A) and hot plate (Figure 2-11B) assays. The force needed for paw withdrawal upon filament pressure on the foot and the time needed for response to heat stimulus on a hotplate were similar between the two genotypes. Thus, there was no motor or sensory deficit measurable in the PKD1 mutant mice.

Because of the patient history of epileptic seizures and the possible involvement of KCC3 in seizure susceptibility (Boettger et al., 2002), we utilized a kainate-induced seizure model in PKD1 mutant mice compared to wild-type littermates (Figure 2-12). After intra-peritoneal injection of 20 mg/Kg kainic acid, mice were observed for 60 min and the latency to stage 3 myoclonic seizures (see methods) was measured. $PRKD1^{+/E77X}$ mice had a clear increase in seizure susceptibility and severity compared to wild-type mice (Figure 2-12A, C). In addition, $PRKD1^{+/E77X}$ mice exhibited a significantly larger number of myoclonic jerks than their wild-type counterparts (Figure 2-12B). Since changes in corpus callosum are associated with changes in brain weight (Shekarabi et al., 2012) and KCC3 loss of function is linked to ACCPN (Howard et al., 2002) and increased seizure susceptibility (Boettger et al., 2003), we were interested in measuring brain weight of $PRKD1^{+/E77X}$ mice. There was no observed difference in averaged brain weights among WT and $PRKD1^{+/E77X}$ mice (Figure 2-12D), concluding that the effect of PKD1 on seizures might act independently of the relationship between KCC3 and brain cell volume.

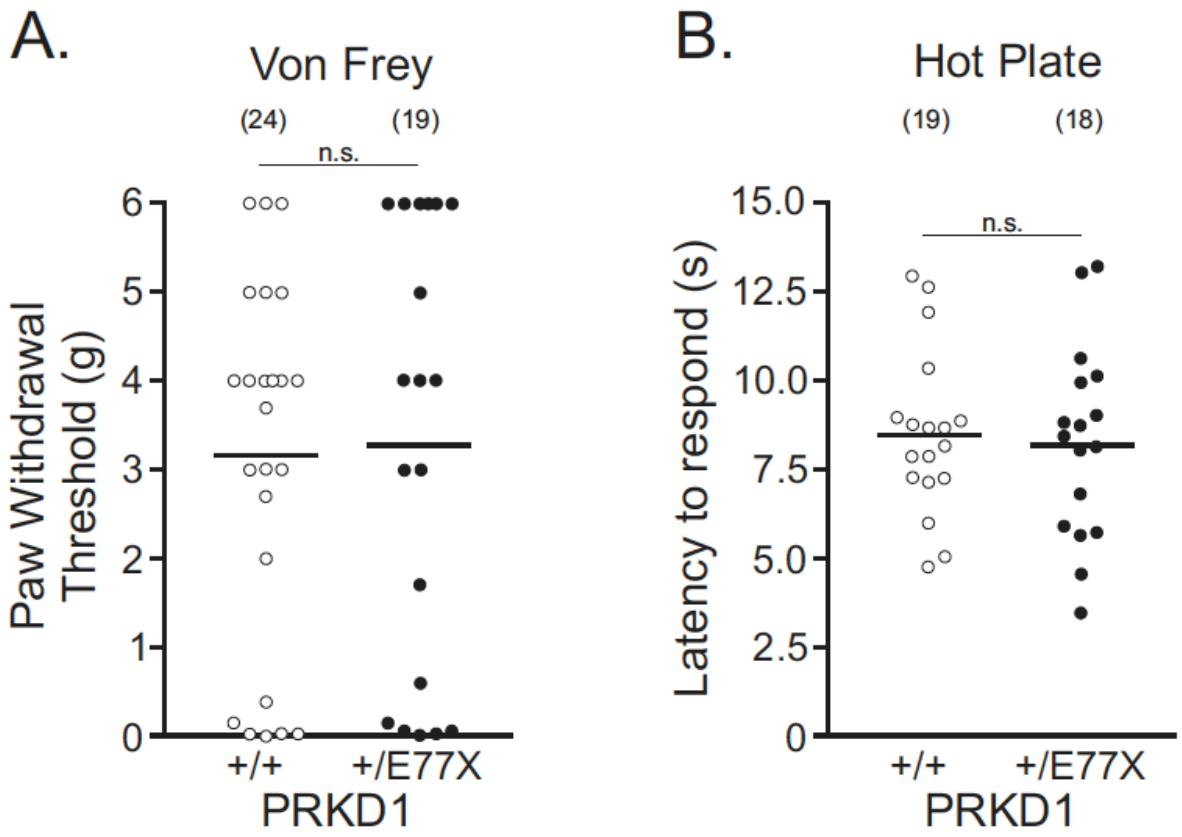

Figure 2-11. Sensory assessment through force and nociception in WT PRKD1 $^{+/E77X}$ mice. (A) Von-Frey filaments were used to test paw withdrawal threshold in WT (n = 24) and in PRKD1 $^{+/E77X}$ (n = 19) mice. (B) WT (n = 19) and PRKD1$^{+/E77X}$ (n = 18) mice were subjected to the hot plate assay at 52^{o}C with a cut-off time of 15 seconds to prevent injury. The latency (in sec) to respond to the noxious stimulus was measured using a stopwatch. Student's t-test, n.s.

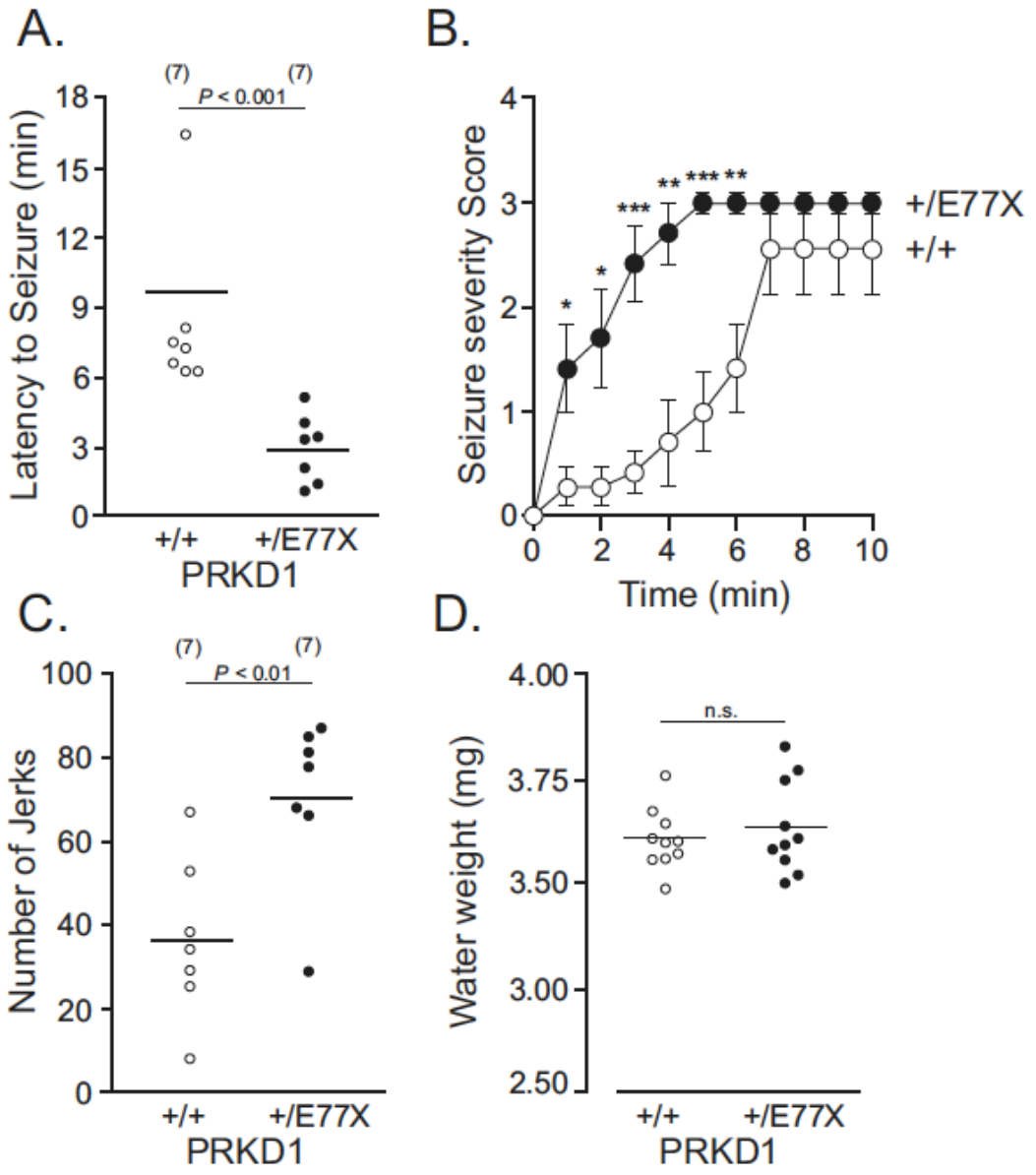

Figure 2-12. Seizure susceptibility and brain water content in WT and PRKD1$^{+/E77X}$ mice. (A-B) Seizure susceptibility measured in WT (n = 7) and in PRKD1$^{+/E77X}$ (n = 7) mice, by measuring the latency (in minutes) to exhibit myoclonic jerks (stage 3 of the Racine scale, Table 2-1) following kainic acid injection. (B) Seizure severity following kainic acid injection occurring in WT (n = 7) and in PRKD1$^{+/E77X}$ (n = 7) mice over a 30 min period. (B) Number of myoclonic jerk events following kainic acid injection occurring in WT (n = 7) and in PRKD1 $^{+/E77X}$ (n = 7) mice over a 30 min period. Student's unpaired t-test, *p< 0.05, **p< 0.01, ***p< 0.0001. (D) water content (mg) measured in WT (white, n = 10) and in PRKD1$^{+/E77X}$ (black, n = 10) mice.

Final Conclusions and Discussion

The present study was undertaken to assess the role of a *de novo* loss-of-function mutation in PKD1 identified in a young female patient with peripheral neuropathy and seizures. Our study provides the first link between PKD1 and neurodegenerative disease in humans, while heterozygous missense mutations in the kinase had been identified in 6 individuals with congenital heart defects (Sifrim et al., 2016). In 2008, Fielitz and coworkers reported the embryonic lethality of the PKD1 global knockout mouse and cardiomyopathies resulting from a cardiac-specific deletion of PKD1 in mice (Fielitz et al., 2008). From both the human patients and the mouse studies, PKD1 seems to play an important role in heart function. Note that there are no known cases of patients with homozygous mutations in PKD1.

Because of the substitution of a glutamic acid residue (coded by GAG) at position 79 with a stop codon (coded by TAG), the mutation reported here terminates the translation of the PKD1 protein prematurely. Thus, the patient carries one wild-type allele and one knockout allele, reducing the level of protein expression. To better establish causality with the neurological phenotype of the patient and further study the impact of the mutation, we reproduced the mutation in mice using CRISPR/Cas9. In addition to observing similar tomacula pathology in sections of sural nerves (Figure 5H-I vs. Figure 1D), but we also demonstrated an overall increase in myelin thickness, leading to a decrease in g ratio (as the fiber diameter remained constant). Note that the tomacula pathology, the decrease in g-ratio, and the increase in myelin thickness were only observed in the sural nerves of homozygote mice. It is interesting that from the many heterozygous breeding schemes that were initiated, 2-3 viable homozygote mice were produced,

indicating that the embryonic lethality was not fully penetrant. The absence of homozygote mice hindered our behavioral studies as only large numbers of wild-type and heterozygote mice could be produced. All behavioral assays testing locomotion were consistent in observing no phenotype between heterozygote PKD1 mutant mice and wild-type mice. These included open field, accelerated rotarod, balance beam, and footprint pattern. Similarly, no sensory phenotype could be detected in the mutant mouse through the von Frey (testing mechano-sensation) and hotplate (testing thermo-sensation) assays. Our data therefore suggest that the mutant mice carrying one mutant allele, unlike the patient, do not exhibit any locomotor deficits. This species discrepancy is rather frequent in the field of peripheral nerve disorders (Kahle et al., 2016; Howard et al., 2002; Ding & Delpire, 2014). For instance, we recently reported the case of a patient with sensorimotor neuropathy and heterozygous gain-of-function mutation in KCC3. While defects could be seen in the peripheral nerves of heterozygote mice, locomotor deficits could only be detected in the homozygote mice (Kahle et al., 2016). Another example of a dominant mutation causing human disease which can be only recapitulated in the homozygote state in the mouse is lamin A, a nuclear envelope protein associated with dilated cardiomyopathy and muscular dystrophy (N195K) (Fatkin et al., 1999l; Mounkes et al., 2005).

One possible mechanism of PKD1 action on peripheral nerve fibers affects the K-Cl cotransporter-3, or KCC3 (Figure 2-13). The cotransporter is intimately involved in the health of peripheral nerve fibers through hydration and/or cell volume. Indeed loss-of function mutations in KCC3 lead to axonal swelling (Byun and Delpire, 2007; Ding and Delpire, 2014) and give rise to sensorimotor neuropathy in both humans and mice (Boettger et al., 2003; Howard et al., 2002).

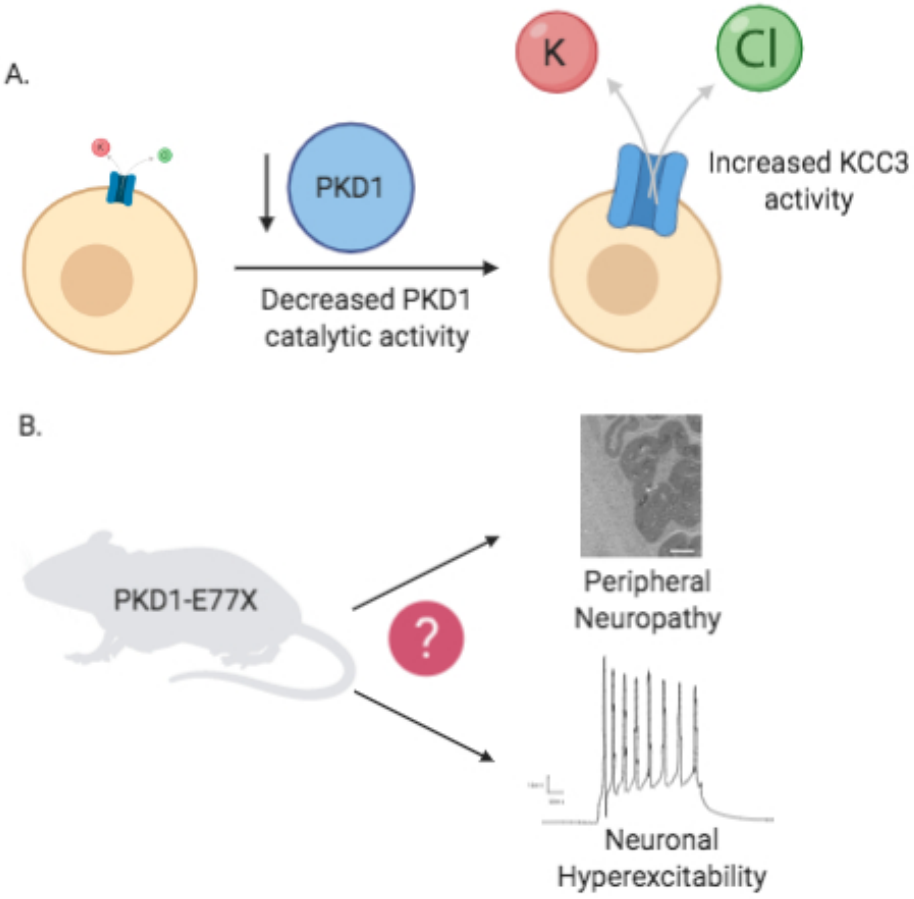

Figure 2-13. Schematic model illustrating the effect of catalytically inactive PKD1 on KCC3 activity, peripheral nerve integrity, and neuronal hyperexcitability. (A) In vitro cell based assays assessing the effect of a catalytically inactive PKD1 resulted in increased KCC3 activity. (B) Generating a translatable mouse model expressing the PKD1-E77X mutation reproduced the patient's peripheral neuropathy phenotype in mice. Mice expressing the PKD1-E77X mutation, displayed neuronal hyperexcitability in the form of increased seizure susceptibility. How and whether PKD1-E77X results in the observed phenotypes, directly through KCC3 activity, or independent of it, remains to be determined.

In addition, a gain-of-function mutation in KCC3 leads to axonal shrinkage (Flores et al., 2019) and peripheral neuropathy in both humans and mice (Kahle et al., 2016). The cotransporter is regulated by phosphorylation through the WNK-SPAK signaling cascade (Garzón-Muvdi et al., 2007; Pacheco-Alvarez and Gamba, 2011). Additional kinases such as PKCθ (Liedtke et al., 2003; Smith et al., 2008) and PKCθ (Li et al., 2004) have also been shown to affect the pathway, so the idea that PKD1 might also modulate the kinase pathway regulating KCC3 is plausible. In fact, Zhang and colleagues (Zhang et al., 2016) identified PKD1 as an interacting partner with KCC3 in a kinomic screen. They showed that knocking down PKD1 via RNAi, reduced the levels of P^{T991}-KCC3 and P^{T1048}-KCC3, suggesting increased KCC3 activity. Our flux data in *Xenopus laevis* oocytes show that expression of a dominant-negative PKD1 kinase yields increased KCC3 flux, consistent with inactivation of the terminal kinase which suppresses KCC3 function. In addition, we showed that the kinase and the cotransporter co-localize at the membrane of transfected HEK293 cells and no indication that cell surface expression was enhanced by expressing the catalytically dead kinase.

It is also possible that the PKD1 mutation results in peripheral nerve disease in a KCC3-independent manner (Figure 2-13). PKD1 has also been identified as a target of protein-activated receptor 2 (PAR(2)) (Amadesi et al., 2009). In response to inflammation and injury, PAR (2) in primary sensory neurons is activated leading to a cascade of phosphorylation involving PKCθ, PKD1, and the transient receptor potential vanilloid (TRPV1) channel. TRPV1 expression is increased following nerve injury, indicating that it plays a role in myelin regeneration and

inflammatory responses (Zakir et al., 2012). Consequently, inactive PKD1 could lead to improper TRPV1 expression resulting in abnormal sensory feedback and peripheral nerve disease.

Inactivation of one PKD1 allele in mice resulted in increased seizure susceptibility as demonstrated by the significant reduction in the latency to seizures following injection of a low dose of kainic acid (Fig. 11A, C) and significant increase in the number of observed jerks (Fig. 11B). Whether this phenotype can also be attributed to a change in KCC3 function is unknown. There are no indications that the KCC3-T991A patient previously reported (Kahle et al 2016), with increased KCC3 activity, experiences epileptic seizures. In addition, possible increases in chemically-induced seizure susceptibility was not tested in KCC3-T991A mice (Kahle et al., 2016). The small increase in KCC3 activity that we measured in *Xenopus laevis* oocytes might not result in long-term changes in volume or ion homeostasis in PKD1 heterozygous mice. Other transport mechanisms might be able to counter the increased KCC3 activity in central neurons of PKD1 heterozygous mice. No difference in water content could be detected in the brain of PKD1 heterozygous mice, compared to wild-type mice (Fig. 11D). While the seizure phenotype needs to be chemically induced in mice, it is spontaneous in the patient which again suggests clear differences in species. Our data thus indicate that humans might be more susceptible to the loss of one PKD1 allele compared to mice.

CHAPTER III

A MUTATION IN THE NA-K-2Cl COTRANSPORTER-1 LEADS TO CHANGES IN CELLULAR METABOLISM

Introduction

The second part of my dissertation work is based on a patient expressing a *de novo* (heterozygous) 11 base pair deletion in *SLC12A2*, the gene encoding the Na-K-2Cl cotransporter-1 (NKCC1) (Delpire et al., 2016). The patient was referred to the Undiagnosed Diseases Program (UDP) at the NIH with symptoms such as decreased energy and fatigue, obstructive apnea, vomiting and dehydration, exercise intolerance, dilated cardiomyopathy in the left ventricle, and seizure like episodes. She also experienced multi-organ dysfunction involving the gastrointestinal, urinary, and exocrine systems. Thus, as the patient's organs kept 'failing', and she showed clear signs of excessive sleeping, hypotonia, and exercise intolerance, clinicians postulated that she suffered from some type of mitochondrial or metabolic syndrome. Clinical tests at age 7 revealed elevated liver and muscle glycogen levels and an increased mitochondrial DNA copy number. On this basis, she was enrolled in the NIH Epi-743 clinical trial at the UDP to improve energy production.

Genomic analysis revealed additional mutations in the *PCNT* (pericentrin) and *FMN2* (formin 2) genes. However, none of the diseases associated with PCNT or FMN2 mutations were observed in the patient. The 11 bp deletion in *SLC12A2* was found in exon 22, leading to a frameshift and

the introduction of a premature stop codon resulting in the truncation of 200 amino acids from the carboxyl-terminal tail of the cotransporter. The mutant was called NKCC1-DFX for the last "intact" residue, aspartic acid residue (D), followed by a new residue, phenylalanine (F), and a stop codon (X) (Delpire et al., 2016). Functional analyses revealed absence of function of the mutant transporter and absence of dominant negative effects in *Xenopus laevis* oocytes and fibroblasts (Delpire et al., 2016). In contrast, a dominant negative effect was observed in epithelial cells with the mutant transporter mistrafficking to the apical and subapical pole of the cells and through dimerization, it carries with it some wild-type transporters to the apical membrane (Koumangoye et al., 2018). Improper trafficking is due to the loss of a dileucine motif located close to the extreme COOH-terminus of the protein (Koumangoye et al., 2019). In addition, improper trafficking was confirmed in a mouse model recapitulating the patient mutation. The mutant mouse exhibited signs of gastrointestinal deficits, including decreased fluid secretion, abnormal mucus release, and bacterial invasion of the epithelial layer, consistent with the patient gastrointestinal issues (Koumangoye et al., 2020).

Detailed analyses of intracellular compartments revealed that the mutant transporter was able to clear the endoplasmic reticulum (ER) and was found principally at the apical membrane, in Rab5-positive apical early endosomes, and in lysosomes (Koumangoye et al., 2019). Because overexpression of truncated transporters often results in their accumulation in the ER (Nezu et al., 2009), we postulated that the mutant transporter to clear the ER might require additional energy. Increased mitochondrial respiration is an adaptive cellular response to protein misfolding in the ER, by reducing ROS accumulation from the ER and promoting cell survival (Knupp et al.,

2019). Alternatively, NKCC1 activity in cells affects intracellular levels of Na^+, K^+, and Cl^- and the Na^+ concentration in particular might affect intracellular Ca2+ levels through plasma membrane Na^+/Ca^{2+} exchangers. Thus, changes in NKCC1 function might lead to changes in mitochondrial function through Na^+ and Ca^{2+} levels. In this paper, we examine the consequences of expressing the mutant NKCC1 cotransporter on mitochondrial function. We show that the fibroblasts from the patient have increased basal mitochondrial respiration rate, as do MDCK cells overexpressing the mutant transporter and mouse fibroblasts natively expressing the defective transporter. In addition, fibroblasts lacking NKCC1 function demonstrate increased hydrogen peroxide production and peroxidase activity, hallmarks of increased oxidative stress. When combined with the observation that proteins involved in the unfolded protein response demonstrate reduced expression, our data suggest that cells expressing the mutant transporter behave like they are deprived of key nutrients or in a state of starvation.

Materials and Methods

Cell lines

Primary human fibroblasts isolated from two healthy individuals and fibroblasts from the NKCC1-DFX patient and immortalized by the Undiagnosed Diseases Program were obtained and cultured in 10-cm dishes in DMEM:F12 medium containing 10% fetal bovine serum and 200 U penicillin + 200 μg/mL streptomycin and kept at 37°C under 95% air, 5% CO2. At the time of experiments, the fibroblasts were used at low (up to 3) passages. The wild-type and mutant NKCC1 plasmids used to transfect MDCK cells were described previously (Delpire et al., 2016). MDCK cells expressing wild-type and mutant cotransporters were grown in selection media

(DMEM supplemented with 5% FBS, 1% penicillin and streptomycin, and 500 µg/ml of Geneticin). Previous studies had shown that the addition of fluorescent markers to the N-terminus of NKCC1 did not affect cotransporter expression, trafficking, and function (Gagnon et al., 2006; Koumangoye, et al., 2018). Primary mouse fibroblasts were isolated from tails of wild-type (WT) mice, mice heterozygous for the NKCC1-DFX mutation ($NKCC1^{WT/DFX}$), and mice homozygous for the NKCC1-DFX mutation ($NKCC1^{DFX/DFX}$), as described below. The generation of these mice were described in a previous paper (Koumangoye et al., 2018).

Seahorse assays

Cells were plated in a 96-well plate at 15 x 10^3 cells per well in Seahorse Assay Media and assessed on the Seahorse XFe 96 Extracellular Flux Analyzer (Agilent Technologies, Santa Clara, CA). The Seahorse assay media was DMEM-based and contained 2 mM of L-glutamine (as L-alanyl-glutamine or GlutaMAX) and no glucose (Agilent Technologies, catalog #102365-100). For the mitochondrial stress test, assay media were supplemented with 10 mM glucose, and cells were sequentially treated with 1 mM oligomycin, 1 mM FCCP, and 0.5 mM of antimycin A and rotenone (all from Agilent Technologies). Basal respiration was quantified as the difference between the last rate measurement before oligomycin injection, and the minimum rate measurement after rotenone/antimycin A injection. Maximum respiration is the difference between the maximum rate measurement after FCCP injection and the minimum rate measurement after rotenone/antimycin A injection. For the glycolysis stress test, cells were sequentially treated with 10 mM glucose (Sigma-Aldrich, St. Louis, MO), 1 mM oligomycin, and 50 mM 2-deoxyglucose (2-DG) (Sigma-Aldrich). Glycolysis was quantified as the difference

between the maximum rate measurement before oligomycin injection and the last rate measurement before glucose injection. Glycolytic capacity was quantified as the difference between the maximum rate measurement after oligomycin injection and the last rate measurement before glucose injection. For both mitochondrial and glycolysis stress tests, some cells were pretreated with 20 M of bumetanide (Sigma-Aldrich). A Bio Rad TC20™ Automated Cell Counter was used to ensure that the same numbers of cells were used in each assay. Statistical analyses were performed using Prism (GraphPad Software, Inc.) using one-way analysis of variance (ANOVA) to determine any statistical significance of differences between the means of two or more independent groups.

Mitochondrial density

Mitochondrial density was measured in primary human fibroblasts isolated from healthy individuals and fibroblasts from the NKCC1-DFX patient; and fibroblasts isolated from WT, $NKCC1^{WT/DFX}$ and $NKCC1^{DFX/DFX}$ mice using the MITO-ID® Green detection kit (Enzo Life Sciences, ENZ-51022-0100). The same numbers of cells were used for each assay by counting cells using a Bio Rad TC20™ Automated Cell Counter. Cells were stained with 0.33 ul/ml of MITO-ID® Green and 0.25 ul/ml of Hoescht 33342 Nuclear Stain. Cells were incubated in the dark for 30 minutes at 37°C in 5% CO_2 in phenol-red free DMEM with 4.5 g/L D-Glucose, no glutamine or pyruvate. Mean fluorescence intensity of each cell was detected using a 5-laser LSRll flow cytometer. The FlowJo software package was utilized to analyze the mean fluorescence intensity of each sample. Cell sorting within FlowJo allowed isolation of fibroblasts from cell debris and dead cells. The software plots the side scatter of single cells (SSC) based on granularity (Y-axis of Figure 1A) as a

function of the level of FITC fluorescence (FITC on X-axis) within each cell. Single cell mitochondrial density was obtained from the level of fluorescence intensity from each cell. Statistical analysis was performed using one-way analysis of variance (ANOVA).

Generation of the NKCC1-DFX mouse

Two attempts were made to generate the NKCC1-DFX allele. In the first attempt, a 20 bp sequence (AGAATACTATAGATGTCTGG) located in exon 22 of mouse Slc12a2, and followed by TGG (coding for the second of two adjacent tryptophan residues) as proto-spacer adjacent motif, was selected to create a target-specific guide RNA molecule. The sequence flanked by BbsI sites was ligated in pX330, a vector expressing the guide RNA under a strong U6 promoter and cas9 under a hybrid chicken β-actin (Cbh) promoter. The vector was injected alongside a 195 base repair oligonucleotide into 961 mouse embryos. The repair oligo contained 91 base homology arms, a codon substituting valine residue 1020 to phenylalanine, a unique ClaI restriction site, and a few additional third-base mutations to introduce two stop codons and prevent targeting of cas9 to the repair DNA. Out of 961 embryos injected, 687 were transferred to 30 pseudo-pregnant females to generate 110 pups. At weaning, genotyping was done by amplifying a 421 bp fragment followed by sequencing. A large number of mutant alleles were produced, but none of them carried the designed mutation. In our second and successful attempt, the 20 bp target sequence was shifted three residues for the protospacer adjacent motif (PAM) to encode the first tryptophan residue (GGAAGAATACTATAGATGTC, boxed in Fig.3-2A), and the 163 repair oligonucleotide consisted of different size homology arms, 11 bases deleted as in the patient, and a third-base mutation to introduce a unique ClaI restriction site. Twenty pups were generated out of 213 embryos injected and 142 embryos transferred to 6 pseudo-pregnant

females. Again, a large number of mutant alleles were generated, including the designed DFX allele (Figure 3-2C).

Isolation of mouse tail fibroblasts

The generation of the NKCC1-DFX mouse is stated above. Experiments with mice were approved by the Vanderbilt University Medical Center Institutional Animal Care and Use Committee. To isolate fibroblasts, the tip of the tail (< 5 mm) of a mouse was minced with a sharp razor blade in 35-mm tissue culture dish containing 2 ml DMEM supplemented with 10 mM HEPES, penicillin/streptomycin, and 2 mg/ml collagenase D. The 2 ml medium with minced tissue was then added to 3 ml identical medium in a 15 ml conical tube, rotated overnight at room temperature. The next day, 5 ml of complete medium (DMEM/F12 + 10% fetal bovine serum + penicillin/streptomycin) was added to the tube, which was mixed by inversion, and the large undigested tissue fragments were allowed to sediment to the bottom of the tube by gravity (20-30 sec). The majority of the supernatant was then pipetted out, placed in a fresh tube, and spun at 900 rpm for 5 min. The supernatant was discarded and the pellet was resuspended into 500 ul of complete medium, which was plated in a 24-well plate for expansion. The total number of passages did not exceed 3 passages.

Transmission electron microscopy

Pelleted human fibroblasts and mouse intestinal sections were fixed with 2.5% glutaraldehyde in 0.1 M sodium cacodylate buffer, in water for 1 hour at room temperature (RT) and then at 4°C overnight. The Vanderbilt Electron Microscopy core further processed the fibroblast samples by washing them and fixing in 1% osmium tetroxide solution for 1 hour at RT

and then with 0.5% osmium for 24 hours. The tissue samples underwent a series of ethanol dehydration steps (50% for 5 min, 75% for 15 min, 95% two times for 15 min, 100% three times for 20 min) before they were embedded in Spurr resin at 60°C for 24 to 48 hours. Semi-thin sections (500 nm) were stained with toluidine blue and examined for positioning. Ultra-thin sections (80 nm) were then stained with uranyl acetate and lead citrate and placed on copper grids. Images were observed using a Philips/FEI T-12 transmission electron microscope

Horseradish peroxidase assay

Peroxidase activity in cell lysates was determined using the Amplex® red hydrogen peroxide/peroxidase assay kit (Invitrogen, Carlsbad, CA). Briefly, fibroblasts from WT, $NKCC1^{WT/DFX}$ and $NKCC1^{DFX/DFX}$ mice were lysed with a hypotonic lysis buffer (10 mM Tris·HCl pH 7.5) supplemented with protease inhibitors (Roche Applied Science, Indianapolis, IN), and diluted in 1x reaction buffer composed of 28 ml of 0.25 M sodium phosphate at pH 7.4, to a final protein concentration of 5 g/ l, measured by Biorad protein assay. 50 ul H_2O_2 mixture (4.45 ml of 1x Reaction Buffer + 500 20 mM H_2O_2 + 50 Amplex® Red reagent) were then added to 50 ul cell lysates placed into individual wells of a 96-well plate. The same amount of mixture was added to 50 l of a standard curve containing 0, 0.25, 0.5, 1, and 2 mU/ml horse radish peroxidase. Reactions, protected from light, were incubated at RT for 30 min before reading the fluorescence using a microplate reader with excitation at 530–560 nm and emission at 590 nm. Readings were corrected for background fluorescence by subtracting the values derived from the no-HRP control well from the raw fluorescence values. Statistical analysis was performed using one way analysis of variance (ANOVA).

Hydrogen Peroxide Assay

The amount of hydrogen peroxide in cells was determined using the same red hydrogen peroxide/peroxidase assay kit (Invitrogen). Supernatant was obtained from fibroblasts of WT, $NKCC1^{WT/DFX}$ and $NKCC1^{DFX/DFX}$ mice. 50 ul HRP mixture (4.85 ml of 1x Reaction Buffer + 100 ul HRP stock (10 U/ml) + 50 ul Amplex® Red reagent) were then added to 50 ul of sample placed into individual wells of a 96-well plate. The same amount of mixture was added to 50 ul of a standard curve containing 0, 2, 4, 6, 8, and 10 mM H_2O_2. Reactions, protected from light, were incubated at RT for 30 min before reading the fluorescence using a microplate reader with excitation at 530–560 nm and emission at 590 nm. Readings were corrected for background fluorescence by subtracting the values derived from the no-HRP control wells from the raw fluorescence values. Statistical analysis was performed using one way analysis of variance (ANOVA).

Quantitative reverse transcription PCR (RT-qPCR)

Expression of ER-stress markers BiP, Xbp1 and Dcnajc3 was quantitated by RT-qPCR. Fibroblasts were isolated from WT, $NKCC1^{WT/DFX}$ and $NKCC1^{DFX/DFX}$ mice and 20-30 mg tissue was lysed and processed using the RNeasy mini kit (Qiagen). RNA quality and quantity were assessed by measuring absorbance at 260, 280, and 320 nm. Reverse-Transcription was performed by incubating 1 ug RNA with random hexamers, dNTPs, and SuperScript II (Invitrogen), for 1 hour at 37°C, followed by denaturation for 5 min at 95°C. Quantitative PCR reactions contained SYBRTM Green PCR master mix (Applied Biosystems, Foster City, CA), each primer at 40 nM and 1 ul cDNA. mRNA expression is represented as the fold change normalized to WT, calculated using the delta Ct method. Statistical analysis was performed using one way analysis of variance (ANOVA).

Primers (mouse genes):

Target	Forward primer (5'-3')	Reverse primer (5'-3')
Xbp1	TCAAATGTCCTTCCCCAGAG	AAAGGGAGGCTGGTAAGGAA
Hspa5(BiP)	TGCAGCAGGACATCAAGTTC	TTTCTTCTGGGGCAAATGTC
Dnajc3	GACAGCTAGCCGACGCCTTA	GTCACCATCAACTGCAGCGT
Slc12a2 (NKCC1)	AGTGGACACCACCAGCAGTACTA	GTGTGCCGGTAGTGGTCGAT
Gapdh	AGGTCGGTGTGAACGGATTTG	GGGGTCGTTGATGGCAACA

Results

Fibroblasts isolated from the NKCC1-DFX patient show increased mitochondrial density

Laboratory tests conducted on the NKCC1-DFX patient muscle cells identified an increase in mitochondrial DNA copy number, compared to normal range (Delpire et al., 2016). Clinical cases of patients suffering from mitochondrial diseases also exhibit an increase in mitochondria number (Pfeffer & Chinnery, 2013). To confirm that the increase in mitochondrial DNA copy number found in the UDP patient was due to the number of mitochondria, we quantified mitochondrial density in fibroblasts isolated from the patient, compared to fibroblasts from two healthy individuals (Figure 3-1A, B). Fibroblasts from the NKCC1-DFX patient demonstrated an increase in mitochondrial density compared to control human fibroblasts, confirming the patient lab reports. To assess whether this increase was due to the NKCC1 mutation, we used fibroblasts isolated from a mouse model that recapitulates the patient 11 bp deletion in the SLC12A2 (NKCC1) gene. The mice were backcrossed for several generations to C57BL/6J mice to ensure that possible *off target* events due to CRISPR/cas9 were eliminated through breeding (Figure 3-2

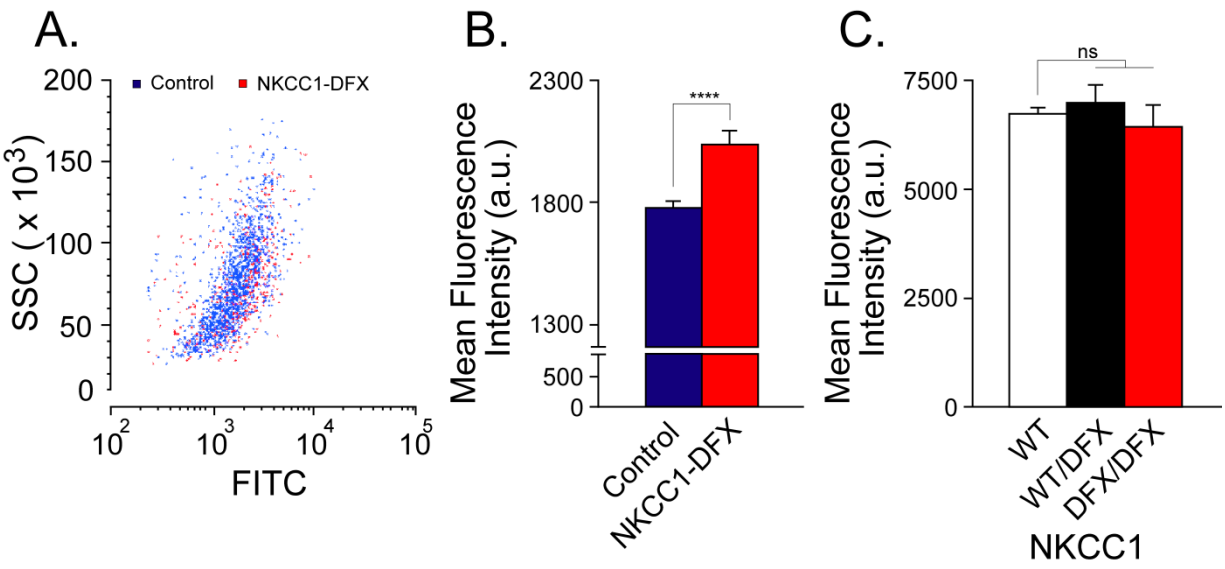

Figure 3-1. Human fibroblasts expressing NKCC1-DFX have increased mitochondrial density. (A) Flow cytometry analysis of mitochondria in fibroblasts stained with MITO-ID green in control fibroblasts (blue) and NKCC1-DFX fibroblasts (red). Y-axis = Side Scatter (SSC) of single cells; X-axis = level of FITC fluorescence (FITC) from mitochondria. (B) Mean fluorescence intensity of mitochondria in control (n = 1440 cells) and NKCC1-DFX (n = 523 cells) fibroblasts, 3 biological replicates. Higher mitochondrial density observed in NKCC1-DFX fibroblasts. Unpaired t-test, ****p < 0.0001. (C) Mean fluorescence intensity of mitochondria from WT (n = 30,000 cells), $NKCC1^{WT/DFX}$ (n = 30,000 cells) and $NKCC1^{DFX/DFX}$ (n = 20,000 cells) fibroblasts, one-way ANOVA, P > 0.05, ns = non-significant.

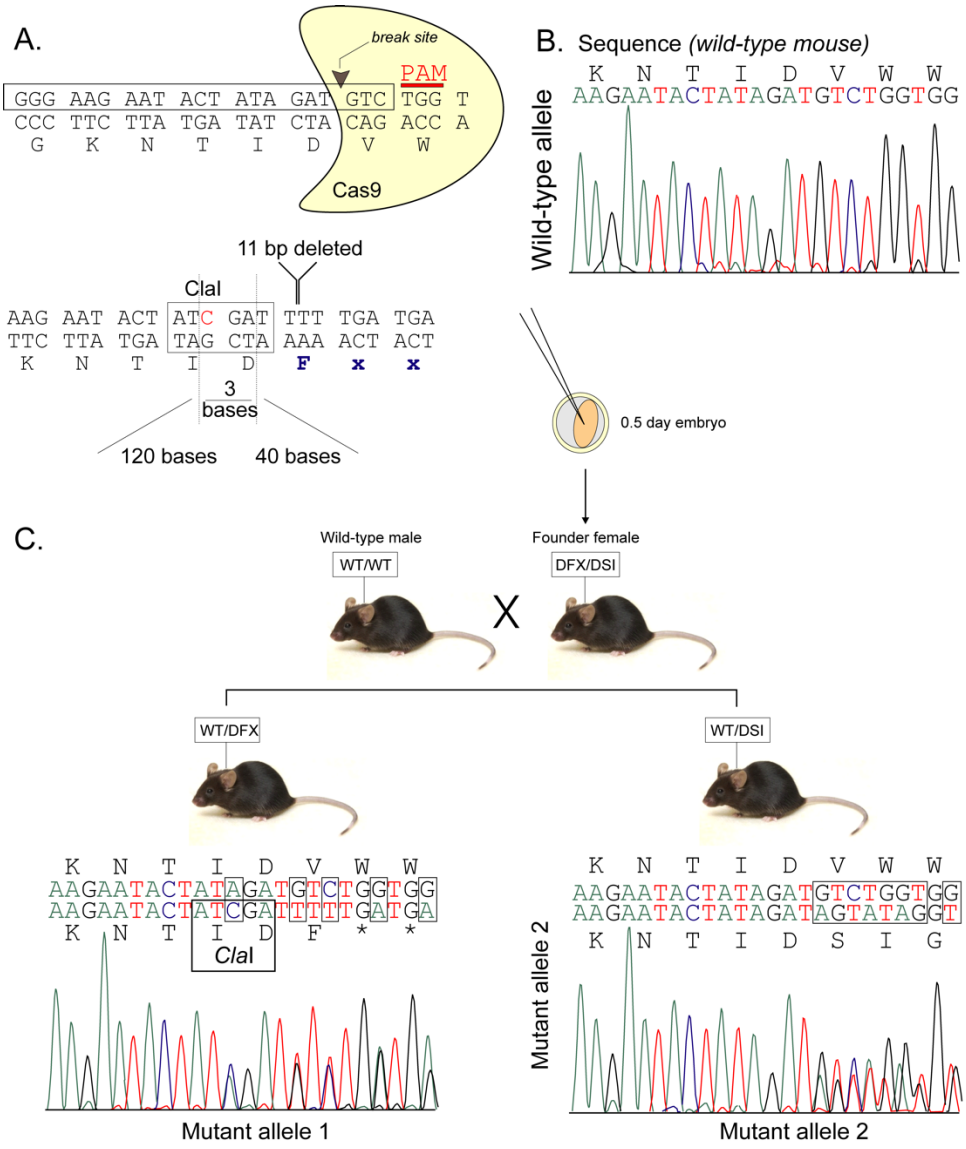

Figure 3-2. Generation of the CRISPR/cas9 NKCC1-DFX mouse. (A) Targeting design of the Slc12a2 allele at exon 22 are shown. Boxed sequence on the forward strands were used to guide cas9. Guide sequences are followed by TGG as protospacer adjacent motif (PAM) sequences. Location of the DNA break sites is indicated by arrowheads. Design of DNA repair shows arms of recombination surrounding 3 bp mutated sequences. A ClaI site is inserted to facilitate genotyping. (B) chromatograph showing sequence of wild-type allele. (C) Chromatographs showing separation of the two mutant alleles in the progeny of the unique NKCC1-DFX female. Mutant allele 1 alongside a wild-type allele reveals exact mutations as designed in (A). Mutant allele 2 alongside a wild-type allele reveals DNA repair through unspecific insertion/deletion. NKCC1, Na^+-K^+-$2Cl^-$ cotransporter-1; Slc12a2, solute carrier family 12, member 2.

). We measured mitochondrial density in fibroblasts isolated from WT, NKCC1$^{WT/DFX}$, and NKCC1$^{DFX/DFX}$ mice and observed no difference between the groups (Figure 3-1C). Thus, mutation of NKCC1 or loss of NKCC1 was not enough to explain the patient's increase in mitochondria number.

Fibroblasts isolated from the NKCC1-DFX patient demonstrate deficits in energy homeostasis

Since an increase in mitochondrial density was observed in the NKCC1-DFX patient fibroblasts, we were interested in investigating whether this increase affected mitochondrial function and glycolysis. Fibroblasts isolated from the patient as well as from two healthy individuals were subjected to seahorse mitochondrial and glycolysis stress tests. The seahorse mitochondrial stress & glycolysis stress tests measure mitochondrial function in cells through the measurement of key parameters such as oxygen consumption rate (OCR) or extracellular acidification rate (ECAR), respectively. The patient fibroblasts demonstrated elevated levels of basal and maximal mitochondrial respiration, as quantified by OCR (Figure 3-3A, 3-3B). By measuring the rate of extracellular acidification, we show that the patient fibroblasts demonstrated a significant decrease in glycolysis when compared to control fibroblasts (Figure 3-3C, D). These data indicate that the increased respiration is fueled by a substrate other than glucose.

MDCK cells expressing the non-functional NKCC1 mutation also exhibit increased mitochondrial respiration but no change in glycolysis

Since the patient fibroblasts carry additional mutations, we needed to explore more directly the role of NKCC1 on mitochondrial respiration and glycolysis. In our previous study of

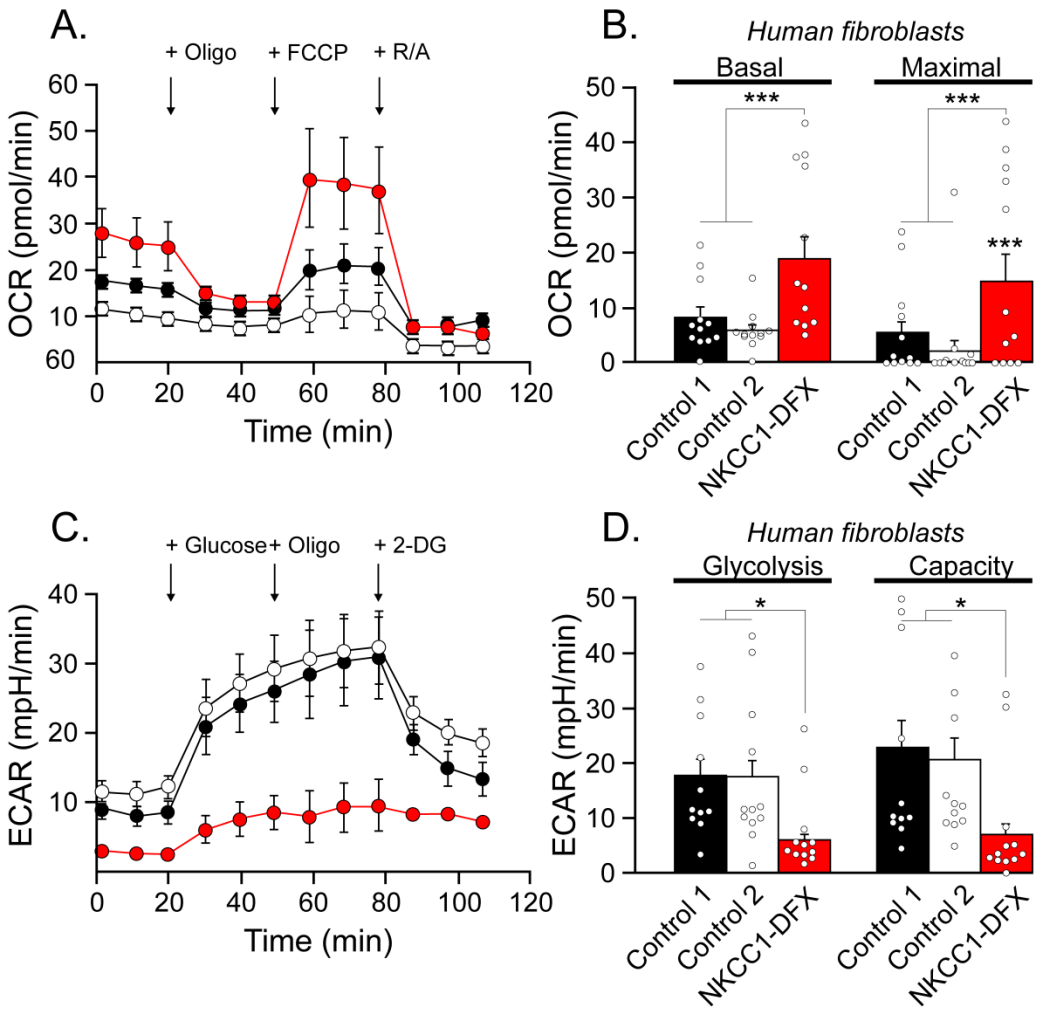

Figure 3-3. Human fibroblasts expressing NKCC1-DFX result in elevated mitochondrial respiration and decreased glycolytic respiration. (A) Seahorse assay mitochondrial stress test results for oxygen consumption rate (OCR) of fibroblasts isolated from healthy individuals (black n = 12, and white n = 12) and patient expressing NKCC1-DFX (red n = 12) at 3.5 x 10^4 cells/well, in real time under basal conditions in response to mitochondrial inhibitors as indicated (oligo = oligomycin injected at 20 min, FCCP injected at 60 min, AA&R = Antimycin and Rotenone injected at 80 min). (B) Basal respiration is the value just before oligomycin injection, and maximal respiration is the highest value after FCCP injection. NKCC1-DFX fibroblasts result in elevated basal and maximal respiration. (C) Cellular glycolytic activity as shown by the Seahorse assay glycolysis stress test in fibroblasts isolated from healthy individuals (n = 12), and patient expressing NKCC1-DFX (n = 12). Extracellular acidification rate (ECAR) was measured in real time under basal conditions in response to sequential use of glucose, oligomycin (to block mitochondrial respiration and force the cells to rely on glycolysis for ATP production), and 2-deoxyglucose (2-DG), a glucose analog and inhibitor of glycolytic ATP production). Glucose is injected at 20 min, oligomycin at 60 min, and 2-DG at 80 min. (D) Quantification of glycolysis (the value after glucose injection) and glycolytic capacity of (the value after oligomycin injection) (C). Lower glycolysis in NKCC1-DFX fibroblasts. One-way ANOVA *p < 0.05, ***p < 0.001, ****p < 0.0001.

NKCC1 polarity and trafficking in epithelial cells, we created MDCK cell lines overexpressing GFP-tagged wild-type and GFP-tagged NKCC1-DFX transporters (Koumangoye et al., 2018). The presence of the fluorescent tags did not affect expression, trafficking, and function of the transporter but was useful in visualizing the location of the transporter within cells. We used these cells to conduct mitochondrial stress tests and assess basal respiration and maximal respiration. Cells expressing NKCC1-DFX showed increased basal and maximal respiration relative to untransfected cells, whereas cells overexpressing wild-type NKCC1 did not exhibit such an increase (Figure 3-4A, B). These data indicate that the presence of the mutant transporter affected mitochondrial respiration and it was not a result of protein overexpression as this was not observed with overexpression of the wild-type cotransporter. There was no change in glycolysis, as demonstrated from the similar extracellular acidification rates following an increase in the glucose concentration (Figure 3-4C, D).

Bumetanide treatment does not affect basal mitochondrial respiration or glycolysis

As the patient fibroblasts have reduced NKCC1 activity as well as expression of a mutant protein, we assessed whether the increase in mitochondrial respiration could be attributable to one or both of these factors. Experiments with transfected MDCK cells indicate that expression of the mutant transporter leads to increased mitochondrial respiration. Here, we use a pharmacological approach to assess mitochondrial respiration in MDCK cells treated with a NKCC1-specific inhibitor. Native untransfected MDCK cells were treated with DMSO (vehicle for bumetanide) or DMSO + 20 μM of bumetanide. Upon addition of bumetanide, we observed no change in basal respiration, but a significant increase in maximal respiration, similar to the mitochondrial respiration of MDCK cells overexpressing NKCC1-DFX protein (Figure 3-5 A, B).

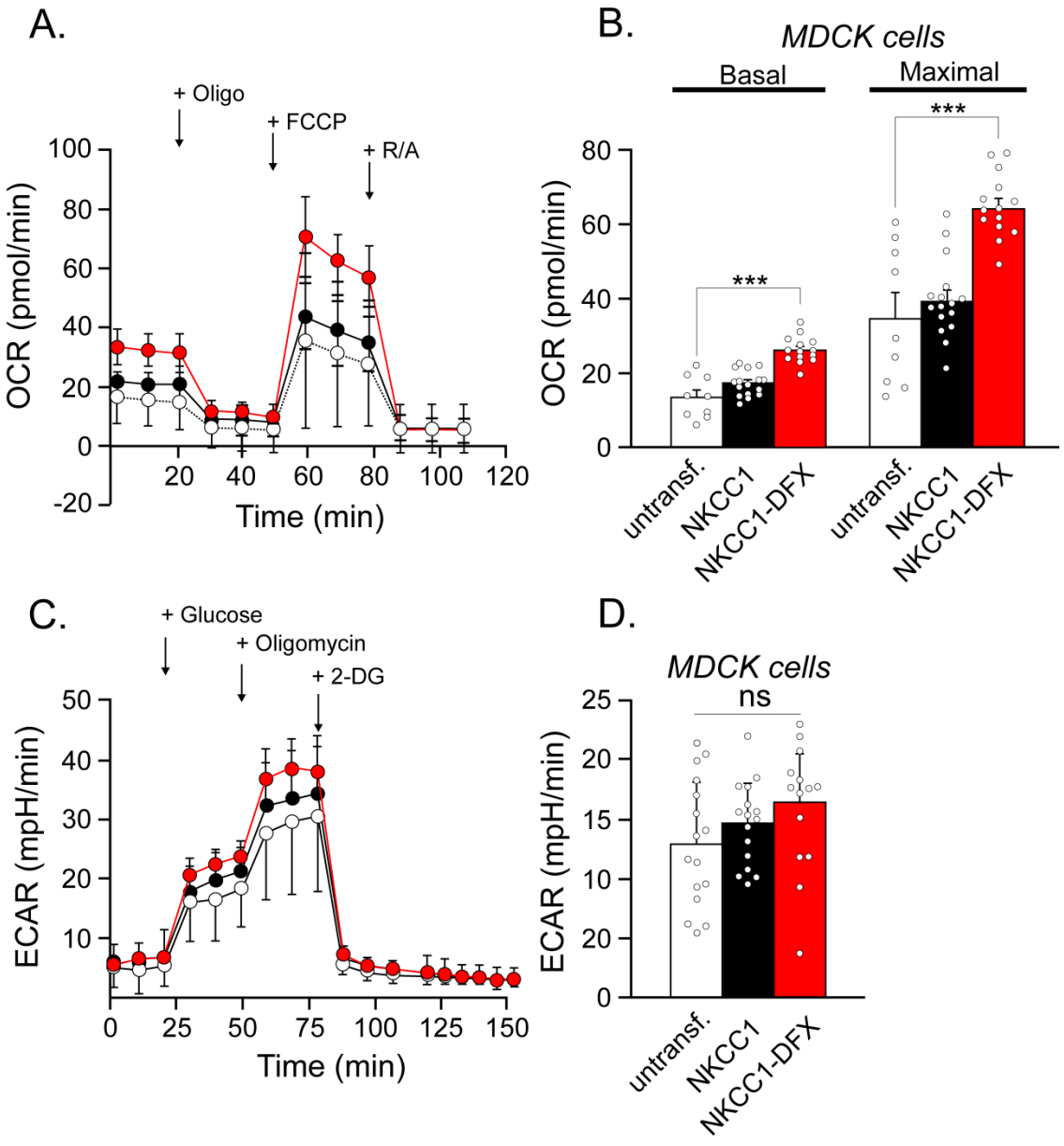

Figure 3-4. MDCK cells expressing transfected NKCC1-DFX display increased mitochondrial respiration. (A) Seahorse assay mitochondrial stress test shows OCR in untransfected MDCK cells (black, n = 10) and MDCK cells transfected with NKCC1-DFX (red, n = 29). (B) Quantification of basal and maximal respiration revealed elevated basal and maximal respiration in MDCK cells transfected with NKCC1-DFX. (C) Seahorse assay glycolysis stress test in untransfected MDCK cells (white, n = 16), MDCK cells over-expressed with WT NKCC1 (black, n = 16), and MDCK cells expressing NKCC1-DFX (n = 14). (D) Quantification of glycolysis and glycolytic capacity of (C), demonstrated no significant difference in glycolysis between groups. One-way ANOVA, ***$p < 0.001$.

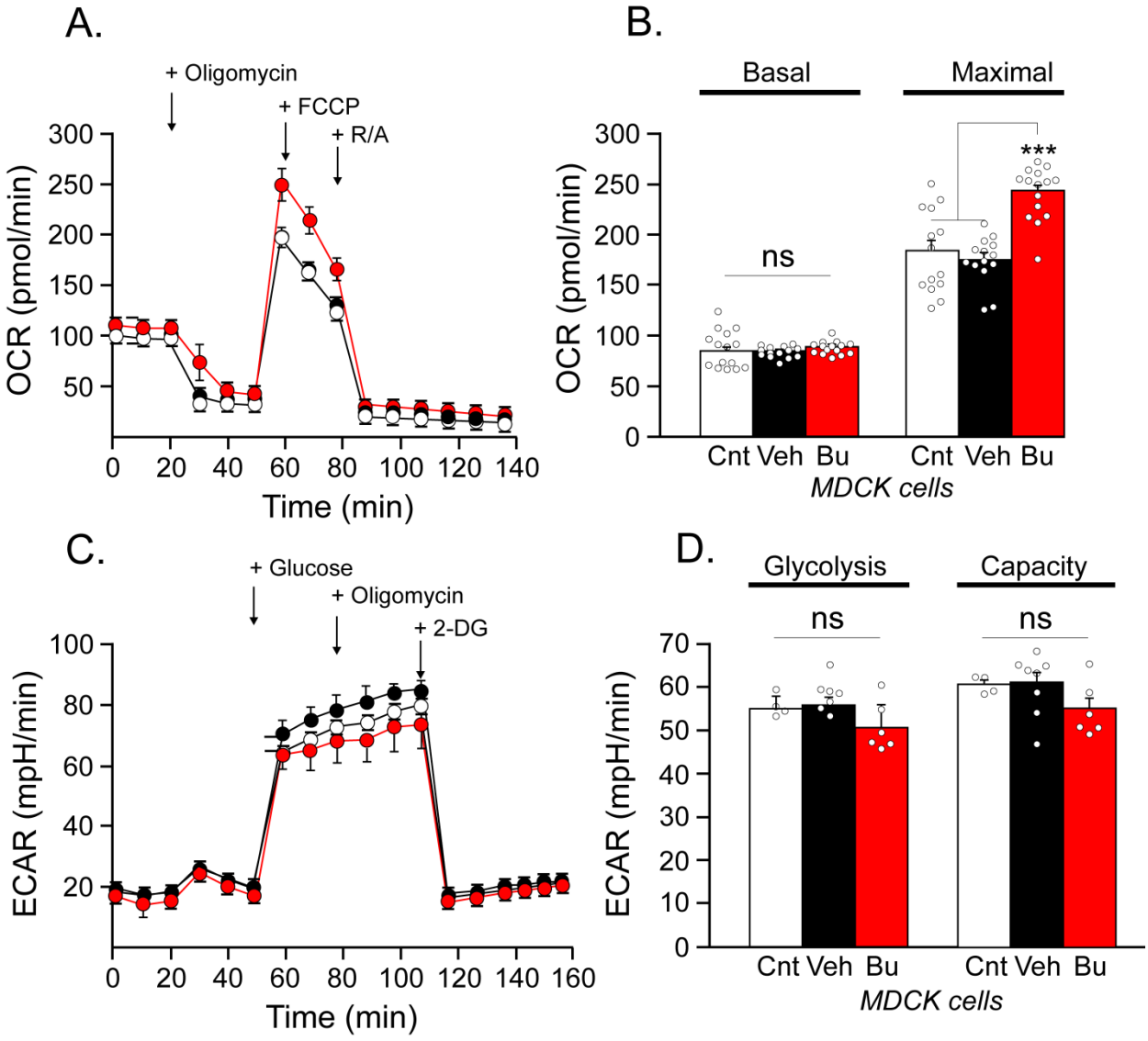

Figure 3-5. Bumetanide leads to an increase in mitochondrial respiration capacity in MDCK cells. (A) Seahorse assay mitochondrial stress test shows OCR in native untreated MDCK cells (white, n = 14), treated with DMSO as vehicle (black, n = 14), and treated with 20 M bumetanide (red n = 15). (B) Quantification of basal respiration and maximal respiration demonstrated an increase in basal but not maximal respiration of cells treated with bumetanide. (C) Seahorse assay glycolysis stress test results of untransfected and untreated MDCK cells (white, n = 4), treated with DMSO as vehicle (black, n = 8), and treated with 20 M bumetanide (red, n = 6). (D) Quantification of glycolysis and glycolytic capacity. One-way ANOVA, ***$p < 0.001$.

Absence of a change in basal respiration indicates that the cells under bumetanide treatment have no need for additional ATP. The increase in maximal respiration suggests that substrate availability was increased or substrate oxidation upstream of the proton circuit was affected upon addition of bumetanide. The mechanism is unknown. Application of bumetanide also did not affect the rate of acidification induced by addition of glucose, i.e. glycolytic respiration (Figure 3-5C, D).

Fibroblasts isolated from NKCC1$^{WT/DFX}$ and NKCC1$^{DFX/DFX}$ also show increased mitochondrial respiration

To further establish the connection between the cotransporter and mitochondrial respiration we also utilized fibroblasts isolated from a mouse model that reproduced the unique mutation in NKCC1 without carrying the additional mutations of the patient (Delpire et al., 2016). Mitochondrial stress tests were performed on fibroblasts isolated from WT, NKCC1$^{WT/DFX}$, and NKCC1$^{DFX/DFX}$ mice. Fibroblasts expressing mutant NKCC1-DFX also showed increased basal respiration and maximal respiration compared to fibroblasts isolated from wild-type mice (Figure 3-6). This demonstrated increase was consistent with the increase in mitochondrial respiration that we observed in human fibroblasts. These results therefore suggest that NKCC1-DFX is solely responsible for the increase in mitochondrial respiration observed in the NKCC1-DFX patient fibroblasts.

Mouse fibroblasts expressing NKCC1DFX/DFX have increased hydrogen peroxide levels and peroxidase activity

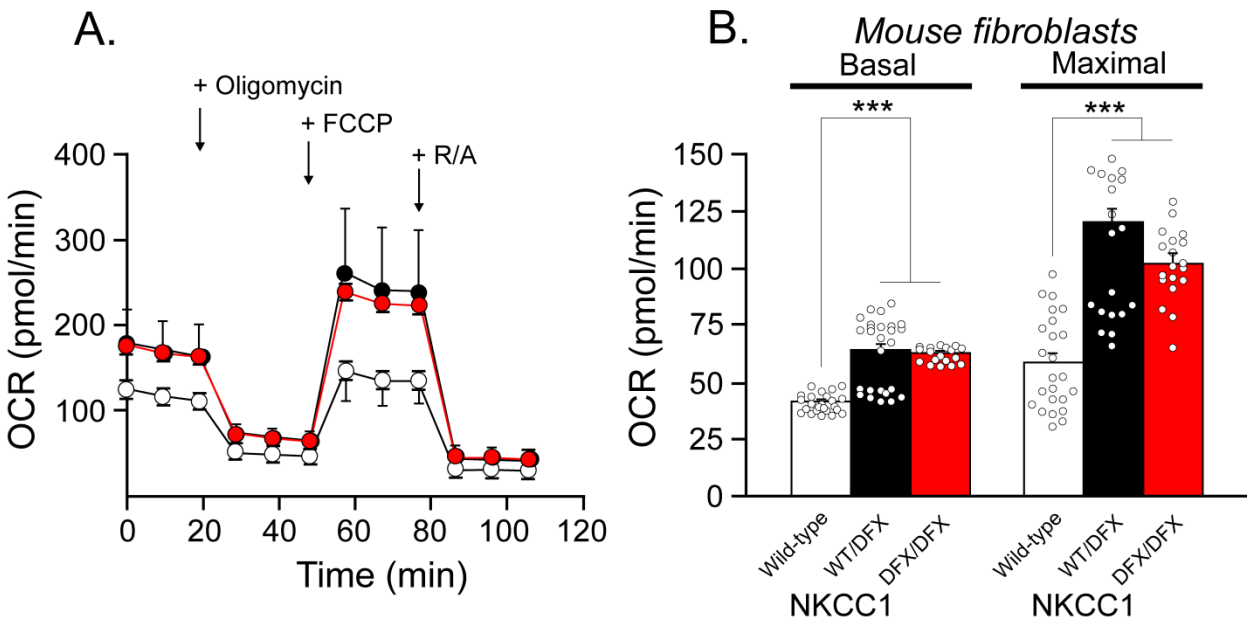

Figure 3-6. NKCC1$^{WT/DFX}$, and NKCC1$^{DFX/DFX}$ mouse fibroblasts display elevated mitochondrial respiration. (A) Seahorse assay mitochondrial stress test shows OCR in fibroblasts isolated from WT (white, n = 24), NKCC1$^{WT/DFX}$ (black, n = 26), and NKCC1$^{DFX/DFX}$ (red, n = 19) mice. (B) Quantification of basal and maximal respiration display elevated basal and maximal respiration in mouse fibroblasts expressing either one or two copies of NKCC1-DFX. One-way ANOVA ***p < 0.001, n.s. = non-significant.

An increase in mitochondrial respiration leads to changes in key cellular functions, including release of reactive oxygen species (ROS) (Brown, 1992, 1995; Chance & Williams, 1955; Murphy, 2009; Wallace et al., 2010). Reactive oxygen species take several forms, such as hydroxyl radicals, superoxide (O_2.-), hydrogen peroxide (H_2O_2) (Cadenas & Davies, 2000). Excess hydrogen peroxide in cells can lead to an increase in hydroxyl radicals. In turn, peroxidase catalyzes the oxidation of organic compounds using hydrogen peroxide. This chemical reaction can be utilized to investigate the level of hydrogen peroxide present in cells. Both hydrogen peroxide levels and peroxidase activity were measured in fibroblasts isolated from WT, NKCC1$^{WT/DFX}$, and NKCC1$^{DFX/DFX}$ (Figure 3-7). Fibroblasts expressing NKCC1$^{DFX/DFX}$ showed an increase in hydrogen peroxide levels as well as peroxidase activity compared to WT and NKCC1$^{WT/DFX}$ fibroblasts. These results indicate that the increase in hydrogen peroxide levels and peroxidase activity cannot be attributed to increased mitochondrial respiration as it was not observed in cells expressing one copy of the mutant transporter, while these cells demonstrated similar increase in mitochondrial respiration.

The NKCC1-DFX mutant allele decreases expression of ER stress proteins

In a previous study, we showed that the NKCC1-DFX protein is cleared from the ER and accumulated in the lysosome (Koumangoye et al., 2019). Although the mutant protein was seemingly cleared from the endoplasmic reticulum (ER), we sought to investigate whether its transit through the endoplasmic reticulum led to ER stress. Typically, accumulation of misfolded proteins in the ER causes ER stress leading to the increased expression of a variety of protein involved in the unfolded protein response (UPR) pathway (Bertolotti et al., 2000; Schröder &

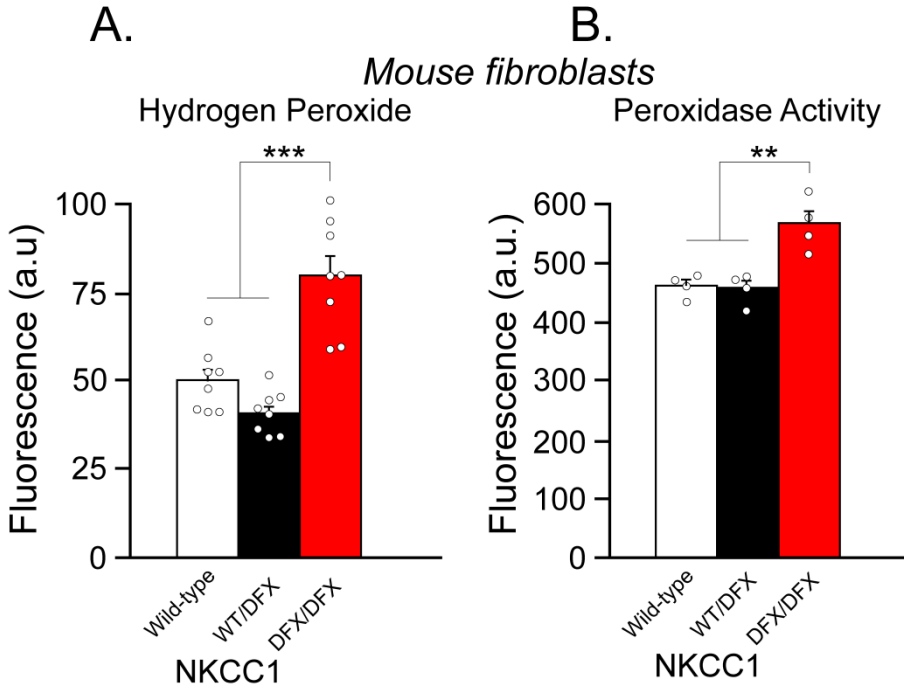

Figure 3-7. NKCC1$^{DFX/DFX}$ mouse fibroblasts elicit increase in hydrogen peroxide levels and in peroxidase activity. (A) Fluorescence intensity of extracellular hydrogen peroxide of fibroblasts isolated from WT (white, n = 4 wells), NKCC1$^{WT/DFX}$ (black, n = 4 wells), and NKCC1$^{DFX/DFX}$ (red, n = 4 wells) mice. (B) Fluorescence intensity of intracellular peroxidase activity in fibroblasts isolated from WT (white, n = 4 wells), NKCC1$^{WT/DFX}$ (black, n = 4 wells), and NKCC1$^{DFX/DFX}$ (red, n = 4 wells) mice. NKCC1$^{DFX/DFX}$ mouse fibroblasts demonstrated elevated hydrogen peroxide and peroxidase activity. One-way ANOVA, **p < 0.01, ***p < 0.001.

Kaufman, 2005; Walter & Ron, 2011; Yoshida et al., 1998). These proteins are tasked with relieving ER stress through a variety of means. Some proteins serve as chaperones where they assist with proper folding; others clear mis-folded protein aggregates from the ER and send them to the proteasome for degradation; while others prevent further protein synthesis to prevent additional aggregation in the ER (Hetz & Saxena, 2017). The proteins involved in the UPR can be utilized as markers for ER stress, and an elevation of expression in any one or all of these proteins is indicative of ER stress (Estébanez et al., 2018). We analyzed the level of mRNA expression of BiP, Dnajc3, and Xbp1 in fibroblasts isolated from WT, NKCC1$^{WT/DFX}$, and NKCC1$^{DFX/DFX}$ mice (Figure 3-8). Interestingly, we observed a decrease in mRNA expression of BiP, Dnajc3 and Xbp1 in NKCC1$^{WT/DFX}$ and NKCC1$^{DFX/DFX}$ mouse fibroblasts, compared to wild-type fibroblasts.

Expression of NKCC1-DFX alters the morphology of mitochondria in intestinal cells

The effect of NKCC1-DFX on mitochondrial respiration led to the investigation of mitochondrial morphology in cells expressing NKCC1-DFX. We utilized transmission electron microscopy to analyze the morphology of mitochondria in tissues from wild-type, NKCC1$^{WT/DFX}$, and NKCC1$^{DFX/DFX}$ mice. As indicated in Figure 3-9, we observed the presence of large dense inclusion bodies in the colon of both mutant mice, compared to wild-type mice. Only droplets of very small sizes were observed in the colon of wild-type mice. Quantitation revealed a significant increase in the number of droplets in mitochondria from heterozygote mice (108/382 mitochondria, 15 fields, 3 mice, $P < 0.01$) and homozygote mice (125/356, 15, 3, $P < 0.001$), compared to mitochondria from wild-type mice (59/447, 15, 3). Note that these structures were not present in the mitochondria of fibroblasts isolated from the NKCC1-DFX patient or healthy

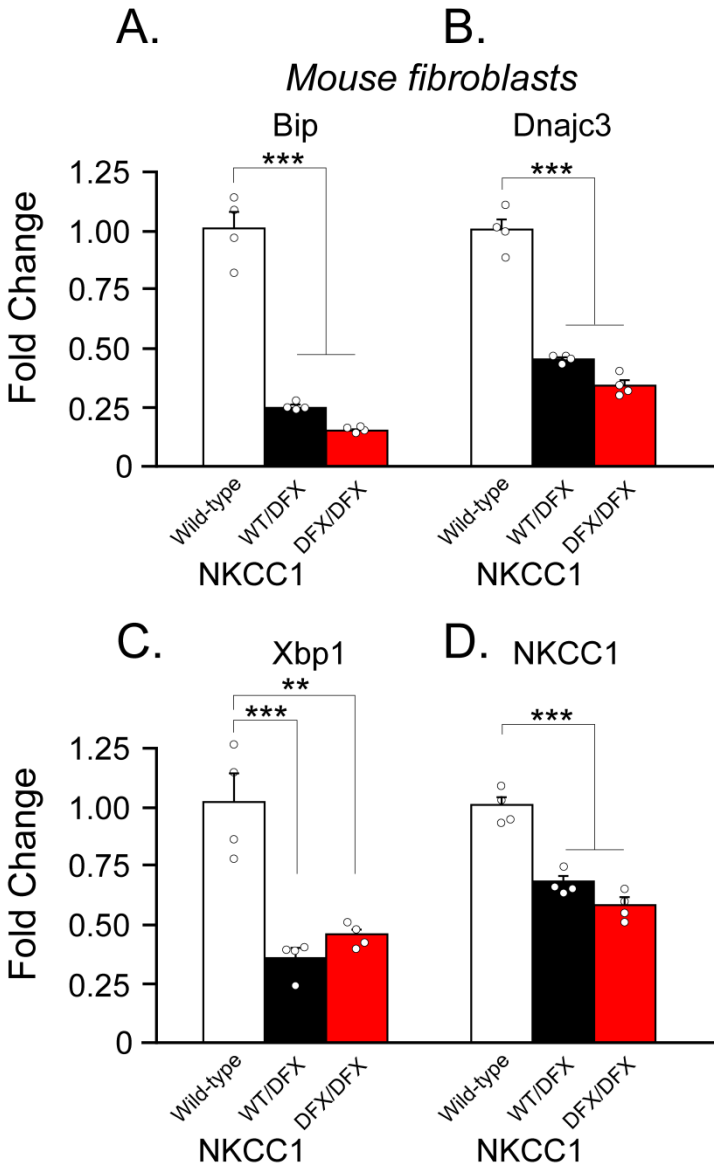

Figure 3-8. mRNA expression of ER stress markers and NKCC1 are decreased in NKCC1$^{WT/DFX}$, and NKCC1$^{DFX/DFX}$ fibroblasts. (A-C) Fold change of mRNA expression levels in fibroblasts of WT (white, n = 4), NKCC1$^{WT/DFX}$ (black, n = 4), and NKCC1$^{DFX/DFX}$ (red, n = 4). (D) mRNA expression of NKCC1 in same genotypes. One-way ANOVA **p < 0.01, ***p < 0.001, n.s. = non-significant. Fold change is normalized to WT and is calculated by the delta Ct method.

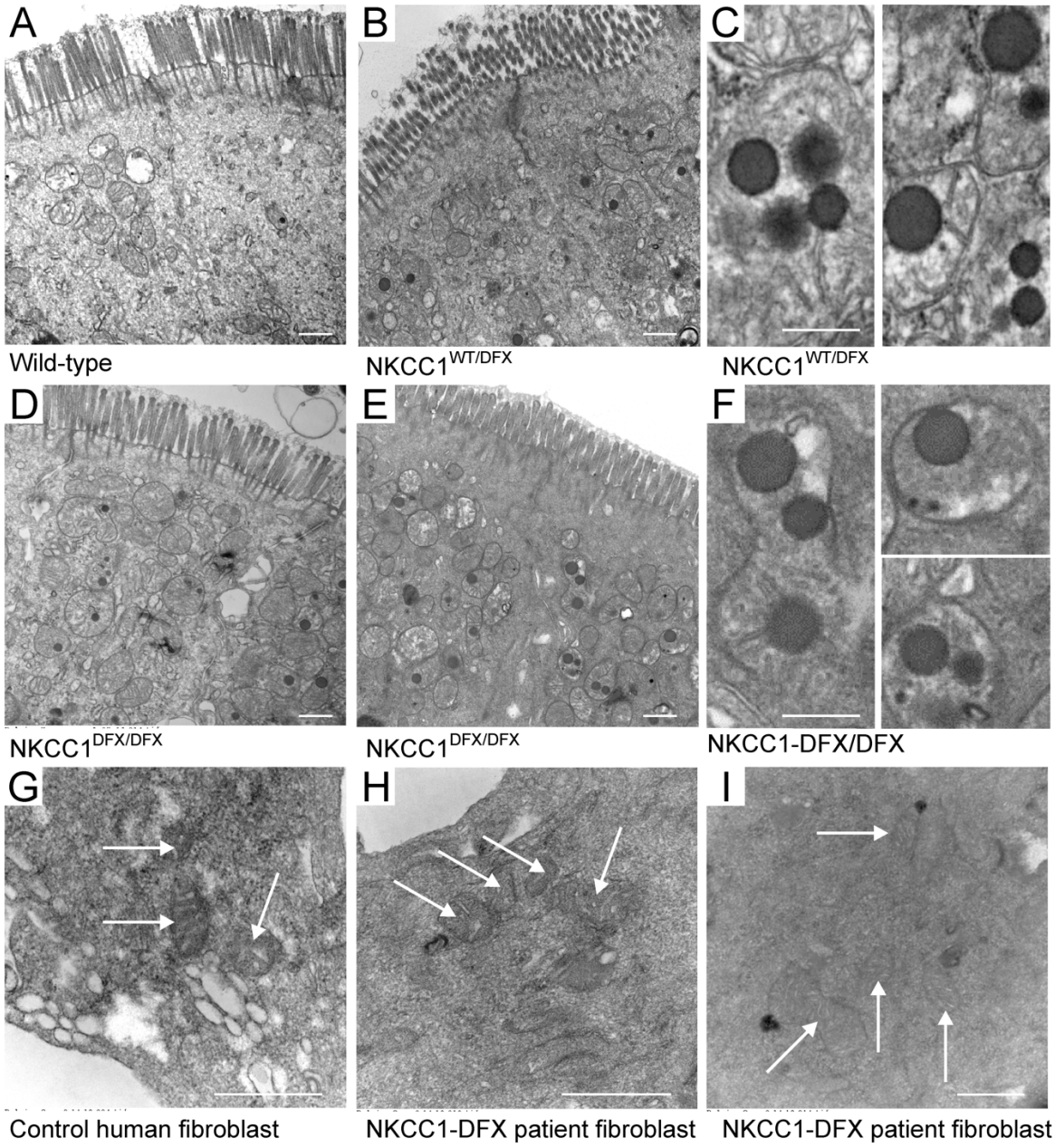

Figure 3-9. Loss of NKCC1 function alters the morphology of mitochondria. Typical transmission electron microscopy images of (**A**) WT, (**B, C**) NKCC1$^{WT/DFX}$ and (**D, E and F**) NKCC1$^{DFX/DFX}$ mouse colon sections. In this experiment, 3 mice per group and 20-50 micrographs per mouse section were analyzed. Dense inclusion bodies could be seen in panels **B** (NKCC1$^{WT/DFX}$) and in **D-E** (NKCC1$^{DFX/DFX}$). Bars = 500 m. Higher magnification of the dense bodies in (**C**) NKCC1$^{WT/DFX}$ and (F) NKCC1$^{DFX/DFX}$ mouse colon sections. Bars = 250 m. Electron microscopy images of (G) human fibroblasts from healthy individual, and (H-I) Human patient with NKCC1-DFX mutation. Bars = 500 m.

individuals (Figure 3-9G-I), indicating that this abnormality might be tissue-specific.

Final Conclusions and Discussion

This study was undertaken to establish a possible connection between the Na-K-2Cl cotransporter, NKCC1, and cellular energy metabolism. As mentioned above, an undiagnosed diseases program patient with a truncation mutation in NKCC1 was first diagnosed with mitochondrial disease. Liver and muscle biopsies revealed increased glycogen levels and mitochondria DNA copy number (173% of the mean value of age and tissue matched controls). The increase in mtDNA content possibly indicated a compensatory amplification due to mitochondrial dysfunction. This was substantiated by her co-enzyme Q10 levels in skeletal muscle, which were 222% of the normal reference mean, and 7.1 standard deviations above the mean. Because the patient carries mutations in additional genes (Delpire et al., 2016), we sought to address the role of NKCC1 in metabolism deficits. Our data clearly establish that the mutation in NKCC1 affects mitochondrial respiration, as expression of the mutant transporter in MDCK cells and mouse fibroblasts resulted in elevated mitochondrial respiration. In contrast, we demonstrated that while the patient fibroblasts have lower glycolysis rates than fibroblasts isolated from control individuals, this difference was not reproduced in our NKCC1 manipulation experiments. The lower glycolysis rate and capacity measured in the patient fibroblasts are consistent with the elevated glycogen levels measured in her muscle and liver cells, as glycolysis leads to the breakdown of glycogen (Delpire et al., 2016). However, as the fibroblasts are isolated and cultured *in vitro* for several passages, their properties are intrinsic to the cells and therefore no longer dependent of events that occur in other tissues in the patient. Thus, the decrease in

glycolysis rate and capacity that we measured in Figure 3-3 are intrinsic properties of the fibroblasts of the UDP patient. It is unclear why the manipulation of NKCC1 function did not reproduce these findings, but this suggests that the decreased glycolysis is possibly due to other genetic factors. The fact that glycolysis in the patient cells is reduced while mitochondrial respiration is increased suggests that the mitochondria in that case utilize substrates other than glucose. Examples could be long chain fatty acids or glutamine oxidation.

Elevated basal mitochondrial respiration was observed in cells expressing the mutant transporter but not in cells exposed to bumetanide, the cotransporter inhibitor. This indicates that the function of the transporter *per se* is not linked to mitochondrial respiration. This is consistent with the electroneutral transport function of Na^+, K^+ and Cl^- ions at the plasma membrane of cells, a process that is unrelated to Ca^{2+} homeostasis. On the other hand, expression of a mutant protein can affect the endoplasmic reticulum of the cell and stimulate the unfolded protein response (UPR). Many studies have shown that mitochondrial respiration is often increased upon UPR activation, thus promoting survival from endoplasmic reticulum stress (Bravo et al., 2011; Knupp et al., 2019; Senft & Ronai, 2015). This enhanced mitochondrial respiration is likely due to the release of Ca^{2+} from the ER and increased influx of the divalent cation in mitochondria (Peng & Jou, 2010).

Expression of a mutant protein, particularly a truncated protein, is anticipated to affect the endoplasmic reticulum (Ellgaard et al., 1999). In fact, expression of C-terminal truncated NKCC1 was previously shown to result in accumulation of the mutant transporter in the ER (Nezu

et al., 2009). In this case, however, to assess trafficking, the mutant transporter was expressed in HEK-293 cells and co-localization with ER markers could have been due to microscopy resolution issues due to HEK293 cells being flat. We recently demonstrated that in polarized MDCK cells, the NKCC1-DFX protein readily clears the ER and is trafficked to the apical plasma membrane, rab5 early endosomes, and lysosomes (Koumangoye et al., 2019). As one has to worry that over-expression of mutant proteins in cells might result in ER stress, we did not only measure the effect of expressing the NKCC1-DFX in MDCK cells, but we also measured the effect of mutant transporter in mouse fibroblasts where expression of the transporter is driven by the native *slc12a2* (NKCC1) promoter. In both cases, we measured similar increases in mitochondrial respiration (Figures 3-4 & 3-6). The fact that the transporter clears the ER and proceeds to downstream compartments, does not exclude the fact that the cells might have needed additional energy to process the transporter through the ER. Increased ER stress is typically demonstrated through the activation of the unfolded protein response and increased expression of a variety of proteins, such as BiP1, Dnac3j, Xbp1 (Gülow et al., 2002; Lee et al2003; Yan et al., 2002). BiP is one of the most abundant proteins in the ER where it is the major chaperone (Bakunts et al., 2017). Several studies have identified its role in its recruitment of misfolded proteins in attempts to correct misfolded proteins (Behnke et al., 2015; Hartl et al., 2011; Kampinga & Craig, 2010). This recruitment in turn leads to activation of the UPR pathway where BiP has been suggested to act as a direct ER stress sensor. However, consistent with the clearance of NKCC1-DFX from the ER, we did not observe activation of the unfolded protein response in mouse fibroblasts expressing NKCC1-DFX. Instead, we saw a significant decrease in BiP, Xbp1, and Dnac3j mRNA levels. A significant decrease in BiP expression has been observed in the liver

of calorie restricted mice as well as mouse embryonic fibroblasts deprived of serum (Pfaffenbach et al., 2012). Similarly, BiP expression is markedly decreased in the liver of diabetic mice (Yamagishi et al., 2012). In a recent paper, Daniela Rotin demonstrated that NKCC1 through an interaction with the leucine transporter LAT1 was a negative regulator of the PI3K/AKT/mTOR pathway in colonic organoids and colon. She showed that suppression of NKCC1 resulted in the activation of Akt, Erk, and mTORC1 (Demian et al., 2019). Thus, there seems to be a relationship between the cotransporter and the PI3K/AKT/mTORC1 pathway. This is relevant because BiP function was also shown to be regulated by the PI3K/AKT/mTORC1 axis, independently of the canonical UPR (Pfaffenbach et al., 2012). Our data showing decreased BiP expression indicate that cells expressing the mutant transporter might be in a state of starvation, which could explain why the NKCC1-DFX patient is in a constant state of fatigue and explain the belief from the physicians treating the patient that her cells behave like starving cells. Additionally, lysosomal degradation is activated during states of cell starvation (Yu et al., 2010; Zhou et al., 2013), consistent with the increase in NKCC1 lysosomal degradation that we observed in MDCK cells (Koumangoye et al., 2019), and the measured increased respiration rate that we observed in this study with cells expressing the NKCC1-DFX mutant protein. As glycolysis was not decreased in MDCK cells or in mouse fibroblasts expressing the mutant transporter, we hypothesize that access to glucose is not affected in the cells. This likely means that cells have the capacity to increase their energy production by using energy sources independent of glucose. The fact that fibroblasts isolated from $NKCC1^{DFX/DFX}$ mice but not $NKCC1^{WT/DFX}$ mice show increased hydrogen peroxide production and peroxidase activity while they both demonstrate increase in mitochondrial respiration suggests that the increased ROS measured does not originate in the

mitochondria. As we demonstrated previously that NKCC1-DFX accumulates in rab5-positive endosomes and lysosomes (Koumangoye et al., 2019), and increased substrate load in lysosomes is known to induce oxidative stress (Martínez-Fábregas et al., 2018), one possible explanation for the increase in hydrogen peroxide production and peroxidase activity would be lysosomal overload in cells expressing NKCC1-DFX from two mutant alleles. In conclusion, one possible mechanism explaining the deficits in cell metabolism is explained in Figure 3-10. A suppression in the UPR pathway allows NKCC1-DFX to be trafficked to the plasma membrane. However, due to a non-functioning NKCC1-DFX at the plasma membrane, the transporter is readily endocytosed for lysosomal degradation. This process is energetically demanding, which might explain the elevation of mitochondrial respiration. A substrate overload of NKCC1-DFX can also lead to elevated ROS, also contributing to the elevation of mitochondrial respiration.

One additional observation that we made by electron microscopy while we were studying intestinal epithelial cells from NKCC1-DFX heterozygote and homozygote mice, was the presence of large electron-dense particles or vesicles within mitochondria. These structures were only seen in very small sizes and lower numbers in the intestine of wild-type animals and not present in fibroblasts of the patient. At this point, we have no information on the composition of these particles, whether they are surrounded by a membrane, and what their role is in mitochondrial function, or whether it is a result of oxidative stress (lipid peroxidation). These particles, however, have been previously described in the intestinal cells of NLRP6 knockout mice which like the NKCC1-DFX mice (Koumangoye et al., 2020) have a deficit in goblet cell-mediated mucus secretion and increased susceptibility to bacterial infection (Wlodarska et al., 2015). These

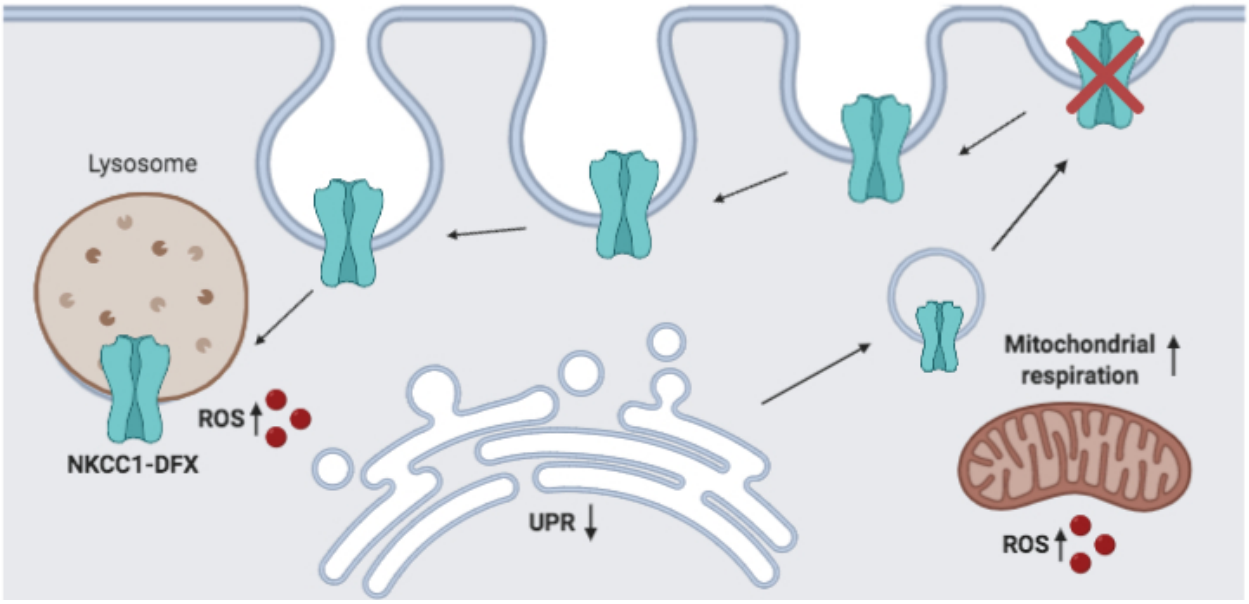

Figure 3-10. Schematic model explaining the effects of NKCC1-DFX on cellular metabolism. A suppression in the UPR pathway allows NKCC1-DFX to be trafficked to the plasma membrane. However, due to a non-functioning NKCC1-DFX at the plasma membrane, it is readily endocytosed for lysosomal degradation. This process is energetically demanding, which explains the elevation of mitochondrial respiration. A substrate overload of NKCC1-DFX can also lead to elevated ROS, also contributing to the elevation of mitochondrial respiration.

structures might thus be related to the inflammatory response of the epithelium to bacterial infection.

CHAPTER IV

CONCLUSIONS AND FUTURE DIRECTIONS

Summary

The characterization of human mutations in PKD1 and NKCC1 *in vivo* by generating two novel mouse models, helped us gather compelling evidence as to the importance of these proteins to human health (Koumangoye et al., 2018b). Generating both mouse models allowed for the successful recapitulation of phenotypes of the respective individuals carrying the mutations. We were fortunate to collaborate with groups of clinicians and contribute to their understanding of the pathology at the basis of the clinical presentation of their patients. Although generating a homozygous mouse model of PKD1-E77X revealed difficult, it corroborated previous findings that showed embryonic lethality of the PRKD1 KO mouse (Rozengurt 2011; Ellwanger & Hausser 2013). Because of the lethality, we were forced to study the effect of an inactive PKD1 on sensorimotor neurobehavior in heterozygous mice which are typically resistant to nerve diseases. This prompted us to utilize a stressor to reveal a phenotype in the heterozygote mouse. The stressor was a seizure induction compound, kainate, resulting in the discovery that PKD1 plays a role in on seizure susceptibility in mice. We are now convinced that the PKD1-E77X mutation in the heterozygous state is insufficient to produce a locomotor phenotype that can be assessed through basal behavioral studies. Prior to generating this *in vivo* mouse model, the effect of PKD1 on KCC3 was established in *Xenopus laevis* oocytes, ex vivo, where we confirmed that inactivating PKD1 resulted in an increase in KCC3 activity, without affecting the expression of the

cotransporter at the plasma membrane. More importantly, EM studies focusing on peripheral nerve integrity in heterozygous and a few homozygous PKD1-E77X mice revealed that nerve fiber g-ratios were smaller, due to an increased myelin diameter with increasing copy number of PKD1-E77X. The most profound finding of the nerve fiber studies in the mutant mouse was the observation of the same nerve tomacula pathology reported in sural nerve biopsies of the patient carrying the PKD1 mutation. On that note, the patient was also suffering from generalized seizures, in addition to gait abnormalities. Although we were not able to recapitulate the locomotor aspect in the mice, increased seizure susceptibility was observed in the heterozygous PKD1-E77X mice, confirming a CNS deficit.

In addition to creating and studying the PKD1 mouse mutant, I investigated the role of NKCC1 in metabolism. This work was driven by the demonstration that a patient with an NKCC1 mutation was diagnosed with some sort of mitochondrial disease and metabolic disorder (Delpire et al., 2016), and I assisted with generating the mouse model of this particular disease mutation (Koumangoye et al., 2018b). In addition, the role of NKCC1 in metabolism has never been studied. This project allowed me to address the problem through multiple approaches, namely the use of stable MDCK cell lines expressing wild-type and mutant transporters, the use of a more native system by utilizing cells from the mouse model, the use of pharmacological agents, and the use of fluorescent-based metabolic assays. After confirming that the patient fibroblasts had elevated mitochondrial respiration levels, and reduced glycolysis compared to fibroblasts isolated from control individuals, I addressed the metabolic properties of MDCK cells expressing the mutant transporter. Once I demonstrated that MDCK cells expressing the NKCC1-DFX mutation displayed

elevated mitochondrial respiration (but no decreased in glycolysis), I was interested in assessing mitochondrial respiration in isolated fibroblasts from control and mutant NKCC1 mice. As expected based on my previous data, fibroblasts from the mutant mice also demonstrated higher mitochondrial respiration levels than wild-type fibroblasts. I then showed that this led to higher production of reactive oxygen species. These findings have unveiled a previously unknown role for a plasma membrane transporter and thus, advanced our understanding of the physiology of the Na-K-2Cl cotransporter. Although the two projects discussed in my thesis have contributed to our understanding of the cotransporters and the proteins that regulate their activity, additional work needs to be done to further understand the biology of the transporters and their regulatory kinases.

PKD1 effect on KCC3

The novel effect of PKD1 on KCC3 that was observed in *Xenopus laevis* oocytes opens an entirely new avenue of investigation into the regulation of the cotransporters. Our knowledge of the mechanisms by which the cotransporters are regulated by the kinases and phosphatases is still relatively limited and for the first time this work identifies PKD1 as a novel player in the regulation of the cotransporter. The identification of SPAK and OSR1, two mammalian Ste20p kinases, as terminal kinases binding, phosphorylating, and inactivating the cotransporter has significantly advanced the field. The discovery that WNK kinases act upstream of SPAK/OSR1 was also a major advance in the field, but the WNK kinases are not the only kinases that modulate the activity of SPAK/OSR1. Indeed, kinases such as PKC-theta (Li et al., 2004) and PKC-delta Smith et al., 2008) have been shown to interact and modulate SPAK activity. The biology of the WNK

kinases is also fascinating. These kinases have a Cl^- binding site that makes them sensitive to the intracellular Cl^- concentration (Piala et al., 2014). In addition, their expression is highly regulated by two proteins of the ubiquitin pathway: protein cullin 3 (CUL3) and the substrate adaptor kelch-like 3 (KLHL3) protein (McCormick et al., 2014). On the other hand, a previous study demonstrated that PKD1 knockdown in cells via shRNA led to increased phosphorylation of KCC3 at positions Thr991 and Thr1048 (Zhang et al., 2016). Our study did not elaborate on the mechanism by which PKD1 might affect KCC3 activity. This could be through modulating expression and/or function of SPAK/OSR1, modulating expression and/or function of the WNK kinases, or through a still unknown mechanism. Whether overall expression, expression at the plasma membrane, or just modulation of activity of transporters already existing at the membrane is affected is still unknown. Future work should focus on this particular aspect of PKD1 regulation of KCC3.

Effect of PKD1 in the PNS and CNS

Our group has extensively studied and demonstrated that mutations in *SLC12A6* causing deficits or increase in KCC3 function, results in abnormal myelination, axonopathies, and sensory/locomotor behavior in mice (Byun & Delpire 2007b; Ding & Delpire 2014b; Howard et al., 2002; Kahle et al., 2016). These studies carried out by Dr. Nellie Byun and current PhD candidate Bianca Flores in our laboratory highlighted phenotypes in mice that were similar to those in humans carrying LOF or GOF mutations in KCC3. Although KCC3 is expressed in both the CNS and PNS, only peripheral neuropathy was identified as a phenotype. There is still a rather large gap in knowledge in identifying the molecular mechanisms by which a LOF or GOF in KCC3

results in peripheral neuropathy. Here, I provide insights into PKD1 as a potential contributor to KCC3 related peripheral neuropathies. Through *ex vivo* electron microscopy analyses of homozygous PRKD1$^{E77X/E77X}$ sciatic nerves discussed in chapter 2, it is pretty clear that absence of PKD1 affects the structure/histology of peripheral nerves. Considering that not enough PRKD1$^{E77X/E77X}$ mice were generated for neurobehavioral analyses, we could not fully address the role of PKD1 in sensory and motor phenotypes. It is possible that targeting deletion of PKD1 in specific tissues, e.g. sensory neurons, motor neurons, etc. would allow us to go around the lethality issue of the global knockout. Further studies are therefore needed.

KCC3 is widely distributed in the brain and many individuals with LOF mutations in KCC3 demonstrate partial or complete agenesis of the corpus callosum (Howard et al., 2002; Uyanik et al., 2006; Shekarabi et al., 2011b). Thus, it is clear that KCC3 plays a role in the development and function of central neurons. It is also worth noting that a study conducted in KCC3 knockout mice, demonstrated lower seizure thresholds and increase in spontaneous high-voltage spike-wave-like complexes in electrocorticograms (Boettger et al., 2003). The role of KCC3 in affecting brain excitability is still poorly understood, especially since KCC2 is the predominant K-Cl cotransporter in central neurons, and its function is to strengthen hyperpolarizing GABA/glycine responses. Studies have shown that mutations in KCC2 in humans and in mice affects brain excitability (Chen et al., 2017; Kahle et al., 2014). The fact that KCC3 and KCC2 through interaction might be molecular partners in neurons provides a possible explanation for the role of KCC3 in neuronal hyperexcitability. Interestingly, I also demonstrated that pharmacological induction of seizures resulted in increased seizure susceptibility in PRKD1$^{+/E77X}$ mice, with lower thresholds than wild-

type littermates, recapitulating the patient seizure symptoms. A potential mechanism underlying the increased seizure susceptibility in PRKD1$^{+/E77X}$ mice, could be an increased GABA inhibition due to over-active KCC3 in interneurons. Our laboratory has identified a role for KCC3 in parvalbumin-positive (PV+) cells, some of which are inhibitory interneurons responsible for providing the main source of somatic inhibition (Ding & Delpire 2014b). Thus, an increase in KCC3 activity in interneurons could lead to increased Cl^- extrusion resulting in a lower E_{Cl}, facilitating inhibition. Thus, inhibiting the effect of inhibitory interneurons might lead to increased neuronal firing, thereby accounting for the lower seizure threshold observed in PRKD1$^{+/E77X}$ mice.

Whether the seizure effect of PKD1 is in direct or indirect relationship to KCC3 activity and/or to interneurons needs to be further addressed. Ideally, immunohistochemistry assays would be conducted with hippocampal slices from WT, PRKD1$^{+/E77X}$, and PRKD1$^{E77X/E77X}$ mice stained against phospho-KCC3 and PKD1 antibodies. The role of interneurons could be addressed by selective deletion of KCC3 and PKD1 in the interneuronal lineage (e.g. driven by Dlx5-CRE). In additional experiments, we could directly determine the activity of KCC3 in cells isolated from wild-type, PKD1-E77X heterozygous, and homozygous mice. A limitation of these assays is that it does not identify the K-Cl cotransporter isoform that is affected. Indeed, if the experiment is done in neurons, KCC2 activity which is prevalent could also be affected. This would need to be sorted out. Heterologous expression in *Xenopus laevis* oocytes or KCC-deficient HEK293 cells could be used to sort out the effect, but it is very likely that regulation would be similar in all the K-Cl cotransporter tested. In conclusion, our work has generated many questions that remain to be answered: whether PKD1 results in peripheral neuropathy and in increased seizure susceptibility

by acting directly on KCC activity, or whether this effect is independent of the cotransporter; which cell type, i.e. interneurons or other are affected by the deficit in PKD1 expression.

NKCC1 in metabolism

The expression and function of NKCC1 have been well-studied by our and other groups (Delpire et al., 1994a; 1999). Several recent studies from us have highlighted the importance and the pathogenetic role of NKCC1 in the inner ear, nervous system, intestine, salivary gland, lung, and testis (Delpire et al., 1999; Flagella et al 1999, Dixon et al., 1999, Evans et al., 2000, Pace et al., 2000, Grubb et al., 2000, Grubb et al., 2001, Delpire et al., 2016; Koumangoye et al., 2019). Other investigators such as Sergei Orlov have studied NKCC1 in smooth muscle cell function, where the cotransporter plays an indirect role in the proper maintenance of intracellular Ca^{2+} levels necessary for smooth muscle cell (SMC) contraction (Orlov et al., 2010). The main source of Ca^{2+} for the tonic contractile activity of muscle is thought to come from extracellular stores channeled through L-type Ca^{2+} channels, although Ca^{2+} is additionally obtained from intracellular stores such as the sarcoplasmic reticulum (Kitamura & Yamazaki 2001). L-type Ca^{2+} channels are voltage operated Ca^{2+} channels expressed at the plasma membrane that open in response to membrane depolarization. The activation of Cl^- channels leading to membrane depolarization is a determining factor for the opening of L-type Ca^{2+} channels. It is believed that this Cl^- channel depolarization is helped by the accumulation of Cl^- provided by the activity of NKCC1. Indeed, high E_{Cl} in smooth muscle cells is maintained in part by the cotransporter. Because smooth muscle cells are in many different organs, e.g. vasculature, intestine, bladder, etc., it might not be surprising that a patient expressing a mutant form of NKCC1 suffers from multi-organ

dysfunction. In addition, because of the vital role that nerve afferents play in sensory feedback and the important role that NKCC1 plays in modulating the return of sensory information, the multi-organ failure could also have some neurological origins. Thus, two major physiological processes sustained by NKCC1 function could account for the patient multi-system disorder.

So far, we have determined that loss of NKCC1 function results in impaired intestinal secretion and chronic inflammation in mice (Koumangoye et al., 2020), where electron microscopy and immunofluorescence studies were used to analyze mucous release and layer formation in the colon and immune cell infiltration. This study is consistent with severe gastrointestinal deficits identified in a separate patient who is a functional knockout of NKCC1. Although we have some understanding of the mechanisms by which the two NKCC1 patients suffer from gastrointestinal deficits, we have yet to tackle the idea that smooth muscle function is impaired in NKCC1 mutant mice. In addition, the muscle and liver cells of the NKCC1-DFX patient exhibit an abnormal elevation in mitochondrial DNA content, and an increase in glycogen content. This property was of particular interest to me since the role of NKCC1 in metabolic and energy homeostasis has been poorly investigated. Given the necessity of intracellular Cl^- maintenance for Ca^{2+} uptake, and Ca^{2+} uptake is important for proper mitochondrial, glycolytic, and ER function, it was important to study the effect of NKCC1-DFX on mitochondrial activity, glycolysis, and ER stress (Finkel et al., 2015; Brox, Petermann & Frunder, 1977). Additionally, the patient's elevated amount in DNA copy number, is a hallmark of metabolic disease, which was another factor contributing to my curiosity and desire to investigate the role of NKCC1 in metabolism (Malik & Czajka, 2013). I first confirmed that the NKCC1-DFX patient had elevated

mitochondrial DNA copy number, and elevated glycogen content by assessing mitochondrial and glycolytic respiration in isolated fibroblasts from the patient, compared to fibroblasts isolated from healthy individuals. There was a significant increase in the oxygen consumption rate (mitochondrial respiration), and a significant decrease in extracellular acidification rate (glycolysis) in fibroblasts expressing NKCC1-DFX. Due to the NKCC1-DFX patient expressing several other mutations, mitochondrial respiration and glycolysis was analyzed in MDCK epithelial cells and mouse fibroblasts expressing NKCC1-DFX. We found that in both cases, cells expressing NKCC1-DFX recapitulated the patient fibroblasts of elevated mitochondrial respiration. There was no difference in glycolysis. When cells were treated with the NKCC1 specific inhibitor bumetanide, the cells had higher mitochondrial respiration, further confirming that NKCC1 leads to the increase in mitochondrial activity.

Furthermore, due to the patient's large amount of mitochondrial DNA copy number, I confirmed there was a higher mitochondrial density in her fibroblasts, compared to fibroblasts from healthy individuals. There was no difference in mitochondrial density when repeated in fibroblasts isolated from $NKCC1^{DFX/+}$ and $NKCC1^{DFX/DFX}$. Although this is unlike what was observed in the NKCC1-DFX patient, it speaks to the participation of NKCC1 in mitochondrial respiration, where a disruption in NKCC1 function, affects mitochondrial respiration without increasing the mitochondrial content. One outcome of an abnormal increase in mitochondrial respiration can be oxidative stress in the form of reactive oxidative species (Tiwari et al., 2002). An abundance in reactive oxidative species may lead to a negative cell fate, such as cell death (Maryanovich and Gross 2013). It was therefore sensible to test the level of reactive oxidative species in

heterozygous and homozygous NKCC1-DFX mouse fibroblasts. Interestingly, there was a significant increase in reactive oxidative species in NKCC1$^{DFX/DFX}$ fibroblasts, suggesting that one functional copy of NKCC1 is enough to alleviate or prevent from oxidative stress. To understand whether a nonfunctional NKCC1 affects the ER, major markers of ER stress were analyzed in fibroblasts of NKCC1$^{DFX/+}$ and NKCC1$^{DFX/DFX}$ mice. There was a significant decrease in ER stress markers compared to WT in NKCC1$^{DFX/+}$ and NKCC1$^{DFX/DFX}$ mouse fibroblasts. These results were intriguing since we recently demonstrated that NKCC1-DFX was able to clear the ER, even if partially misfolded. The ER is equipped with several chaperones and machinery in the UPR pathway, responsible for identifying misfolded protein to either correctly fold or target them for proteasomal degradation (Kadowaki & Nishitoh 2013). However, in the case of the NKCC1-DFX mutant, we have established in a recent study that it is not until NKCC1-DFX reaches the plasma membrane that it is targeted for lysosomal degradation (Koumangoye et al., 2019; 2018b). Here, I established that several ER stress markers are in fact suppressed, possibly contributing to the NKCC1-DFX mutant being able to avoid the UPR pathway.

In my studies, I have determined that a genetic and pharmacological abrogation of NKCC1 function, causes an increase in mitochondrial respiration, elevation in oxidative stress, and decreased ER stress response. The next step would be to decipher the mechanism by which NKCC1 is linked to mitochondrial respiration, and ER stress. This could be approached in several ways. First, mitochondrial respiration in mouse fibroblasts should be assessed under different osmotic conditions. NKCC1 is active in hypertonic solutions, and inactive in hypotonic conditions. I would expect to see lower mitochondrial respiration in cells exposed to hypertonic solutions,

than isotonic, and hypotonic ones. However, since NKCC1 is not necessarily "inhibited" or abnormally functioning in isotonic or hypotonic conditions, one might not expect to see any difference. To determine whether different concentrations of Na^+ and K^+ affect mitochondrial respiration and glycolysis, cells would be exposed through ionophores to different concentrations of Na^+ and K^+. Additionally, the relationship between intracellular Na^+ and intracellular Ca^{2+} (through Na^+/Ca^{2+} exchanger) could also be investigated in respect to changes in mitochondrial function. These studies would determine more directly whether NKCC1 contributes to mitochondrial respiration through its transport activity (and through which ion(s)), or through its expression at the plasma membrane.

Calcium is also involved in proper ER function, and abnormalities in ER Ca^{2+} levels has been linked to contributing to several disease states (Carreras-Sureda et al., 2018; Mekahli et al., 2011). Since Ca^{2+} influx in SMCs is affected in part by intracellular Cl^- levels, and NKCC1 plays a part in the maintenance of intracellular Cl^- in SMCs, it would be interesting to assess whether NKCC1-DFX affects calcium levels in NKCC1-DFX mouse fibroblasts. Calcium levels would be measured by calcium fluorescent assays, using chemical indicators such as fura-2, fluo-4, or fluo-8. Through understanding calcium levels, mitochondrial respiration and glycolysis in response to changes in osmolarity and ion concentrations, a mechanism of NKCC1 action in metabolism might unfold.

Overall, because the individuals with rare diseases described in Chapters 2 and 3 are single clinical cases carrying unique mutations, the causality is difficult to make. The power of linking diseases with mutations in multiple members of a family and multiple families is not

available to us. By generating a mouse model carrying the PKD1-E77X, I was able to 1) reproduce the pathology observed in the nerve of the patient, and 2) demonstrate that loss of PKD1 results in neuronal hyperexcitability. On the other hand, by generating a mouse model expressing the NKCC1-DFX mutation I was able to reproduce and study the metabolic deficits observed in the NKCC1-DFX patient. The mutation results in: 1) elevated mitochondrial respiration, 2) suppressed UPR pathway, and 3) increase in ROS levels. In conclusion, the studies outlined in this dissertation might serve as foundation for future work that could contribute to our understanding of NKCC1 and PKD1/KCC3 function and lead the development of novel therapeutic drugs to treat clinical conditions related to cation-chloride cotransporters.

REFERENCES

Abbas, L., and Whitfield, T. (2009). Nkcc1 (Slc12a2) Is Required for the Regulation of Endolymph Volume in the Otic Vesicle and Swim Bladder Volume in the Zebrafish Larva. *Development,* 136 (16): 2837–48.

Adragna, N. C., and Lauf P. K. (2007). K–Cl Cotransport Function and Its Potential Contribution to Cardiovascular Disease. *Pathophysiology,* 14 (3–4): 135–46.

Agez, M., Schultz, P., Medina I., Baker D. J, Burnham M. P., Cardarelli R. A., C. Conway L. C., et al., (2017). Molecular Architecture of Potassium Chloride Co-Transporter KCC2. *Scientific Reports,* 7 (1).

Akaishi, T. (2018). Saltatory Conduction as an Electrostatic Compressional Wave in the Axoplasm. *Tohoku Journal of Experimental Medicine,* 244 (2): 151–61.

Aldskogius, Håkan, Lars-Gösta Elfvin, and Catarina Andersson Forsman. (1986). Primary Sensory Afferents in the Inferior Mesenteric Ganglion and Related Nerves of the Guinea Pig. *Journal of the Autonomic Nervous System* 15 (2): 179–90.

Alessi, D. R., Zhang, J., Khanna, A., Hochdörfer, T., Shang, Y., and Kahle T. K. (2014). The WNK-SPAK/OSR1 Pathway: Master Regulator of Cation-Chloride Cotransporters. *Science Signaling,* 7 (334): re3.

Alvarez-Leefmans, F. J., and Delpire, E. (2009). *Physiology and Pathology of Chloride Transporters and Channels in the Nervous System : From Molecules to Diseases*. Elsevier/Academic.

Alvarez-Leefmans, F. J., Gamiño S. M., Giraldez, F., and Noguerón, I. (1988). Intracellular Chloride Regulation in Amphibian Dorsal Root Ganglion Neurones Studied with Ion-Selective Microelectrodes. *The Journal of Physiology,* 406 (1): 225–46.

Amadesi, S., Grant, A. D., Cottrell, G. S., Vaksman, N., Poole, D. P., Rozengurt, E., and Bunnett N. W. (2009). Protein Kinase D Isoforms Are Expressed in Rat and Mouse Primary Sensory Neurons and Are Activated by Agonists of Protease-Activated Receptor 2. *The Journal of Comparative Neurology*, 516 (2): 141–56.

Amorim, J. B.O., Bailey M. A., Musa-Aziz, R., Giebisch, G., and Malnic, G.. (2003). Role of Luminal Anion and PH in Distal Tubule Potassium Secretion. *American Journal of Physiology - Renal Physiology,* 284 (2 53-2).

Andreasen, F., and Mikkelsen, E. (1977). Distribution, Elimination and Effect of Furosemide in Normal Subjects and in Patients with Heart Failure. *European Journal of Clinical Pharmacology,* 12 (1): 15–22.

Aptel, H, Hilaire, C., Pieraut, S., Boukhaddaoui, H., Mallié, S., Valmier, J., and Scamps, F. (2007). The Cav3.2/A1H T-Type Ca2+ Current Is a Molecular Determinant of Excitatory Effects of GABA in Adult Sensory Neurons. *Molecular and Cellular Neuroscience,* 36 (2): 293–303.

Auer, Roland N, Janet L Laganière, Yves O Robitaille, John Richardson, Patrick A Dion, Guy A Rouleau, and Masoud Shekarabi. (2016). KCC3 Axonopathy: Neuropathological Features in the Central and Peripheral Nervous System. *Nature Publishing Group* 29.

Austin, T.M., and Delpire, E. (2011). Inhibition of KCC2 in Mouse Spinal Cord Neurons Leads to Hypersensitivity to Thermal Stimulation. *Anesthesia and Analgesia,* 113 (6): 1509–15.

Bachmann, S., Velázquez, H., Obermüller, N., Reilly, R.F., Moser, D., and Ellison, D. H. (1995). Expression of the Thiazide-Sensitive Na-Cl Cotransporter by Rabbit Distal Convoluted Tubule Cells. *Journal of Clinical Investigation,* 96 (5): 2510–14.

Bakunts, A., Orsi, A., Vitale, M., Cattaneo, A., Lari, F., Tadè, L., Sitia, R., Raimondi, A., van Anken, E. (2017). Ratiometric sensing of BiP-client versus BiP levels by the unfolded protein response determines its signaling amplitude. *Elife, 6*, e27518.

Barrell, K., and Smith A. G. (2019). Peripheral Neuropathy. *Medical Clinics of North America*, 103 (2): 383-397.

Bazzini, C., Vezzoli, V., Sironi, C., Dossena, S., Ravasio, A., De Biasi, S., Garavaglia, M.L., et al., (2005). Thiazide-Sensitive NaCl-Cotransporter in the Intestine: Possible Role of Hydrochlorothiazide in the Intestinal Ca2+ Uptake. *Journal of Biological Chemistry,* 280 (20): 19902–10.

Behnke, J., Feige, M. J., & Hendershot, L. M. (2015). BiP and its nucleotide exchange factors Grp170 and Sil1: mechanisms of action and biological functions. *J. Mol. Biol., 427*(7), 1589-1608.

Ben-Ari, Y., Cherubini, E., Corradetti, R., & Gaiarsa, J. L. (1989). Giant synaptic potentials in immature rat CA3 hippocampal neurones. *The Journal of Physiology*, *416*(1), 303–325.

Bencsik, N., Szíber, Z., Liliom, H., Tárnok, K., Borbély, S., Gulyás, M., Rátkai, A., et al., (2015). Protein Kinase D Promotes Plasticity-Induced F-Actin Stabilization in Dendritic Spines and Regulates Memory Formation. *The Journal of Cell Biology,* 210 (5): 771–83.

Bertolotti, A., Zhang, Y., Hendershot, L. M., Harding, H.P., and Ron. D. (2000). Dynamic Interaction of BiP and ER Stress Transducers in the Unfolded-Protein Response. *Nature Cell Biology,* 2 (6): 326–32.

Bisbal, M., Conde, C. , Donoso, M., Bollati, F., Sesma, J., Quiroga, S., Diaz Anel, A., Malhotra V., Marzolo, M. P., and Caceres, A. (2008). Protein Kinase D Regulates Trafficking of Dendritic

Membrane Proteins in Developing Neurons. *Journal of Neuroscience,* 28 (37): 9297–9308.

Blaesse, Peter, Matti S. Airaksinen, Claudio Rivera, and Kai Kaila. (2009). Cation-Chloride Cotransporters and Neuronal Function. *Neuron,* 61 (6): 820–38.

Blaesse, P., Guillemin, I., Schindler, J., Schweizer, M., Delpire, E., Khiroug, L., Friauf, E., and Nothwang, H.G. (2006). Oligomerization of KCC2 Correlates with Development of Inhibitory Neurotransmission. *Journal of Neuroscience,* 26 (41): 10407–19.

Boettger, T., Hübner, C. A., Maier, H., Rust, M.B., Beck, F.X., and Jentsch, T.J. (2002). Deafness and Renal Tubular Acidosis in Mice Lacking the K-Cl Co-Transporter Kcc4. *Nature,* 416 (6883): 874–78.

Boettger, T., Rust, M.B., Maier, H., Seidenbecher, T., Schweizer, M., Keating, D. J., Faulhaber, J.,et al., (2003). Loss of K-Cl Co-Transporter KCC3 Causes Deafness, Neurodegeneration and Reduced Seizure Threshold. *EMBO Journal,* 22 (20): 5422–34.

Boulenguez, P., Liabeuf, S., Bos, R., Bras, H., Jean-Xavier, C., Brocard, C., Stil, A., et al., (2010). Down-Regulation of the Potassium-Chloride Cotransporter KCC2 Contributes to Spasticity after Spinal Cord Injury. *Nature Medicine,* 16 (3): 302–7.

Bourke, E. (1976). Furosemide, bumetanide, and ototoxicity. *The Lancet,* 307 (7965): 917–18.

Bravo, R., Vicencio, J.M., Parra, V., Troncoso, R., Munoz, J.P., Bui, M., Quiroga, C., et al., (2011). Increased ER-Mitochondrial Coupling Promotes Mitochondrial Respiration and Bioenergetics during Early Phases of ER Stress. *Journal of Cell Science*. 124 (pt 13): 2143-52.

Brown, G. C. (1992). Control of Respiration and ATP Synthesis in Mammalian Mitochondria and Cells. *Biochemical Journal*, 254 (pt1): 1-13

Brown, G.C. (1995). Nitric Oxide Regulates Mitochondrial Respiration and Cell Functions by Inhibiting Cytochrome Oxidase. *FEBS Letters* 369 (2–3): 136–39.

Brox, D, Petermann, B., and Frunder, H. (1977). The Effects of Calcium on Glycolysis and ATP Concentration in Complete and Membrane-Poor Hemolyzates of Human Erythrocytes. *Acta Biologica et Medica Germanica,* 36 (5–6): 611–19.

Brunet, G. M., Gagnon, E., Simard, C. F., Daigle, N. D., Caron, L., Noël, M., Lefoll, M.H., Bergeron, M. J., and Isenring, P. (2005). Novel Insights Regarding the Operational Characteristics and Teleological Purpose of the Renal Na+-K+-Cl- Cotransporter (NKCC2s) Splice Variants. *Journal of General Physiology,* 126 (4): 325–37.

Byun, N., and Delpire, E. (2007a). Axonal and Periaxonal Swelling Precede Peripheral Neurodegeneration in KCC3 Knockout Mice. *Neurobiology of Disease,* 28 (1): 39–51.

Cadenas, E., and Davies, K.J.A. (2000). Mitochondrial Free Radical Generation, Oxidative Stress, and Aging. *Free Radical Biology and Medicine,* 29 (3–4): 222–30.

Calder, J.A., Schachter, M., and Sever, P.S. (1992). Direct Vascular Actions of Hydrochlorothiazide and Indapamide in Isolated Small Vessels. *European Journal of Pharmacology,* 220 (1): 19–26.

Carmosino, M., Giménez, I., Caplan, M., and Forbush, B. (2008). Exon Loss Accounts for Differential Sorting of Na-K-Cl Cotransporters in Polarized Epithelial Cells. *Molecular Biology of the Cell,* 19 (10): 4341–51.

Carreras-Sureda, A., Pihán, P., and Hetz, C. (2018). Calcium Signaling at the Endoplasmic Reticulum: Fine-Tuning Stress Responses. *Cell Calcium*. 70: 24-31

Casaubon, L. K., Melanson, M., Lopes-Cendes, I., Marineau, C., Andermann, E., Andermann, F., Weissenbach, J., et al., (1996). The Gene Responsible for a Severe Form of Peripheral Neuropathy and Agenesis of the Corpus Callosum Maps to Chromosome 15q. *American Journal of Human Genetics,* 58 (1): 28–34.

Casula, S., Shmukler, B. E., Wilhelm, S., Stuart-Tilley, A.K., Su, W., Chernova, M. N., Brugnara, C., and Alper, S. L. (2001). A Dominant Negative Mutant of the KCC1 K-Cl Cotransporter: Both N- and C-Terminal Cytoplasmic Domains Are Required for K-Cl Cotransport Activity. *Journal of Biological Chemistry,* 276 (45): 41870–78.

Casula, S., Zolotarev, A.S., Stuart-Tilley, A.K., Wilhelm, S., Shmukler, B. E., Brugnara, C., and Alper, S. L. (2009). Chemical Crosslinking Studies with the Mouse Kcc1 K-Cl Cotransporter. *Blood Cells, Molecules, and Diseases,* 42 (3): 233–40.

Chance, B., and Williams, G. R. (1955). Respiratory Enzymes in Oxidative Phosphorylation. III. The Steady State. *The Journal of Biological Chemistry,* 217 (1): 409–27.

Chen, H., Albertson, T.E., and Olson, K.R. (2016). Treatment of Drug-induced Seizures. *British Journal of Clinical Pharmacology,* 81 (3): 412–19.

Chen, L., Zheng Wu, L., Ren, W., Huang, Y., Qian, B., and Wang, Y. (2017). KCC2 Downregulation Facilitates Epileptic Seizures. *Scientific Reports,* 7 (1): 156.

Chen, Y., Chou, C., Ellory, J.C., and Shen, M. (2010). The Emerging Role of KCl Cotransport in Tumor Biology. *American Journal of Translational Research,* 2 (4): 345–55.

Chen, Y., Chou, C.Y., Wilkins, R. J., Ellory, J. C. , Mount, D. B. and Shen, M. (2009). Motor Protein-Dependent Membrane Trafficking of KCl Cotransporter-4 Is Important for Cancer Cell Invasion. *Cancer Research,* 69 (22): 8585–93.

Chew, T. A., Orlando, B. J., Zhang, J., Latorraca, N.R., Wang, A., Hollingsworth, S.A., Chen, D., Dror, R. O., Liao, M.,and Feng, L. (2019). Structure and Mechanism of the Cation–Chloride Cotransporter NKCC1. *Nature,* 572 (7770): 488–92.

Chipperfield, A.R., and Harper, A.A.. (2000). Chloride in Smooth Muscle. *Progress in Biophysics and Molecular Biology,* 74 (3): 175–221.

Chiu, T. T., Leung, W., Moyer M., Strieter, R.M., and Rozengurt, E. (2007). Protein Kinase D $_2$ Mediates Lysophosphatidic Acid-Induced Interleukin 8 Production in Nontransformed Human Colonic Epithelial Cells through NF-KB. *American Journal of Physiology-Cell Physiology,* 292 (2): C767–77.

Clayton, G. H., Owens, G. C., Wolff, J. S., & Smith, R. L. (1998). Ontogeny of cation-Cl- cotransporter expression in rat neocortex. *Developmental Brain Research*, *109*(2), 281–292.

Crable, S. C., Hammond, S.M., Papes, R., Rettig, R. K., Zhou, G.P., Gallagher, P.G., Joiner, C.H., and Anderson, K. P. (2005). Multiple Isoforms of the KC1 Cotransporter Are Expressed in Sickle and Normal Erythroid Cells. *Experimental Hematology,* 33 (6): 624–31.

Cremaschi, D., Porta, C., Bottà, G., Bazzini, C., Baroni, M. D., and Garavaglia, M. (2000). Apical Na^+-Cl^- Symport in Rabbit Gallbladder Epithelium: A Thiazide-Sensitive Cotransporter (TSC). *The Journal of Membrane Biology,* 176 (1): 53–65.

Cutler, C.P., and Cramb, G. (2002). Two Isoforms of the Na+/K+/2Cl- Cotransporter Are Expressed in the European Eel (Anguilla Anguilla). In *Biochimica et Biophysica Acta - Biomembranes*, 1566:92–103.

Cutler, C.P., and Cramb, G. (2008). Differential Expression of Absorptive Cation-Chloride-Cotransporters in the Intestinal and Renal Tissues of the European Eel (Anguilla Anguilla). *Comparative Biochemistry and Physiology - B Biochemistry and Molecular Biology,* 149 (1): 63–73.

de Los Heros, P., Alessi, D.R., R., Gourlay, D., Campbell, G., Deak, M., Macartney, T.J., Kahle, K.T., and Zhang, J. (2014). The WNK-Regulated SPAK/OSR1 Kinases Directly Phosphorylate and Inhibit the K+ -Cl- Co-Transporters. *Biochemical Journal,* 458 (3): 559–73.

de Los Heros, P., Kahle, K.T., Rinehart, J., Bobadilla, N.A., Vázquez, N., San Cristobal, P., Mount, D.B., Lifton, R.P., Hebert, S.C., and Gamba, G. (2006). WNK3 Bvpasses the Tonicity Requirements for K-Cl Cotransporter Activation via a Phosphatase-Dependent Pathway. *Proceedings of the National Academy of Sciences of the United States of America,* 103 (6): 1976–81.

Deeb, T. Z., Lee, H.H.C., Walker, J. A., Davies, P. A., and Moss, S. J. (2011). Hyperpolarizing GABAergic Transmission Depends on KCC2 Function and Membrane Potential. *Channels*, 5 (6): 475–81.

Delpire, E. (2000). Cation-Chloride Cotransporters in Neuronal Communication. *News Physiol. Sci.* 15: 309–12.

Delpire, E., and Austin, T.M. (2010). Kinase Regulation of Na^+-K^+-$2Cl^-$ Cotransport in Primary Afferent Neurons. *The Journal of Physiology,* 588 (Pt 18): 3365–73.

Delpire, E., and Gagnon, K.B. (2011). Kinetics of Hyperosmotically Stimulated Na-K-2Cl Cotransporter in Xenopus Laevis Oocytes. *American Journal of Physiology - Cell Physiology,* 301 (5).

Delpire, E., Gagnon, K.B., Ledford, J., and Wallace, J. (2011). Housing and husbandry of *Xenopus laevis* impact the quality of oocytes for heterologous expression studies. *J. Am. Assoc. Lab. Anim. Sci.* 50: 46-53.

Delpire, E., Lu, J., England, R., Dull, C., and Thorne, T. (1999). Deafness and Imbalance Associated with Inactivation of the Secretory Na-K-2Cl Co-Transporter. *Nature Genetics* 22: 192–95.

Delpire, E., Rauchman, M.I., Beier, D.R., Hebert, S.C., and Gullans, S.R. (1994a). Molecular Cloning and Chromosome Localization of a Putative Basolateral Na^+-K^+-$2Cl^-$ Cotransporter from Mouse Inner Medullary Collecting Duct (MIMCD-3) Cells. *Journal of Biological Chemistry,* 269 (41): 25677–83.

Delpire, E., and Weaver, C.D. (2016). Challenges of Finding Novel Drugs Targeting the K-Cl Cotransporter. *ACS Chemical Neuroscience,* 7 (12): 1624–27.

Delpire, E. Wolfe, L., Flores, B., Koumangoye, R., Schornak, C.C., Omer, S., Pusey, B., Lau, C., Markello, T., and Adams, D.R. (2016). A Patient with Multisystem Dysfunction Carries a Truncation Mutation in Human SLC12A2, the Gene Encoding the Na-K-2Cl Cotransporter, NKCC1. *Cold Spring Harbor Molecular Case Studies,* 2 (6): a001289.

Demian, W.L., Persaud, A., Jiang, C., Coyaud, É., Liu, S., Kapus, A., Kafri, R., Raught, B., and Rotin, D. (2019). The Ion Transporter NKCC1 Links Cell Volume to Cell Mass Regulation by Suppressing MTORC1. *Cell Reports,* 27 (6): 1886-1896.e6.

Deng, L., and Chen, G. (2003). Cyclothiazide Potently Inhibits γ-Aminobutyric Acid Type A Receptors in Addition to Enhancing Glutamate Responses. *Proceedings of the National Academy of Sciences of the United States of America*, 100 (22): 13025–29.

Desarmenien, M., Santangelo, F., Loeffler, J.P., and Feltz, P. (1984). Comparative Study of GABA-Mediated Depolarizations of Lumbar A Delta and C Primary Afferent Neurones of the Rat. *Experimental Brain Research,* 54 (3): 521–28.

Devor, M. (1999). Unexplained Peculiarities of the Dorsal Root Ganglion. *Pain,* Suppl 6: S27-35.

Dharmsathaphorn, K., Mandel, K. G., Masui, H. and McRoberts, J. A. (1985). Vasoactive Intestinal Polypeptide-Induced Chloride Secretion by a Colonic Epithelial Cell Line. Direct Participation of a Basolaterally Localized Na^+,K^+,Cl^- Cotransport System. *Journal of Clinical Investigation,* 75 (2): 462–71.

Ding, J., and Delpire, E. (2014a). Deletion of KCC3 in Parvalbumin Neurons Leads to Locomotor Deficit in a Conditional Mouse Model of Peripheral Neuropathy Associated with Agenesis of the Corpus Callosum. *Behavioural Brain Research,* 274: 128–36.

Ding, J., Ponce-Coria, J., and Delpire. E. (2013). A Trafficking-Deficient Mutant of KCC3 Reveals Dominant-Negative Effects on K–Cl Cotransport Function. *PLoS ONE,* 8 (4): e61112.

Disse-Nicodeme, S., Achard, J., Desitter, I., Houot, A., Fournier, A., Corvol, P., and Jeunemaitre, X. (2000). A New Locus on Chromosome 12p13.3 for Pseudohypoaldosteronism Type II, an Autosomal Dominant Form of Hypertension. *American Journal of Human Genetics,* 67 (2): 302–10.

Dong, C., Wei, P., Jian, X., Gibbs, R., Boerwinkle, E., Wang, K., and Liu, X. (2015). Comparison and integration of deleteriousness prediction methods for nonsynonymous SNVs in whole exome sequencing studies. *Human Molecular Genetics,* 24: 2125-2137.

Doucet, A. (1988). Function and Control of Na-K-ATPase in Single Nephron Segments of the Mammalian Kidney. *Kidney International,* 34 (6): 749–60.

Dunham, P. B., Stewart, G. W., and Ellory, J. C. (1980). Chloride-Activated Passive Potassium Transport in Human Erythrocytes. *Proceedings of the National Academy of Sciences of the United States of America,* 77 (3 I): 1711–15.

Dvorak, M.M., De Joussineau, C., Carter, D.H., Pisitkun, T., Knepper, M. A., Gamba, G., Kemp, P.J., and Riccardi, D. (2007). Thiazide Diuretics Directly Induce Osteoblast Differentiation and Mineralized Nodule Formation by Interacting with a Sodium Chloride Co-Transporter in Bone. *Journal of the American Society of Nephrology,* 18 (9): 2509–16.

Dzhala, V.I., Talos, D.M., Sdrulla, D.A., Brumback, A.C., Mathews, G.C., Benke, T.A., Delpire, E., Jensen, F.E., and Staley, K.J. (2005). NKCC1 Transporter Facilitates Seizures in the Developing Brain. *Nature Medicine,* 11 (11): 1205–13.

Ellgaard, L., Molinari, M.,and Helenius, A. (1999). Setting the Standards: Quality Control in the Secretory Pathway. *Science*. 286 (5446), 1882-8

Ellison, D.H., Velazquez, H. and Wright, F. S. (1987). Thiazide-Sensitive Sodium Chloride Cotransport in Early Distal Tubule. *American Journal of Physiology - Renal Fluid and Electrolyte*

Physiology, 253 (3): F546-54

Ellwanger, K., and Hausser, A. (2013). Physiological Functions of Protein Kinase D in Vivo. *IUBMB Life*. 65 (2), 98-107

Estébanez, B. De Paz, J.A., Cuevas, M.J., and González-Gallego, J. (2018). Endoplasmic Reticulum Unfolded Protein Response, Aging and Exercise: An Update. *Frontiers in Physiology*, 9, 1744

Fatkin, D., MacRae, C., Sasaki, T., Wolff, M.R., Porcu, M., Frenneaux, M., Atherton, J., Vidaillet, H.J., Jr., Spudich, S., De Girolami, U., et al. (1999). Missense mutations in the rod domain of the lamin A/C gene as causes of dilated cardiomyopathy and conduction-system disease. *New Eng. J. Med.* 341: 1715-1724.

Feeney, D.M., Gonzalez, A., and Law, W.A. (1982). Amphetamine, Haloperidol, and Experience Interact to Affect Rate of Recovery after Motor Cortex Injury. *Science,* 217 (4562): 855–57.

Ferguson, P.L., Smith, G.M., Wannamaker, B.B., Thurman, D.J., Pickelsimer, E.E., and Selassie, A.W. (2010). A Population-Based Study of Risk of Epilepsy after Hospitalization for Traumatic Brain Injury. *Epilepsia,* 51 (5): 891–98.

Fielitz, J., Kim, M.S., Shelton, J. M., Qi, X., Hill, J. A., Richardson, J. A., Bassel-Duby, R., and Olson, E.N. (2008). Requirement of Protein Kinase D1 for Pathological Cardiac Remodeling. *Proceedings of the National Academy of Sciences,* 105 (8): 3059–63.

Finkel, T., Menazza, S., Holmström, K.M., Parks, R.J., Liu, J., Sun, J., Liu, J., Pan, X., and Murphy, E. (2015). The Ins and Outs of Mitochondrial Calcium. *Circulation Research*, 116 (11), 1810-9

Flagella, M., Clarke, L. L., Miller, M. L., Erway, L. C., Giannella, R. A., Andringa, A., … Shull, G. E. (1999). Mice lacking the basolateral Na-K-2Cl cotransporter have impaired epithelial chloride secretion and are profoundly deaf. *Journal of Biological Chemistry*, 274(38), 26946–26955.

Flemmer, A.W., Giménez, I., Dowd, B.F.X., Darman, R.B., and Forbush. B., (2002). Activation of the Na-K-Cl Cotransporter NKCC1 Detected with a Phospho-Specific Antibody. *Journal of Biological Chemistry,* 277 (40): 37551–58.

Flores, B., Schornak, C.C., and Delpire, E. (2018). A Role for KCC3 in Maintaining Cell Volume of Peripheral Nerve Fibers. *Neurochemistry International*, 123: 114-124

Forbush, B., and Palfrey, H.C. (1983). [3H]Bumetanide Binding to Membranes Isolated from Dog Kidney Outer Medulla. Relationship to the Na,K,Cl Co-Transport System. *The Journal of Biological Chemistry,* 258 (19): 11787–92.

Franceschi, L., Villa-Moruzzi, E., Biondani, A., Siciliano, A., Brugnara, C., Alper, S.L., Lowell, C.A., and Berton, G. (2006). Regulation of K-Cl Cotransport by Protein Phosphatase 1α in Mouse

Erythrocytes. *Pflugers Archiv European Journal of Physiology,* 451 (6): 760–68.

Fujii, Takuto, Kyosuke Fujita, Noriaki Takeguchi, and Hideki Sakai. (2011). Function of K^+-Cl^- Cotransporters in the Acid Secretory Mechanism of Gastric Parietal Cells. *Biological and Pharmaceutical Bulletin*. 34 (6), 810-2

Gagnon, K.B.E, England, R., and Delpire, E. (2006). Characterization of SPAK and OSR1, Regulatory Kinases of the Na-K-2Cl Cotransporter. *Molecular and Cellular Biology,* 26 (2): 689–98.

Gagnon, K.B.E, and Delpire, E. (2013a). Physiology of SLC12 Transporters: Lessons from Inherited Human Genetic Mutations and Genetically Engineered Mouse Knockouts. *American Journal of Physiology-Cell Physiology,* 304 (8): C693–714.

Gagnon, K.B.E., England, R., and Delpire, E. (2006). Volume Sensitivity of Cation-Cl- Cotransporters Is Modulated by the Interaction of Two Kinases: Ste20-Related Proline-Alanine-Rich Kinase and WNK4. *American Journal of Physiology - Cell Physiology,* 290 (1): C134–42.

Galan, A., and Cervero, F. (2005). Painful Stimuli Induce in Vivo Phosphorylation and Membrane Mobilization of Mouse Spinal Cord NKCC1 Co-Transporter. *Neuroscience,* 133 (1): 245–52.

Gallagher, J.P., Higashi, H., and Nishi, S. (1978). Characterization and Ionic Basis of GABA-Induced Depolarizations Recorded in Vitro from Cat Primary Afferent Neurones. *The Journal of Physiology* 275: 263–82.

Gamba, G., Saltzberg, S. N., Lombardi, M., Miyanoshita, A., Lytton, J., Hediger, M.A., Brenner, B.M., and Hebert, S.C. (1993). Primary Structure and Functional Expression of a CDNA Encoding the Thiazide-Sensitive, Electroneutral Sodium-Chloride Cotransporter. *Proceedings of the National Academy of Sciences of the United States of America,* 90 (7): 2749–53.

Gamba, G. (2005). Molecular Physiology and Pathophysiology of Electroneutral Cation-Chloride Cotransporters. *Physiological Reviews,* 85 (2): 423–93.

Gamba, G., Miyanoshita, A., Lombardi, M., Lytton, J., Lee, W., Hediger, M.A., and Hebert, S.C. (1994). Molecular Cloning, Primary Structure, and Characterization of Two Members of the Mammalian Electroneutral Sodium-(Potassium)-Chloride Cotransporter Family Expressed in Kidney. *Journal of Biological Chemistry,* 269 (26): 17713–22.

Ganguly, K., Schinder, A.F., Wong, S.T., and Poo, M. (2001). GABA Itself Promotes the Developmental Switch of Neuronal GABAergic Responses from Excitation to Inhibition. *Cell*, 105 (4): 521–32.

Garzón-Muvdi, T., Pacheco-Alvarez, D., Gagnon, K.B.E., Vázquez, N., Ponce-Coria, J., Moreno, E., Delpire, E., and Gamba. G. (2007). WNK4 Kinase Is a Negative Regulator of K^+-Cl^- Cotransporters. *American Journal of Physiology - Renal Physiology,* 292 (4).

Geck, P., Pietrzyk, C., Burckhardt, B.C., Pfeifferl, B., and Heinz, E. (1980). Electrically Silent Cotransport of Na^+, K^+ and Cl^- in Ehrlich Cells. *Biochimica et Biophysica Acta - Biomembranes,* 600 (2): 432–47.

Gelderd, J.B., and Chopin, S.F. (1977). The Vertebral Level of Origin of Spinal Nerves in the Rat. *The Anatomical Record,* 188 (1): 45–47.

Gillen, C.M., Brill, S., Payne, J.A., and Forbush, B. (1996). Molecular Cloning and Functional Expression of the K-Cl Cotransporter from Rabbit, Rat, and Human: A New Member of the Cation-Chloride Cotransporter Family. *Journal of Biological Chemistry*, 271 (27): 16237–44.

Giménez, I., Isenring, P.,and Forbush, B. (2002). Spatially Distributed Alternative Splice Variants of the Renal Na-K-Cl Cotransporter Exhibit Dramatically Different Affinities for the Transported Ions. *Journal of Biological Chemistry,* 277 (11): 8767–70.

Golyala, A., and Kwan, P. (2017). Drug Development for Refractory Epilepsy: The Past 25 Years and Beyond. *Seizure*. 44, 147-156

Granados-Soto, V., Arguelles, C.F., and Álvarez-Leefmans, F.J. (2005). Peripheral and Central Antinociceptive Action of Na^+–K^+–$2Cl^-$ Cotransporter Blockers on Formalin-Induced Nociception in Rats. *Pain,* 114 (1): 231–38.

Greger, R. (1985). Ion Transport Mechanisms in Thick Ascending Limb of Henle's Loop of Mammalian Nephron. *Physiological Reviews*, 65(3), 760-97

Greger, R., and Schlatter, E. (1981). Presence of Luminal K^+, a Prerequisite for Active NaCl Transport in the Cortical Thick Ascending Limb of Henle's Loop of Rabbit Kidney. *Pflugers Archiv : European Journal of Physiology,* 392 (1): 92–94.

Gregoriades, J. M. C., Madaris, A., Alvarez, F. J., & Alvarez-Leefmans, F. J. (2019). Genetic and pharmacological inactivation of apical Na^+-K^+-$2Cl^-$ cotransporter 1 in choroid plexus epithelial cells reveals the physiological function of the cotransporter. *American Journal of Physiology - Cell Physiology*, *316*(4), C525–C544.

Guha, S., Tanasanvimon, S., Sinnett-Smith, J., and Rozengurt, E. (2010). Role of Protein Kinase D Signaling in Pancreatic Cancer. *Biochemical Pharmacology*, 80 (12), 1946-54

Gülow, K., Bienert, D., and Haas, I.G. (2002). BiP Is Feed-Back Regulated by Control of Protein Translation Efficiency. *Journal of Cell Science,* 115 (11): 2443–52.

Harrison, B. C., Kim, M.S., van Rooij, E., Plato, C. F., Papst, P. J., Vega, R. B., McAnally, J. A., et al., (2006). Regulation of Cardiac Stress Signaling by Protein Kinase D1. *Molecular and Cellular Biology,* 26 (10): 3875–88.

Hartl, F. U., Bracher, A., and Hayer-Hartl, M. (2011). Molecular chaperones in protein folding and proteostasis. *Nature, 475* (7356): 324-332.

World Health Organization (2019). Neurological Disorders, Including Epilepsy. https://www.who.int/mental_health/management/neurological/en/.

Henrar, S., and Arickx, F., (2016). Negotiating prices of drugs for rare diseases. *Bulletin of the World Health Organization.* 94:779-781

Hetz, C., and Saxena, S. (2017). ER Stress and the Unfolded Protein Response in Neurodegeneration. *Nature Reviews Neurology*, 13 (8): 477-491

Hiki, K., D'Andrea, R.J., Furze, J., Crawford, J., Woollatt, E., Sutherland, G.R., Vadas, M.A., and Gamble, J.R. (1999). Cloning, Characterization, and Chromosomal Location of a Novel Human K + -Cl - Cotransporter. *Journal of Biological Chemistry,* 274 (15): 10661–67.

Hoffmann, E K, and P B Dunham. (1995). Membrane Mechanisms and Intracellular Signalling in Cell Volume Regulation. *International Review of Cytology,* 161: 173–262.

Hoffmann, E.K., Lambert, I.H., and Pedersen, S.F., (2009). Physiology of Cell Volume Regulation in Vertebrates. *Physiological Reviews,* 89 (1):193-277.

Hogan, Quinn H. (2010). Labat Lecture: The Primary Sensory Neuron. *Regional Anesthesia and Pain Medicine,* 35 (3): 306–11.

Howard, H.C., Mount, D.B., Rochefort, D., Byun, N., Dupré, N., Lu, J., Fan, X., et al., (2002). The K-Cl Cotransporter KCC3 Is Mutant in a Severe Peripheral Neuropathy Associated with Agenesis of the Corpus Callosum. *Nature Genetics*, 32: 384–392.

Huang, H., Song, S., Banerjee, S., Jiang, T., Zhang, J., Kahle, K.T., Sun, D.,and Zhang, Z. (2019). The WNK-SPAK/OSR1 Kinases and the Cation-Chloride Cotransporters as Therapeutic Targets for Neurological Diseases. *Aging and Disease,* 10 (3): 626.

Huberfeld, G., Wittner, L., Clemenceau, S., Baulac, M., Kaila, K., Miles, R., and Rivera, C. (2007). Perturbed Chloride Homeostasis and GABAergic Signaling in Human Temporal Lobe Epilepsy. *Journal of Neuroscience,* 27 (37): 9866–73.

Hübner, C.A., Stein, V., Hermans-Borgmeyer, I., Meyer, T., Ballanyi, K., and Jentsch, T.J. (2001a). Disruption of KCC2 Reveals an Essential Role of K-Cl Cotransport Already in Early Synaptic Inhibition. *Neuron,* 30 (2): 515–24.

Humphreys, G. (2012,). Coming together to combat rare diseases. *Bulletin of the World Health Organization*. World Health Organization. 90(6): 406–407.

Hyde, T.M., Lipska, B.K., Ali, T., Mathew, S.V., Law, A.J., Metitiri, O.E., Straub, R.E. et al., (2011). Expression of GABA Signaling Molecules KCC2, NKCC1, and GAD1 in Cortical Development and Schizophrenia. *Journal of Neuroscience,* 31 (30): 11088–95.

Igarashi, P., Heuvel, G.B.V., Payne, J.A., and Forbush, B. (1995). Cloning, Embryonic Expression, and Alternative Splicing of a Murine Kidney-Specific Na-K-Cl Cotransporter. *American Journal of Physiology - Renal Fluid and Electrolyte Physiology,* 269 (3 38-3).

Imad, H., Johan, Z., and Eva, K. (2015). Hypoglycemia and Risk of Seizures: A Retrospective Cross-Sectional Study. *Seizure*, 25: 147–49.

Isenring, P., and Forbush, B. (1997). Ion and Bumetanide Binding by the Na-K-Cl Cotransporter. Importance of Transmembrane Domains. *Journal of Biological Chemistry,* 272 (39): 24556–62.

Isenring, P., Jacoby, S.C., Chang, J., and Forbush. B. (1998). Mutagenic Mapping of the Na-K-Cl Cotransporter for Domains Involved in Ion Transport and Bumetanide Binding. *Journal of General Physiology,* 112 (5): 549–58.

Isenring, P., Jacoby, S.C.,and Forbush, B. (1998). The Role of Transmembrane Domain 2 in Cation Transport by the Na-K-Cl Cotransporter. *Proceedings of the National Academy of Sciences of the United States of America,* 95 (12): 7179–84.

Isenring, P., Jacoby, S.C., Payne, J.A., and Forbush, B. (1998). Comparison of Na-K-Cl Cotransporters NKCC1, NKCC2, AND THE HEK Cell Na-K-Cl Cotransporter. *J Biol Chem,* 273 (18): 11295-301

Ita, S. V. De, Lawand, N. B., Lin, Q., Castañeda-Hernandez, G., & Willis, W. D. (2006). Role of the Na^+-K^+-$2Cl^-$ cotransporter in the development of capsaicin-induced neurogenic inflammation. *Journal of Neurophysiology*, *95*(6), 3553–3561.

Jennings, M.L., and Schulz, R.K. (1991). Okadaic Acid Inhibition of KC1 Cotransport: Evidence That Protein Dephosphorylation Is Necessary for Activation of Transport by Either Cell Swelling or N-Ethylmaleimide. *Journal of General Physiology,* 97 (4): 799–817.

Jin, S.C., Homsy, J., Zaidi, S., Lu, Q., Morton, S., DePalma, S.R., Zeng, X., Qi, H., Chang, W., Sierant, M.C., et al. (2017). Contribution of rare inherited and de novo variants in 2,871 congenital heart disease probands. *Nat. Genet.* 49: 1593-1601.

Johnston, A. M., Naselli, G., Gonez, L. J., Martin, R. M., Harrison, L. C., & DeAizpurua, H. J. (2000). SPAK, a STE20/SPS1-related kinase that activates the p38 pathway. *Oncogene*, 19 (37): 4290–4297.

Jong, J.C.D., Van Der Vliet, W.A., Van Den Heuvel, L.P.W.J., Willems, P.H.G.M., Knoers, N.V.A.M., and Bindels, R.J.M. (2002). Functional Expression of Mutations in the Human NaCl Cotransporter:

Evidence for Impaired Routing Mechanisms in Gitelman's Syndrome. *Journal of the American Society of Nephrology*, 13 (6): 1442–48.

Jong, J.C.D., Willems, P.H.G.M., Mooren, F.J.M., Van Den Heuvel, L.P.W.J., Knoers, N.V.A.M., and Bindels, R.J.M. (2003). The Structural Unit of the Thiazide-Sensitive NaCl Cotransporter Is a Homodimer. *Journal of Biological Chemistry,* 278 (27): 24302–7.

Kadowaki, H., and Nishitoh, H. (2013). Signaling Pathways from the Endoplasmic Reticulum and Their Roles in Disease. *Genes*, *4*(3): 306-333.

Kaeberle, J. (2018). Epilepsy Disorders and Treatment Modalities. *NASN School Nurse (Print)*. NLM (Medline).

Kahle, K.T., Rinehart, J., De Los Heros, P., Louvi, A., Meade, P., Vazquez, N., Hebert, S.C., Gamba, G., Gimenez, I., and Lifton, R.P. (2005). WNK3 Modulates Transport of Cl- in and out of Cells: Implications for Control of Cell Volume and Neuronal Excitability. *Proceedings of the National Academy of Sciences of the United States of America,* 102 (46): 16783–88.

Kahle, K.T., and Staley, K.J. S (2008). The Bumetanide-Sensitive Na-K-2Cl Cotransporter NKCC1 as a Potential Target of a Novel Mechanism-Based Treatment Strategy for Neonatal Seizures. *Neurosurgical Focus,* 25 (3):E22.

Kahle, K.T., Flores, B., Bharucha-Goebel, D., Zhang, J., Donkervoort, S., Hegde, M., Hussain, G., et al., (2016). Peripheral Motor Neuropathy Is Associated with Defective Kinase Regulation of the KCC3 Cotransporter. *Science Signaling,* 9 (439): ra77.

Kahle, K.T., Merner, N.D., Friedel, P., Silayeva, L., Liang, B., Khanna, A., Shang, Y., et al., (2014). Genetically Encoded Impairment of Neuronal KCC 2 Cotransporter Function in Human Idiopathic Generalized Epilepsy. *EMBO Reports,* 15 (7): 766–74.

Kahle, K.T., and Staley, K.J. (2012). Neonatal Seizures and Neuronal Transmembrane Ion Transport. In *Jasper's Basic Mechanisms of the Epilepsies, 4th Edition: NCBI Bookshelf Online Book Version*, 1–12.

Kaji, D.M., and Tsukitani, Y. (1991). Role of Protein Phosphatase in Activation of KCl Cotransport in Human Erythrocytes. *American Journal of Physiology - Cell Physiology,* 260 (1 29-1). C176-80.

Kampinga, H.H., and Craig, E.A. (2010). The HSP70 chaperone machinery: J proteins as drivers of functional specificity. *Nat. Rev. Mol. Cell. Biol., 11* (8): 579-592.

Kaplan, M.R., Plotkin, M.D., Lee, W., Xu, Z., Lytton, J., and Hebert, S.C. (1996). Apical Localization of the Na-K-Cl Cotransporter, RBSC1, on Rat Thick Ascending Limbs. *Kidney International,* 49 (1): 40–47.

Karimy, J. K., Duran, D., Hu, J. K. J. K., Gavankar, C., Gaillard, J. R., Bayri, Y., Rice, H., Michael, L.L., Gerzanich, V., Simard, J.M., Kahle, K. T. (2016). Cerebrospinal fluid hypersecretion in pediatric hydrocephalus. *Neurosurgical Focus*, *41*(5): E10.

Katona, I., and Weis, J. (2018). Diseases of the Peripheral Nerves. *Handbook of Clinical Neurology*, 145:453–74.

Kim, J., and Jung, Y. (2012). Increased Aquaporin-1 and Na^+-K^+-$2Cl^-$ Cotransporter 1 Expression in Choroid Plexus Leads to Blood-Cerebrospinal Fluid Barrier Disruption and Necrosis of Hippocampal CA1 Cells in Acute Rat Models of Hyponatremia. *Journal of Neuroscience Research,* 90 (7): 1437–44.

Kircher, M., Witten, D.M., Jain, P., O'Roak, B.J., Cooper, G.M., and Shendure, J. (2014). A general framework for estimating the relative pathogenicity of human genetic variants. *Nature genetics* 46: 310-315.

Kishi, M., Tanabe, J., Schmelzer, J.D., and Low. P.A., (2002). Morphometry of Dorsal Root Ganglion in Chronic Experimental Diabetic Neuropathy. *Diabetes,* 51 (3): 819–24.

Kitamura, K., and Yamazaki, J. (2001). Chloride Channels and Their Functional Roles in Smooth Muscle Tone in the Vasculature. *Japanese Journal of Pharmacology,* 85 (4): 351–57.

Knupp, J., Arvan, P., and Chang, A. (2019). Increased Mitochondrial Respiration Promotes Survival from Endoplasmic Reticulum Stress. *Cell Death and Differentiation,* 26 (3): 487–501.

Koumangoye, R., Omer S., and Delpire, E. (2018a). Mistargeting of a Truncated Na-K-2Cl Cotransporter in Epithelial Cells. *Am J Physiol Cell Physiol,* 315 (2), C258-C276

Koumangoye, R., Omer S., and Delpire, E. (2019). A Dileucine Motif in the COOH-Terminal Domain of NKCC1 Targets the Cotransporter to the Plasma Membrane. *American Journal of Physiology - Cell Physiology,* 316 (4): C545-C558

Koumangoye, R., Omer S., Kabeer, M., and Delpire, E. (2020). Novel Human NKCC1 Mutations Cause Defects in Goblet Cells Mucus Secretion and Chronic Inflammation. *Cellular and Molecular Gastroenterology and Hepatology*, 9 (2), 239-255.

Krames, E.S. (2014). The Role of the Dorsal Root Ganglion in the Development of Neuropathic Pain. *Pain Medicine,* 15 (10): 1669-85.

Krarup, T., and Dunham, P.B. (1996). Reconstitution of Calyculin-Inhibited K-Cl Cotransport in Dog Erythrocyte Ghosts by Exogenous PP-1. *The American Journal of Physiology,* 270 (3 Pt 1): C898-902.

Krarup, T., Jakobsen, L.D., Jensen, B.S., and Hoffmann, E.K. (1998). Na^+-K^+-$2Cl^-$ Cotransport in

Ehrlich Cells: Regulation by Protein Phosphatases and Kinases. *The American Journal of Physiology,* 275 (1): C239-50.

Kregenow, F.M. (1981). Osmoregulatory Salt Transporting Mechanisms: Control of Cell Volume in Anisotonic Media. *Annual Review of Physiology,* 43 (1): 493–505.

Kregenow, F.M. (1971). The Response of Duck Erythrocytes to Nonhemolytic Hypotonic Media : Evidence for a Volume-Controlling Mechanism. *Journal of General Physiology* 58 (4): 372–95.

Kunau, R.T., Weller, D.R., and Webb. H.L. (1975). Clarification of the Site of Action of Chlorothiazide in the Rat Nephron. *Journal of Clinical Investigation,* 56 (2): 401–7.

Kunchaparty, S., Palcso, M., Berkman, J., Velázquez, H., Desir, G.V., Bernstein, P., Reilly, R.F., and Ellison, D.H. (1999). Defective Processing and Expression of Thiazide-Sensitive Na-Cl Cotransporter as a Cause of Gitelman's Syndrome. *American Journal of Physiology - Renal Physiology,* 277 (4): F643-9.

Kwan, P., and Brodie., M. J. (2000). Early Identification of Refractory Epilepsy. *New England Journal of Medicine,* 342 (5): 314–19.

Laird, J.M.A., García-Nicas, E., Delpire, E., and Cervero., F. (2004). Presynaptic Inhibition and Spinal Pain Processing in Mice: A Possible Role of the NKCC1 Cation-Chloride Co-Transporter in Hyperalgesia. *Neuroscience Letters,* 361 (1–3): 200–203.

Lapato, A.S., Szu, J.I., Hasselmann, J.P.C., Khalaj, A.J., Binder, D.K., and Tiwari-Woodruff, S.K. (2017). Chronic Demyelination-Induced Seizures. *Neuroscience,* 346 (March): 409–22.

Lauf, P. K. (1984). Thiol-Dependent passive K/Cl transport in sheep red cells: IV. Furosemide inhibition as a function of external Rb^+, Na^+, and Cl^-. *The Journal of Membrane Biology*, 77 (1): 57–62.

Lauf, P.K., and Theg, B.E. (1980). A Chloride Dependent K^+ Flux Induced by N-Ethylmaleimide in Genetically Low K+ Sheep and Goat Erythrocytes. *Biochemical and Biophysical Research Communications,* 92 (4): 1422–28.

LaValle, C.R., George, K.M., Sharlow, E.R., Lazo, J.S., Wipf, P., and Wang, Q.J. (2010). Protein Kinase D as a Potential New Target for Cancer Therapy. *Biochimica et Biophysica Acta (BBA) - Reviews on Cancer* 1806 (2): 183–92.

Lek, M., K.J., K., Minikel, E.V. , Samocha, K.E., Banks, E., F., T., O'Donnell-Luria, A.H., Ware, J.S., Hill, A.J., Cummings, B.B., Tukiainen, T., et al. (2016). Analysis of protein-coding genetic variation in 60,706 humans. *Nature,* 536: 285-291.

Lee, A.-H., Iwakoshi, N. N., and Glimcher, L. H. (2003). XBP-1 Regulates a Subset of Endoplasmic

Reticulum Resident Chaperone Genes in the Unfolded Protein Response. *Molecular and Cellular Biology,* 23 (21): 7448–59.

Lek, M., K.J., K., Minikel, E.V. , Samocha, K.E., Banks E2, F., T., O'Donnell-Luria, A.H., Ware, J.S., Hill, A.J., Cummings, B.B., Tukiainen, T., et al. (2016). Analysis of protein-coding genetic variation in 60,706 humans. *Nature*, 536: 285-291.

Lew, V.L., and Bookchin, R.M. (2005). Ion Transport Pathology in the Mechanism of Sickle Cell Dehydration. *Physiological Reviews*, 85 (1): 179-200.

Li, H., and Durbin, R. (2010). Fast and accurate long-read alignment with Burrows-Wheeler transform. *Bioinformatics,* 26: 589-595.

Li, Y., Hu, J., Vita, R., Sun, B., Tabata, H., and Altman, A. (2004). SPAK kinase is a substrate and target of PKCtheta in T-cell receptor-induced AP-1 activation pathway. *Embo J,* 23: 1112-1122.

Liapis, H., Nag, M.,and Kaji, D.M. (1998). K-Cl Cotransporter Expression in the Human Kidney. *American Journal of Physiology - Cell Physiology* 275 (6 44-6).

Liedtke, C.M., Hubbard, M., and Wang, X. (2003). Stability of actin cytoskeleton and PKC-delta binding to actin regulate NKCC1 function in airway epithelial cells. *Am. J. Physiol. Cell Physiol.* 284: C487-C496.

Liu, S., Chang, S., Han, B., Xu, L., Zhang, M., Zhao, C., Yang, W., et al., (2019). Cryo-EM Structures of the Human Cation-Chloride Cotransporter KCC1. *Science,* 366 (6464): 505–8.

Love, S. (2006). Demyelinating Diseases. *Journal of Clinical Pathology,* 59 (11): 1151–59.

Lu, J., Karadsheh, M., & Delpire, E. (1999). Developmental regulation of the neuronal-specific isoform of K-Cl cotransporter KCC2 in postnatal rat brains. *Journal of Neurobiology*, 39 (4): 558–568.

Malik, A.N., and Czajka, A. (2013). Is Mitochondrial DNA Content a Potential Biomarker of Mitochondrial Dysfunction? *Mitochondrion,* 13 (5): 481–92.

Mansfield, T. A., Simon, D. B., Farfel, Z., Bia, M., Tucci, J. R., Lebel, M., Gutkin, M., et al. (1997). Multilocus Linkage of Familial Hyperkalaemia and Hypertension, Pseudohypoaldosteronism Type II, to Chromosomes 1q31-42 and 17p11-Q21. *Nature Genetics,* 16 (2): 202–5.

Mao, S., Garzon-Muvdi, T., Difulvio, M., Chen, Y., Delpire, E., Alvarez-Leefmans, F.J. (2012). Molecular and Functional Expression of Cation-Chloride-Cotransporters in Dorsal Root Ganglion Neurons During Postnatal Maturation. *Journal of Neurophysiology,* 8 (3): 834-52.

Marcus, D.C., Marcus, N.Y., and Greger, R. (1987). Sidedness of Action of Loop Diuretics and

Ouabain on Nonsensory Cells of Utricle: A Micro-Ussing Chamber for Inner Ear Tissues. *Hearing Research,* 30 (1): 55–64.

Martínez-Fábregas, J., Prescott, A., van Kasteren, S., Pedrioli, D. L., McLean, I., Moles, A., Reinheckel, T., Poli, V., Watts, C. (2018). Lysosomal protease deficiency or substrate overload induces an oxidative-stress mediated STAT3-dependent pathway of lysosomal homeostasis. *Nature Commun., 9*, 5343.

Maryanovich, M., and Gross, A. (2013). A ROS Rheostat for Cell Fate Regulation. *Trends in Cell Biology,* 23 (3): 129-34.

Mastroianni, N., De Fusco, M., Zollo, M., Arrigo, G., Zuffardi, O., Bettinelli, A., Ballabio, A.,and Casari, G. (1996). Molecular Cloning, Expression Pattern, and Chromosomal Localization of the Human Na-Cl Thiazide-Sensitive Cotransporter (SLC12A3). *Genomics,* 35 (3): 486–93.

Materson, B.J. (1983). Insights into Intrarenal Sites and Mechanisms of Action of Diuretic Agents. *American Heart Journal,* 106 (1 PART 2): 188–208.

Matthews, J. B., Hassan, I., Meng, S., Archer, S. Y., Hrnjez, B. J., & Hodin, R. A. (1998). Na-K-2Cl cotransporter gene expression and function during enterocyte differentiation. Modulation of Cl- secretory capacity by butyrate. *Journal of Clinical Investigation*, 101 (10): 2072–2079.

Mayan, H., Vered, I., Mouallem, M., Tzadok-Witkon, M., Pauzner, R.,and Farfel, Z. (2002). Pseudohypoaldosteronism Type II: Marked Sensitivity to Thiazides, Hypercalciuria, Normomagnesemia, and Low Bone Mineral Density. *Journal of Clinical Endocrinology and Metabolism,* 87 (7): 3248–54.

McKenna, A., Hanna, M., Banks, E., Sivachenko, A., Cibulskis, K., Kernytsky, A., Garimella, K., Altshuler, D., Gabriel, S., Daly, M., et al. (2010). The Genome Analysis Toolkit: a MapReduce framework for analyzing next-generation DNA sequencing data. *Genome research,* 20: 1297-1303.

McCormick, J.A., Yang, C., Zhang, C., Davidge, B., Blankenstein, K.I., Terker, A.S., Yarbrough, B., et al., (2014). Hyperkalemic Hypertension-Associated Cullin 3 Promotes WNK Signaling by Degrading KLHL3. *Journal of Clinical Investigation,* 124 (11): 4723–36.

Mekahli, D., Bultynck, G., Parys, J.B., de Smedt, H., and Missiaen, L. (2011). Endoplasmic-Reticulum Calcium Depletion and Disease. *Cold Spring Harbor Perspectives in Biology*, 3 (6):a004317

Melo, Z., Cruz-Rangel, S., Bautista, R., Vázquez, N., Castañeda-Bueno, M., Mount, D.B., Pasantes-Morales, H., Mercado, A., and Gamba, G. (2013). Molecular Evidence for a Role for K-Cl Cotransporters in the Kidney. *Am J Physiol Renal Physiol,* 305: 1402–11.

Melo, Z., De Los Heros, P., Cruz-Rangel, S., Vázquez, N., Bobadilla, N.A., Pasantes-Morales, H., Alessi, D.R., Mercado, A., and Gamba, G. (2013). N-Terminal Serine Dephosphorylation Is Required for KCC3 Cotransporter Full Activation by Cell Swelling. *Journal of Biological Chemistry,* 288 (44): 31468–76.

Mercado, A., Broumand, V., Zandi-Nejad, K., Enck, A.H., and Mount, D.B. (2006). A C-Terminal Domain in KCC2 Confers Constitutive K+-Cl - Cotransport. *Journal of Biological Chemistry,* 281 (2): 1016–26.

Mercado, A., Song, L., Vázquez, N., Mount, D.B., and Gamba, G. (2000). Functional Comparison of the K+-Cl- Cotransporters KCC1 and KCC4. *Journal of Biological Chemistry,* 275 (39): 30326–34.

Mercado, A., Vázquez, N., Song, L., Cortés, R., Enck, A.H., Welch, R., Delpire, E., Gamba, G., and Mount, D.B. (2005). NH_2 -Terminal Heterogeneity in the KCC3 K^+ -Cl^- Cotransporter. *American Journal of Physiology-Renal Physiology,* 289 (6): F1246–61.

Misri, S., Chimote, A.A., Adragna, N.C., Warwar, R., Brown, T.L., and Lauf, P.K. (2006). KCC Isoforms in a Human Lens Epithelial Cell Line (B3) and Lens Tissue Extracts. *Experimental Eye Research,* 83 (5): 1287–94.

Monroy, A., Plata, C.,Hebert, S.C.,and Gamba, G. (2000). Characterization of the Thiazide-Sensitive Na+-Cl- Cotransporter: A New Model for Ions and Diuretics Interaction. *American Journal of Physiology - Renal Physiology,* 279 (1).:F161-9

Moore-Hoon, M.L., and Turner, R.J. (2000). The Structural Unit of the Secretory Na+-K+-2Cl-Cotransporter (NKCCl) Is a Homodimer. *Biochemistry,* 39 (13): 3718–24.

Mounkes, L.C., Kozlov, S.V., Rottman, J.N., and Stewart, C.L. (2005). Expression of an LMNA-N195K variant of A-type lamins results in cardiac conduction defects and death in mice. *Hum. Mol. Genet.* 14: 2167-2180.

Mount, D.B., Mercado, A., Song, L., Jason, X., George, A.L., Delpire, E., and Gamba, G. (1999). Cloning and Characterization of KCC3 and KCC4, New Members of the Cation-Chloride Cotransporter Gene Family. *Journal of Biological Chemistry,* 274 (23): 16355–62.

Murphy, M.P. (2009). How Mitochondria Produce Reactive Oxygen Species. *Biochemical Journal*, 417 (1), 1-13.

Nave, K., and Werner, H.B. (2014). Myelination of the Nervous System: Mechanisms and Functions. *Annual Review of Cell and Developmental Biology,* 30 (1): 503–33.

Nezu, A., Parvin, M.N., and Turner, R. J. (2009). A Conserved Hydrophobic Tetrad near the C Terminus of the Secretory Na^+-K^+-$2Cl^-$ Cotransporter (NKCC1) Is Requiredfor Its Correct

Intracellular Processing. *Journal of Biological Chemistry,* 284 (11): 6869–76.

NIH Genetic and Rare Diseases Information Center (GARD) (2017). FAQs About Rare Diseases - an NCATS Program. https://rarediseases.info.nih.gov/diseases/pages/31/faqs-about-rare-diseases

Norman, B. J., and Miller, S.D. (2011). Human Genome Project and Sickle Cell Disease. *Social Work in Public Health*, 26 (4): 405–16.

Oh, S.J., Hemmi, S., and Hatanaka, Y. (2015). On-Nerve Needle Nerve Conduction Study in the Sural Nerve: A New Technique for Evaluation of Peripheral Neuropathy. *Clinical Neurophysiology,* 126 (9): 1811–16.

Orlov, S.N., Tremblay, J., and Hamet, P. (2010). NKCC1 and Hypertension: A Novel Therapeutic Target Involved in the Regulation of Vascular Tone and Renal Function. *Current Opinion in Nephrology and Hypertension*, 19 (2): 163-8

Pace, A. J., Lee, E., Athirakul, K., Coffman, T. M., O'Brien, D. A., & Koller, B. H. (2000). Failure of spermatogenesis in mouse lines deficient in the Na^+-K^+- $2Cl^-$ cotransporter. *Journal of Clinical Investigation*, *105*(4), 441–450.

Pacheco-Alvarez, Diana, and Gerardo Gamba. (2011). WNK3 Is a Putative Chloride-Sensing Kinase. *Cellular Physiology and Biochemistry* 28 (6): 1123–34.

Pain, V.M., Randall, D. P., and Garlick, P. J. (1984). Protein Synthesis in Liver and Skeletal Muscle of Mice Bearing an Ascites Tumor. *Cancer Research,* 44 (3): 1054–57.

Payne, J. A., Xu, J. C., Haas, M., Lytle, C. Y., Ward, D., and Forbush, B. (1995). Primary Structure, Functional Expression, and Chromosomal Localization of the Bumetanide-Sensitive Na-K-Cl Cotransporter in Human Colon. *Journal of Biological Chemistry,* 270 (30): 17977–85.

Payne, J.A. (1997). Functional Characterization of the Neuronal-Specific K-Cl Cotransporter: Implications for $[K^+]_{(o)}$ Regulation. *American Journal of Physiology - Cell Physiology,* 273 (5): C1516-25

Payne, J.A., and Forbush, B. (1994). Alternatively Spliced Isoforms of the Putative Renal Na-K-Cl Cotransporter Are Differentially Distributed within the Rabbit Kidney. *Proceedings of the National Academy of Sciences of the United States of America* 91 (10): 4544–48.

Payne, J.A., Stevenson, T.J., and Donaldson, L.F. (1996). Molecular Characterization of a Putative K-Cl Cotransporter in Rat Brain: A Neuronal-Specific Isoform. *Journal of Biological Chemistry,* 271 (27): 16245–52.

Pearson, M.M, Lu, J., Mount, D.B., and Delpire, E. (2001). Localization of the K^+–Cl^- Cotransporter,

KCC3, in the Central and Peripheral Nervous Systems: Expression in the Choroid Plexus, Large Neurons and White Matter Tracts. *Neuroscience,* 103 (2): 481–91.

Pellegrino, C.M., Rybicki, A.C., Musto, S., Nagel, R.L., and Schwartz, R.S. (1998). Molecular Identification and Expression of Erythroid K:Cl Cotransporter in Human and Mouse Erythroleukemic Cells. *Blood Cells, Molecules and Diseases,* 24 (1): 31–40.

Peng, Tsung I., and Mei Jie Jou. (2010). Oxidative Stress Caused by Mitochondrial Calcium Overload. In *Annals of the New York Academy of Sciences*, 1201:183–88.

Pfaffenbach, K.T., Pong, Mi., Morgan, T.E., Wang, H., Ott, K., Zhou, B., Longo, V.D., and Lee, A.S. (2012). GRP78/BiP Is a Novel Downstream Target of IGF-1 Receptor Mediated Signaling. *Journal of Cellular Physiology,* 227 (12): 3803–11.

Pfeffer, G., and Chinnery, P.F. (2013). Diagnosis and Treatment of Mitochondrial Myopathies. *Annals of Medicine*, 45 (1): 4-16.

Piala, A. T., Moon, T. M., Akella, R., He, H., Cobb, M. H., & Goldsmith, E. J. (2014). Chloride sensing by WNK1 involves inhibition of autophosphorylation. *Science Signaling*, 7 (324): ra41

Piechotta, K., Garbarini, N., England, R., and Delpire, E. (2003). Characterization of the Interaction of the Stress Kinase SPAK with the Na^+ -K^+ -$2Cl^-$ Cotransporter in the Nervous System. *Journal of Biological Chemistry,* 278 (52): 52848–56.

Piechotta, K., Lu, J., and Delpire, E. (2002). Cation Chloride Cotransporters Interact with the Stress-Related Kinases Ste20-Related Proline-Alanine-Rich Kinase (SPAK) and Oxidative Stress Response 1 (OSR1). *Journal of Biological Chemistry,* 277 (52): 50812–19.

Pisciotta, C., and Shy, M.E. (2018). Neuropathy. In *Handbook of Clinical Neurology*, 148: 653–65.

Plotkin, M.D, Kaplan, M. R., Peterson, L. N., Gullans, S. R., Hebert, S. C., and Delpire, E. (1997). Expression of the Na(+)-K(+)-2Cl- Cotransporter BSC2 in the Nervous System. *The American Journal of Physiology,* 272 (1 Pt 1): C173-83.

Plotkin, M.D., Kaplan, M.R., Verlander, J.W., Lee, W., Brown, D., Poch, E., Gullans, S.R., and Hebert, S.C. (1996). Localization of the Thiazide Sensitive Na-Cl Cotransporter, RTSC1, in the Rat Kidney. *Kidney International,* 50 (1): 174–83.

Price, A.L., Patterson, N.J., Plenge, R.M., Weinblatt, M.E., Shadick, N.A., and Reich, D. (2006). Principal components analysis corrects for stratification in genome-wide association studies. *Nat. Genet.* 38: 904-909.

Purcell, S., Neale, B., Todd-Brown, K., Thomas, L., Ferreira, M.A., Bender, D., Maller, J., Sklar, P., de Bakker, P.I., Daly, M.J., et al. (2007). PLINK: a tool set for whole-genome association and

population-based linkage analyses. *Am. J. Hum. Genet.,* 81: 559-575.

Puskarjov, M., Seja, P., Heron, S.E., Williams, T.C., Ahmad, F., Iona, X., Oliver, K.L.,et al., (2014). A Variant of KCC2 from Patients with Febrile Seizures Impairs Neuronal Cl^- Extrusion and Dendritic Spine Formation. *EMBO Reports,* 15 (6): 723–29.

Race, J.E., Makhlouf, F. N., Logue, P. J., Wilson, F. H., Dunham, P. B., andHoltzman, E. J. (1999). Molecular Cloning and Functional Characterization of KCC3, a New K-Cl Cotransporter. *The American Journal of Physiology,* 277 (6): C1210-9.

Randall, J., Thorne, T., & Delpire, E. (1997). Partial cloning and characterization of Slc12a2: The gene encoding the secretory Na^+-K^+-$2Cl^-$ cotransporter. *American Journal of Physiology - Cell Physiology*, *273*(4 42-4).

Reid, M.S., Kern, D.M., and Brohawn, S.G. (2019). Cryo-EM Structure of the Potassium-Chloride Cotransporter KCC4 in Lipid Nanodiscs. *BioRxiv*, 805267.

Richardson, C., akamoto, K., De Los Heros, P., Deak, M., Campbell, D.G., Prescott, A.R., and Alessi, D. R. (2011). Regulation of the NKCC2 Ion Cotransporter by SPAK-OSR1-Dependent and -Independent Pathways. *Journal of Cell Science,* 124 (5): 789–800.

Rinehart, J., Kahle, K.T., De Los Heros, P., Vazquez, N., Meade, P., Wilson, F.H., Hebert, S.C., Gimenez, I., Gamba, G., and Lifton, R.P. (2005). WNK3 Kinase Is a Positive Regulator of NKCC2 and NCC, Renal Cation-Cl - Cotransporters Required for Normal Blood Pressure Homeostasis. *Proceedings of the National Academy of Sciences of the United States of America*, 102 (46): 16777–82.

Rinehart, J., Maksimova, Y.D., Tanis, J.E., Stone, K.L., Hodson, C.A., Zhang, J., Risinger, M.,et al., (2009a). Sites of Regulated Phosphorylation That Control K-Cl Cotransporter Activity. *Cell,* 138 (3): 525–36.

Rivera, C., Voipio, J., Payne, J.A., Ruusuvuori, E., Lahtinen, H., Lamsa, K., Pirvola, U., Saarma, M., and Kaila, K. (1999). The K^+/Cl^- Co-Transporter KCC2 Renders GABA Hyperpolarizing during Neuronal Maturation. *Nature,* 397 (6716): 251–55.

Rocha-González, H.I., Mao, S., and Alvarez-Leefmans, F.J. (2008). Na^+,K^+,$2Cl^-$ Cotransport and Intracellular Chloride Regulation in Rat Primary Sensory Neurons: Thermodynamic and Kinetic Aspects. *Journal of Neurophysiology,* 100 (1): 169–84.

Rosenbluth, J. (2009). Multiple Functions of the Paranodal Junction of Myelinated Nerve Fibers. *Journal of Neuroscience Research*, 87 (15): 3250-8

Rozengurt, E. (2011). Protein Kinase D Signaling: Multiple Biological Functions in Health and Disease. *Physiology,* 26 (1): 23–33.

Rozengurt, E., Rey, O.,and Waldron, R.T. (2005). Protein Kinase D Signaling. *The Journal of Biological Chemistry,* 280 (14): 13205–8.

Rudomin, P., and Schmidt R.F. (1999). Presynaptic Inhibition in the Vertebrate Spinal Cord Revisited. *Experimental Brain Research*, 129 (1), 1-37.

Rust, M.B., Alper, S.L., Rudhard, Y., Shmukler, B.E., Vicente, R., Brugnara, C., Trudel, M., Jentsch, T.J.,and Hübner, C.A. (2007). Disruption of Erythroid K-Cl Cotransporters Alters Erythrocyte Volume and Partially Rescues Erythrocyte Dehydration in SAD Mice. *Journal of Clinical Investigation,* 117 (6): 1708–17.

Sabath, E., Meade, P., Berkman, J., De Los Heros, P., Moreno, E., Bobadilla, N.A., Vázqaez, N., Ellison, D.H.,and Gamba, G. (2004). Pathophysiology of Functional Mutations of the Thiazide-Sensitive Na-Cl Cotransporter in Gitelman Disease. *American Journal of Physiology - Renal Physiology,* 287 (2) F195-203.

Saitsu, H., Watanabe, M., Akita, T., Ohba, C., Sugai, K., Ong, W. P., et al. (2016). Impaired neuronal KCC2 function by biallelic SLC12A5 mutations in migrating focal seizures and severe developmental delay. *Scientific Reports*, *6*: 30072.

San Pietro, A., and Rittenberg, D. (1953). A Study of the Rate of Protein Synthesis in Humans. II. Measurement of the Metabolic Pool and the Rate of Protein Synthesis. *The Journal of Biological Chemistry,* 201 (1): 457–73.

Schröder, M., and Kaufman, R.J. (2005). The Mammalian Unfolded Protein Response. *Annual Review of Biochemistry* 74 (1): 739–89.

Senft, D., and Ronai, Z.A. (2015). UPR, Autophagy, and Mitochondria Crosstalk Underlies the ER Stress Response. *Trends in Biochemical Sciences*, 40 (3): 141-8.

Sharpee, T.O. (2014). Toward Functional Classification of Neuronal Types. *Neuron*, 83 (6): 1329-1334.

Shekarabi, M., Moldrich, R.X., Rasheed, S., Salin-Cantegrel, A., Laganiere, J., Rochefort, D., Hince, P.,et al., (2012). Loss of Neuronal Potassium/Chloride Cotransporter 3 (KCC3) Is Responsible for the Degenerative Phenotype in a Conditional Mouse Model of Hereditary Motor and Sensory Neuropathy Associated with Agenesis of the Corpus Callosum. *Journal of Neuroscience* 32 (11): 3865–76.

Shekarabi, M., Salin-Cantegrel, A., Laganière, J., Gaudet, R., Dion, P., and Rouleau, G.A. (2011a). Cellular Expression of the K^+–Cl^- Cotransporter KCC3 in the Central Nervous System of Mouse. *Brain Research,* 1374: 15–26.

Shorvon, S., and Luciano, A. (2007). Prognosis of Chronic and Newly Diagnosed Epilepsy: Revisiting Temporal Aspects. *Current Opinion in Neurology,* 20 (2): 208–12.

Sifrim, A., Hitz, M., Wilsdon, A., Breckpot, J., Al Turki, S.H., Thienpont, B., McRae, J., et al., (2016). Distinct Genetic Architectures for Syndromic and Nonsyndromic Congenital Heart Defects Identified by Exome Sequencing. *Nature Genetics,* 48 (9): 1060–65.

Simard, Charles F., Marc J. Bergeron, Rachelle Frenette-Cotton, Gabriel A. Carpentier, Marie Eve Pelchat, Luc Caron, and Paul Isenring. (2007). Homooligomeric and Heterooligomeric Associations between K^+-Cl^- Cotransporter Isoforms and between K^+-Cl^- and Na^+-K^+-Cl^- Cotransporters. *Journal of Biological Chemistry* 282 (25): 18083–93.

Simard, C.F., Brunet, G.M., Daigle, N.D., Montminy, V., Caron, L.,and Isenring, P. (2004). Self-Interacting Domains in the C Terminus of a Cation-Cl^- Cotransporter Described for the First Time. *Journal of Biological Chemistry,* 279 (39): 40769–77.

Simon, D.B., Nelson-Williams, C., Bia, M., Ellison, D., Karet, F.E., Molina, A.M., Vaara, I., et al., (1996). Gitelman's Variant of Bartter's Syndrome, Inherited Hypokalaemic Alkalosis, Is Caused by Mutations in the Thiazide-Sensitive Na-Cl Cotransporter. *Nature Genetics.* 12 (1): 24–30.

Singh, R., Almutairi, M.M., Pacheco-Andrade, R., Almiahuob, M.Y.M., and Di Fulvio, M. (2015). Impact of Hybrid and Complex N-Glycans on Cell Surface Targeting of the Endogenous Chloride Cotransporter Slc12a2. *International Journal of Cell Biology,* 2015: 505294

Smith, L., Smallwood, N., Altman, A., and Liedtke, C.M. (2008). PKCdelta acts upstream of SPAK in the activation of NKCC1 by hyperosmotic stress in human airway epithelial cells. J Biol Chem, 283: 22147-22156.

Soo, M.K., Eisner, C., Faulhaber-Walter, R., Mizel, D., Wall, S.M., Briggs, J.P., and Schnermann, J. (2008). Salt Sensitivity of Blood Pressure in NKCC1-Deficient Mice. *American Journal of Physiology - Renal Physiology,* 295 (4). F1230–F1238.

Stafstrom, C.E., and Carmant, L. (2015). Seizures and Epilepsy: An Overview for Neuroscientists. *Cold Spring Harbor Perspectives in Biology,* 7 (5): 1–19.

Starremans, P.G.J.F., Kersten, F.F.J., Knoers, N.V.A.M., Van Den Heuvel, L.P.W.J., and Bindels, R.J.M. (2003). Mutations in the Human Na-K-2Cl Cotransporter (NKCC2) Identified in Bartter Syndrome Type I Consistently Result in Nonfunctional Transporters. *Journal of the American Society of Nephrology,* 14 (6): 1419–26.

Steffensen, A. B., Oernbo, E. K., Stoica, A., Gerkau, N. J., Barbuskaite, D., Tritsaris, K., Rose, C.R., MacAulay, N. (2018). Cotransporter-mediated water transport underlying cerebrospinal fluid formation. *Nature Communications*, 9 (1): 2167.

Stein, V., Hermans-Borgmeyer, I., Jentsch, T.J.,and Hübner, C.A. (2004). Expression of the KCl Cotransporter KCC2 Parallels Neuronal Maturation and the Emergence of Low Intracellular Chloride. *Journal of Comparative Neurology,* 468 (1): 57–64.

Stil, A., Jean-Xavier, C., Liabeuf, S., Brocard, C., Delpire, E., Vinay, L., and Viemari, J. (2011). Contribution of the Potassium-Chloride Co-Transporter KCC2 to the Modulation of Lumbar Spinal Networks in Mice. *European Journal of Neuroscience,* 33 (7): 1212–22.

Stödberg, T., McTague, A., Ruiz, A. J., Hirata, H., Zhen, J., Long, P., et al. (2015). Mutations in SLC12A5 in epilepsy of infancy with migrating focal seizures. *Nature Communications*, *17*, 33: 8038

Storz, P., Doppler, H., and Toker, A. (2005). Protein Kinase D Mediates Mitochondrion-to-Nucleus Signaling and Detoxification from Mitochondrial Reactive Oxygen Species. *Molecular and Cellular Biology,* 25 (19): 8520–30.

Sun, Y.T., Lin, T., Tzeng, S., Delpire, E., and Shen, M. (2010). Deficiency of Electroneutral K^+-Cl^- Cotransporter 3 Causes a Disruption in Impulse Propagation along Peripheral Nerves. *GLIA,* 58 (13): 1544–52.

Sung, K. W., Kirby, M., McDonald, M. P., Lovinger, D. M., and Delpire E. (2000). Abnormal GABAA Receptor-Mediated Currents in Dorsal Root Ganglion Neurons Isolated from Na-K-2Cl Cotransporter Null Mice. *The Journal of Neuroscience* 20 (20): 7531–38.

Takahashi, N., Sequeira Lopez, M.S., Cowhig, J.E., Taylor, M.A., Hatada, T., Riggs, E., Lee, G., Gomez, R. A., Kim, H., and Smithies, O. (2005). Ren1c Homozygous Null Mice Are Hypotensive and Polyuric, but Heterozygotes Are Indistinguishable from Wild-Type. *Journal of the American Society of Nephrology,* 16 (1): 125–32.

Tanis, J.E., Bellemer, A.,Moresco, J.J., Forbush, B., and Koelle, M.R. (2009). The Potassium Chloride Cotransporter KCC-2 Coordinates Development of Inhibitory Neurotransmission and Synapse Structure in Caenorhabditis Elegans. *Journal of Neuroscience,* 29 (32): 9943–54.

Tao, R., Li, C., Newburn, E.N., Ye, T., Lipska, K. B., Herman, M.M., Weinberger, D.R., Kleinman, J.E., and Hyde, T.M. (2012). Transcript-Specific Associations of SLC12A5 (KCC2) in Human Prefrontal Cortex with Development, Schizophrenia, and Affective Disorders. *Journal of Neuroscience,* 32 (15): 5216–22.

Thomas, P. K., Marques, W.J., Davis, M.B., Sweeney, M.G., King, R.H., Bradley, J.L., Muddle, J.R., Tyson, J., Malcolm, S., and Harding, A.E. (1997). The Phenotypic Manifestations of Chromosome 17p11.2 Duplication. *Brain,* 120 (3): 465–78.

Thompson, S.M., Deisz, R.A., and Prince, D.A. (1988). Outward Chloride/Cation Co-Transport in

Mammalian Cortical Neurons. *Neuroscience Letters,* 89 (1): 49–54.

Tiwari, B., Belenghi, B., and Levine, A. (2002). Oxidative Stress Increased Respiration and Generation of Reactive Oxygen Species, Resulting in ATP Depletion, Opening of Mitochondrial Permeability Transition, and Programmed Cell Death. *Plant Physiology,* 128 (4): 1271–81.

Tornberg, J., Segerstråle, M., Kulesskaya, N., Voikar, V.,Taira, T.,and Airaksinen, M.S. (2007). KCC2-Deficient Mice Show Reduced Sensitivity to Diazepam, but Normal Alcohol-Induced Motor Impairment, Gaboxadol-Induced Sedation, and Neurosteroid-Induced Hypnosis. *Neuropsychopharmacology,* 32 (4): 911–18.

Ulzheimer, J.C., Peles, E., Levinson, S. R., and Martini, R. (2004). Altered Expression of Ion Channel Isoforms at the Node of Ranvier in P0-Deficient Myelin Mutants. *Molecular and Cellular Neuroscience,* 25 (1): 83–94.

Uncini, A., and Kuwabara, S. (2015). Nodopathies of the Peripheral Nerve: An Emerging Concept. *Journal of Neurology, Neurosurgery and Psychiatry*, 86 (11), 1186-95

Ushiro, H., Tsutsumi, T., Suzuki, K., Kayahara, T., and Nakano, K. (1998). Molecular Cloning and Characterization of a Novel Ste20-Related Protein Kinase Enriched in Neurons and Transporting Epithelia. *Archives of Biochemistry and Biophysics,* 355 (2): 233–40.

Uvarov, P., Ludwig, A., Markkanen, M., Pruunsild, P., Kaila, K., Delpire, E., Timmusk, T., Rivera, C., and Airaksinen, M.S. (2007). A Novel N-Terminal Isoform of the Neuron-Specific K-Cl Cotransporter KCC2. *Journal of Biological Chemistry,* 282 (42): 30570–76.

Uyanik, G., Elcioglu, N., Penzien, J., Gross, C., Yilmaz, Y., Olmez, A., Demir, E., et al., (2006). Novel Truncating and Missense Mutations of the KCC3 Gene Associated with Andermann Syndrome. *Neurology,* 66 (7): 1044–48.

Van der Auwera, G.A., Carneiro, M.O., Hartl, C., Poplin, R., Del Angel, G., Levy-Moonshine, A., Jordan, T., Shakir, K., Roazen, D., Thibault, J., et al. (2013). From FastQ data to high confidence variant calls: the Genome Analysis Toolkit best practices pipeline. *Curr. Protoc. Bioinformatics,* 43: 11.10.1-11-10-33.

Van der Valk, P., and De Groot, C. J. A. (2000). Staging of Multiple Sclerosis (MS) Lesions: Pathology of the Time Frame of MS. *Neuropathology and Applied Neurobiology,* 26 (1): 2–10.

Van Paassen, B.W., van der Kooi, A. J., van Spaendonck-Zwarts, K.Y., Verhamme, C., Baas, F.,and de Visser, M. (2014). PMP22 Related Neuropathies: Charcot-Marie-Tooth Disease Type 1A and Hereditary Neuropathy with Liability to Pressure Palsies. *Orphanet Journal of Rare Diseases,* 9 (1): 38.

Vargish, T., Benjamin, R., and Shenkman, L. (1970). Deafness from Furosemide. *Annals of*

Internal Medicine, 72 (5): 761.

Vázquez, N., Monroy, A., Dorantes, E., Muñoz-Clares, R.A.,and Gamba, G. (2002). Functional Differences between Flounder and Rat Thiazide-Sensitive Na-Cl Cotransporter. *American Journal of Physiology - Renal Physiology,* 282 (4): F599-607.

Velazquez, H., Good, D. W., and Wright, F. S. (1984). Mutual Dependence of Sodium and Chloride Absorption by Renal Distal Tubule. *American Journal of Physiology - Renal Fluid and Electrolyte Physiology,* 16 (6): F904-11

Velázquez, H., Náray-Fejes-Tóth, A., Silva, T., Andújar, E., Reilly, R.F., Desir, G.V., and Ellison, D.H. (1998). Rabbit Distal Convoluted Tubule Coexpresses NaCl Cotransporter and 11β-Hydroxysteroid Dehydrogenase II MRNA. *Kidney International,* 54 (2): 464–72.

Veríssimo, F., and Jordan, P. (2001). WNK Kinases, a Novel Protein Kinase Subfamily in Multi-Cellular Organisms. *Oncogene,* 20 (39): 5562–69.

Vilen, H., Eerikäinen, S., Tornberg, J., Airaksinen, M. S., and Savilahti, H. (2001). Construction of Gene-Targeting Vectors: A Rapid Mu in Vitro DNA Transposition-Based Strategy Generating Null, Potentially Hypomorphic, and Conditional Alleles. *Transgenic Research,* 10 (1): 69–80.

Vitoux, D., Olivieri, O., Garay, R. P., Cragoe, E. J., Galacteros, F., and Beuzard, Y. (1989). Inhibition of K^+ Efflux and Dehydration of Sickle Cells by [(Dihydroindenyl)Oxy]Alkanoic Acid: An Inhibitor of the K^+ Cl^- Cotransport System. *Proceedings of the National Academy of Sciences of the United States of America,* 86 (11): 4273–76.

Wallace, D.C., Fan, W., and Procaccio, V. (2010). Mitochondrial Energetics and Therapeutics. *Annual Review of Pathology: Mechanisms of Disease,* 5 (1): 297–348.

Wallin, M.T., Culpepper, W.J., Campbell, J.D., Nelson, L.M., Langer-Gould, A., Marrie, R., Cutter, G.R., et al., (2019). The Prevalence of MS in the United States: A Population-Based Estimate Using Health Claims Data. *Neurology,* 92 (10): E1029–40.

Walter, P., and Ron, D. (2011). The Unfolded Protein Response: From Stress Pathway to Homeostatic Regulation. *Science, 334 (6059), 1081-6*

Wang, D. D., and Kriegstein, A. R. (2011). Blocking Early GABA Depolarization with Bumetanide Results in Permanent Alterations in Cortical Circuits and Sensorimotor Gating Deficits. *Cerebral Cortex,* 21 (3): 574–87.

Wang, K., Li, M., and Hakonarson, H. (2010). ANNOVAR: functional annotation of genetic variants from high-throughput sequencing data. *Nucleic Acids Res.* 38: e164.

Waxman, S.G., and Ritchie, J. M. (1993). Molecular Dissection of the Myelinated Axon. *Annals*

of Neurology, 33 (2): 121–36.

Willis, W. D. (1999). Dorsal Root Potentials and Dorsal Root Reflexes: A Double-Edged Sword. *Experimental Brain Research*. 124 (4): 395-421.

Wilson, F. H., Disse-Nicodème, S., Choate, K. A., Ishikawa, K., Nelson-Williams, C., Desitter, I., … Lifton, R. P. (2001). Human hypertension caused by mutations in WNK kinases. *Science*, *293* (5532): 1107–1112.

Wilson, F.H., Kahle, K.T., Sabath, E., Lalioti, M.D., Rapson, A.K., Hoover, R.S., Hebert, S.C., Gamba, G., and Lifton, R.P. (2003). Molecular Pathogenesis of Inherited Hypertension with Hyperkalemia: The Na-Cl Cotransporter Is Inhibited by Wild-Type but Not Mutant WNK4. *Proceedings of the National Academy of Sciences of the United States of America,* 100 (2): 680–84.

Witschi, R., Punnakkal, P., Paul, J., Walczak, J., Cervero, F., Fritschy, J., Kuner, R., Keist, R., Rudolph, U., and Zeilhofer, H. (2011). Presynaptic Alpha2-GABAA Receptors in Primary Afferent Depolarization and Spinal Pain Control. *The Journal of Neuroscience,* 31 (22): 8134–42.

Wlodarska, M., Kostic, A.D., and Xavier, R.J. (2015). An Integrative View of Microbiome-Host Interactions in Inflammatory Bowel Diseases. *Cell Host and Microbe*, 17 (5), 577-91

Woo, N., Lu, J., England, R., McClellan, R., Dufour, S., Mount, D.B., Deutch, A.Y., Lovinger, D.M., and Delpire, E. (2002). Hyperexcitability and Epilepsy Associated with Disruption of the Mouse Neuronal-Specific K-Cl Cotransporter Gene. *Hippocampus,* 12 (2): 258–68.

Wu, Q., Delpire, E., Hebert, S.C.,and Strange, K. (2012). Functional Demonstration of Na^+ -K^+ -$2Cl^-$ Cotransporter Activity in Isolated , Polarized Choroid Plexus Cells. *American Journal of Physiology - Cell Physiology,* 275 (6): C1565-72.

Xu, B. E., English, J. M., Wilsbacher, J. L., Stippec, S., Goldsmith, E. J., & Cobb, M. H. (2000). WNK1, a novel mammalian serine/threonine protein kinase lacking the catalytic lysine in subdomain II. *Journal of Biological Chemistry*, 275 (22): 16795–16801.

Xu, J.Z., Hall, A.E., Peterson, L. N., Bienkowski, M.J., Eessalu, T.E., and Hebert, S.C. (1997). Localization of the ROMK Protein on Apical Membranes of Rat Kidney Nephron Segments. *American Journal of Physiology - Renal Physiology,* 273 (5): F739-48.

Xu, J., Lytle, C., Zhu, T.T., Payne, J.A., Benz, E., and Forbush, B. (1994). Molecular Cloning and Functional Expression of the Bumetanide-Sensitive Na-K-Cl Cotransporter. *Proceedings of the National Academy of Sciences of the United States of America,* 91 (6): 2201–5.

Yamagishi, N., Ueda, T., Mori, A., Saito, Y., and Hatayama, T. (2012). Decreased Expression of Endoplasmic Reticulum Chaperone GRP78 in Liver of Diabetic Mice. *Biochemical and Biophysical Research Communications,* 417 (1): 364–70.

Yan, W., Frank, C.L., Korth, M.J., Sopher, B.L., Novoa, I., Ron, D., and Katze, M.G. (2002). Control of PERK ElF2α Kinase Activity by the Endoplasmic Reticulum Stress-Induced Molecular Chaperone P58IPK. *Proceedings of the National Academy of Sciences of the United States of America,* 99 (25): 15920–25.

Yang, S., Morimoto, T., Rai, T., Chiga, M., Sohara, E., Ohno, M., Uchida, K. et al., (2007). Molecular Pathogenesis of Pseudohypoaldosteronism Type II: Generation and Analysis of a Wnk4D561A/+ Knockin Mouse Model. *Cell Metabolism,* 5 (5): 331–44.

Yoshida, H., Haze, K., Yanagi, H., Yura, T., and Mori, K. (1998). Identification of the Cis-Acting Endoplasmic Reticulum Stress Response Element Responsible for Transcriptional Induction of Mammalian Glucose- Regulated Proteins: Involvement of Basic Leucine Zipper Transcription Factors. *Journal of Biological Chemistry*, 273 (50): 33741–49.

You, Y., Bai, H., Wang, C., Chen, L., Liu, B., Zhang, H., and Gao, G. (2011). Myelin Damage of Hippocampus and Cerebral Cortex in Rat Pentylenetetrazol Model. *Brain Research,* 1381: 208–16.

Yu, L., McPhee, C.K., Zheng, L., Mardones, G.A., Rong, Y., Peng, J., Mi, N., et al., (2010). Termination of Autophagy and Reformation of Lysosomes Regulated by MTOR. *Nature,* 465 (7300): 942–46.

Zaarour, N., Demaretz, S., Defontaine, N., Mordasini, D., and Laghmani ,K . (2009). A Highly Conserved Motif at the COOH Terminus Dictates Endoplasmic Reticulum Exit and Cell Surface Expression of NKCC2. *Journal of Biological Chemistry,* 284 (32): 21752–64.

Zack, M.M., and Kobau, R. (2017). National and State Estimates of the Numbers of Adults and Children with Active Epilepsy — United States, 2015. *MMWR. Morbidity and Mortality Weekly Report,* 66 (31): 821–25.

Zakir, H., Mostafeezur, R., Suzuki, A., Hitomi, S., Suzuki, I., Maeda, T., Seo, K.,et al., (2012). Expression of TRPV1 Channels after Nerve Injury Provides an Essential Delivery Tool for Neuropathic Pain Attenuation. *PLoS ONE,* 7 (9): e44023.

Zamponi, G.W. (2019). Tuning the Regulator: Phosphorylation of KCC2 at Two Specific Sites Is Critical for Neurodevelopment. *Science Signaling,* 12 (603): eaay8960

Zdebik, A.A., Wangemann, P., and Jentsch, T. J. (2009). Potassium Ion Movement in the Inner Ear: Insights from Genetic Disease and Mouse Models. *Physiology,* 24 (5): 307–16.

Zhang, J., Gao, G., Begum, G., Wang, J., Khanna, A. R., Shmukler, B.E., Daubner, G.M., et al., (2016a). Functional Kinomics Establishes a Critical Node of Volume-Sensitive Cation-Cl^- Cotransporter Regulation in the Mammalian Brain. *Scientific Reports* 6 (1): 35986.

Zhou, J., Tan, S., Nicolas, V., Bauvy, C., Yang, N., Zhang, J., Xue, Y., Codogno, P., and Shen, H. (2013). Activation of Lysosomal Function in the Course of Autophagy via MTORC1 Suppression and Autophagosome-Lysosome Fusion. *Cell Research,* 23 (4): 508–23.

Zhu, L., Lovinger, D.,and Delpire, E. (2005). Cortical Neurons Lacking KCC2 Expression Show Impaired Regulation of Intracellular Chloride. *Journal of Neurophysiology,* 93 (3).

Zhu, L., Polley, N., Mathews, G.C., and Delpire, E. (2008). NKCC1 and KCC2 Prevent Hyperexcitability in the Mouse Hippocampus. *Epilepsy Research,* 79 (2–3): 201–12.

Zoons, E., Weisfelt, M., de Gans, J., Spanjaard, L., Koelman, J. H., Reitsma, J. B.,and van de Beek, D. (2008). Seizures in Adults with Bacterial Meningitis. *Neurology,* 70 (22 Pt 2): 2109–15.